Response to Comments from Reviewer #1 AMT-2019-55

The authors would like to sincerely thank the reviewer #1 for the careful review of the manuscript, the quick feedback, and the very constructive comments which helped dramatically improve the manuscript. The reviewer's comments are in italics, the summaries of our responses are in plain font, and the changes in the manuscript are in **bold red text**. Page and line numbers refer to the original document. We also appended a marked-up manuscript version to the end of the responses to better show all the changes made from this review.

Reviewer #1

General Comments:

First, a better description of the algorithm should be supplied. The equations are not matched well with their descriptions in the text, and multiple steps of the process (e.g. the linear regression and Gaussian Process hyperparameter optimization) are described simultaneously. The diagrams of figure 3 are helpful, but not sufficient to clarify the entire process. A complete step-by-step breakdown of an example run of the algorithm could be provided.

Response: We agree with the reviewer on that the algorithm should be better described in Section 2.3. Based on the reviewer's specific comments, we have now provided more details about how the alpha and beta parameters of Equation 3 were determined, how the standardization process was implemented, what it meant to re-calibrate a low-cost node based on its conditional mean, what criteria were used for convergence, and how the predictions were transformed back to the original PM scale. Regarding **1) "The equations are not matched well with their descriptions in the text",** we identified problems such as lack of the description of the $\boldsymbol{y_i}$ term in Equation 3, lack of the description of the Γ term in Equation 4, discrepancy in the Theta notation between Equations 2 and 5, lack of the description of the Theta term in Equations 2 and 5. We have now corrected these issues. Regarding **2) "multiple steps of the process (e.g. the linear regression and Gaussian Process hyperparameter optimization) are described simultaneously"**, we presume that this comment is connected to the reviewer's specific comment on Page 6, Line 19 to Page 7, Line 5. The linear regression step (called low-cost node initialization, corresponding to step 2 in Fig. 3, described on page 6, lines 19-23) and the training/optimization of the hyperparameters of the GPR model (corresponding to step 3 in Fig. 3, described on page 6, lines 23-29, starting from 'After standardizing') were previously described separately. To better highlight this fact and in order to avoid confusion, we have now added additional details to the low-cost node initialization step, have split the descriptions of the two steps into two separate paragraphs, have re-organized the places of Equations 3-5, and have added additional texts to explain the terms in Equations 3-5. Additionally, we have now placed each critical step under a sub-section (e.g., Sect. 2.3.x) to facilitate reading.

Regarding **3) “The diagrams of figure 3 are helpful, but not sufficient to clarify the entire process”,** we have now revised Figure 3 to make it more informative about and more accurately reflect the entire process and we have now expanded the Figure 3 caption to help better carry readers through the algorithm. Regarding 4) **“A complete step-by-step breakdown of an example run of the algorithm could be provided”,** we have now added a detailed algorithm block along with a sub-section number next to each critical step to indicate under which sub-section the details of that step can be found. The Section 2.3 has been completely overhauled.

Modified Section 2.3:

“2.3 Simultaneous GPR and simple linear regression calibration model

The simultaneous GPR and simple linear regression calibration algorithm is introduced here as Algorithm 1. The critical steps of the algorithm are linked to sub-sections under which the respective details can be found. Complementing Algorithm 1, a flow diagram illustrating the algorithm is given in Figure 3.

Algorithm 1: Algorithm of simultaneous GPR and simple linear regression

```
for each reference node (denote: Ref$_k$) in the network do
    leave Ref$_k$ out as test sample (see Sect. 2.3.1 for details)
    for each low-cost node (denote: Low-cost$_i$) in the network do
        find Low-cost$_i$’s closest reference node (denote: Ref$_i$) (Sect. 2.3.2)
        fit a simple linear regression model between Ref$_i$ and Low-cost$_i$’s PM$_{2.5}$: $\boldsymbol{Ref_i} = \alpha_i \cdot \boldsymbol{Low-cost_i} + \beta_i$ (Sect. 2.3.2)
        initialize the simple linear regression calibration factors to $\alpha_i$ (slope) and $\beta_i$ (intercept) for Low-cost$_i$ (Sect. 2.3.2)
        initialize the calibration of Low-cost$_i$ using $\alpha_i$ and $\beta_i$ (Sect. 2.3.2)
    end for
    initialize GPR hyperparameters $\boldsymbol{\Theta} = [\sigma_s^2, l, \sigma_n^2]$ to [0.1, 50, 0.01] (Sect. 2.3.3)
    standardize the 10 calibrated low-cost and 21 reference nodes at once (Sect. 2.3.3)
    while convergence criteria not met do
        update/optimize GPR hyperparameters $\boldsymbol{\Theta}$ using the 31 standardized training nodes (Sect. 2.3.3 and .5)
        for each low-cost node (denote: Low-cost$_i$) in the network do
            for each day (denote: t) of the 59 days do
                calculate Low-cost$_i$’s mean conditional on the remaining 30 nodes on day t (denote $\mu_{A|B}^{it}$) (Sect. 2.3.4 and .5)
            end for
            fit a linear regression between $\boldsymbol{\mu_{A|B}^i} \in \mathbb{R}^{59}$ and Low-cost$_i$: $\boldsymbol{\mu_{A|B}^i} = \alpha_i \cdot \boldsymbol{Low-cost_i} + \beta_i$ (Sect. 2.3.4 and .5)
            update calibration factors $\alpha_i$ and $\beta_i$ for Low-cost$_i$ (Sect. 2.3.4 and .5)
            update the calibration of Low-cost$_i$ using $\alpha_i$ and $\beta_i$ (Sect. 2.3.4 and .5)
        end for
        check convergence criteria (Sect. 2.3.5)
    end while
    use the final GPR model to predict on $\text{Ref}_k$ (Sect. 2.3.6)
    transform the prediction back to original $PM_{2.5}$ scale (Sect. 2.3.6)
    calculate RMSE and percent error (Sect. 2.3.6)
end for
```

2.3.1 Leave one reference node out

Because the true calibration factors for the low-cost nodes **are not know beforehand**, a leave-one-out CV approach (i.e., holding one of the 22 reference nodes out of modelling each run for model predictive performance evaluation) was adopted as a surrogate to estimate our proposed model accuracy of calibrating the low-cost nodes. For each of the 22-fold CV, 31 node locations (denoted $\Gamma = \{\boldsymbol{x}_1, \ldots, \boldsymbol{x}_{31}\}$) were available, where $\boldsymbol{x}_i$ is the latitude and longitude of node *i*. Let y_{it} represent the daily $PM_{2.5}$ measurement of node *i* on day *t* and $\boldsymbol{y}_t \in \mathbb{R}^{31}$ denote the concatenation of the daily $PM_{2.5}$ measurements recorded by the 31 nodes on day *t*. Given a finite number of node locations, a Gaussian Process (GP) becomes a Multivariate Gaussian Distribution over the nodes in the form of:

$$\boldsymbol{y}_t|\Gamma \sim N(\boldsymbol{\mu},\boldsymbol{\Sigma}) \tag{1}$$

where $\boldsymbol{\mu} \in \mathbb{R}^{31}$ represents the mean function (assumed to be $\boldsymbol{0}$ in this study)**;** $\boldsymbol{\Sigma} \in \mathbb{R}^{31\times 31}$ with $\Sigma_{ij} = K(\boldsymbol{x}_i, \boldsymbol{x}_j; \boldsymbol{\Theta})$ represents the covariance function/kernel function and **$\boldsymbol{\Theta}$ is a vector of the GPR hyperparameters.**”

For simplicity’s sake, the kernel function was set to a squared exponential (SE) covariance term to capture the spatially-correlated signals coupled with another component to constrain the independent noise:

“$$K(\boldsymbol{x}_i, \boldsymbol{x}_j; \boldsymbol{\Theta}) = \sigma_s^2\, exp\left(-\frac{\|x_i - x_j\|_2^2}{2l^2}\right) + \sigma_n^2 \boldsymbol{I} \text{ (Rasmussen and Williams, 2006)} \tag{2}$$

where σ_s^2, l, and σ_n^2 are the model hyperparameters (to be optimized) that control the signal magnitude, characteristic length-scale, and noise magnitude, respectively**; $\boldsymbol{\Theta} \in \mathbb{R}^3$ is a vector of the GPR hyperparameters $\boldsymbol{\sigma_s^2}$, $\boldsymbol{l}$, and $\boldsymbol{\sigma_n^2}$.**”

2.3.2 Initialize low-cost nodes’ (simple linear regression) calibrations

What separates our method from standard GP applications is the simultaneous incorporation of calibration for the low-cost nodes using a simple linear regression model into the spatial model. Linear regression has previously been shown to be effective at calibrating PM sensors (Zheng et al., 2018). **Linear regression was first used to initialize low-cost nodes’ calibrations (step two in Fig. 3). In this step**, each low-cost node ***i*** was **linearly** calibrated **to** its closest reference node **using Eq. (3), where the calibration factors $\boldsymbol{\alpha_i}$ (slope) and $\boldsymbol{\beta_i}$ (intercept) were determined by fitting a simple linear**

regression model to all available pairs of daily $PM_{2.5}$ mass concentrations from the uncalibrated low-cost node *i* (independent variable) and its closest reference node (dependent variable). This step aims to bridge disagreements between low-cost and reference node measurements**, which can lead** to a more consistent spatial interpolation and a faster convergence during **the GPR** model optimization.

$$\boldsymbol{r}_i = \begin{cases} \boldsymbol{y}_i, & \text{if reference node} \\ \alpha_i \cdot \boldsymbol{y}_i + \beta_i, & \text{if low} - \text{cost node} \end{cases} \tag{3}$$

where $\boldsymbol{y_i}$ **is either a vector of all the daily $PM_{2.5}$ measurements of reference node *i* or a vector of all the daily raw $PM_{2.5}$ signals of low-cost node *i***; $\boldsymbol{r_i}$ **is either a vector of all the daily $PM_{2.5}$ measurements of reference node *i* or a vector of all the daily calibrated $PM_{2.5}$ measurements of** low-cost node *i*; α_i and β_i are the slope and intercept, respectively, **determined from the fitted simple linear regression** calibration equation **with daily $PM_{2.5}$ mass concentrations of the uncalibrated** low-cost node *i* **as independent variable and $PM_{2.5}$ mass concentrations of low-cost node *i*'s** closest reference node **as dependent variable**.

2.3.3 Optimize GPR model (hyperparameters)

In the next step (step three in Fig. 3), a GPR model was fit to **each day *t*'s** 31 nodes (i.e., 10 initialized low-cost nodes and 21 reference nodes) as described in Eq. (4). **Prior to the GPR model fitting, all the $PM_{2.5}$ measurements of the 31 nodes over 59 valid days used for GPR model hyperparameters training were standardized. The standardization was performed by first concatenating all these training $PM_{2.5}$ measurements (from the 31 nodes over 59 days), then** subtracting **their** mean $\mu_{training}$ and **dividing them by their standard deviation** $s_{training}$ (i.e., transforming **all** the **training** $PM_{2.5}$ measurements to have a zero mean and unit variance). **It is worth noting that assuming the mean function $\boldsymbol{\mu} \in \mathbb{R}^{31}$ to be 0 along with standardizing all the training $PM_{2.5}$ samples in this study is one of the common modelling formulations on the GPR model and the simplest one. More complex formulations including a station-specific mean function (lack of prior information for this project), a time-dependent mean function (computationally expensive), and a combination of both were not considered for this paper. After the standardization of training samples,** the GPR was trained to maximize the log marginal likelihood over all 59 days **using Eq. 5 and** using an L-BFGS-B optimizer (Byrd et al., 1994). To avoid bad local minima, several random hyperparameter initializations were tried and the initialization **that resulted in** the **largest** log marginal likelihood **after optimization** was chosen **(in this paper, $\boldsymbol{\Theta} = [\boldsymbol{\sigma_s^2}, \boldsymbol{l}, \boldsymbol{\sigma_n^2}]$ was initialized to [0.1, 50, 0.01]).**"

$$\boldsymbol{r}_t | \Gamma \sim N(\boldsymbol{\mu}, \boldsymbol{\Sigma}) \tag{4}$$

where *t* ranges from 1 (inclusive) to 59 (inclusive); $\boldsymbol{r_t} \in \mathbb{R}^{31}$ is a vector of all 31 nodes' $PM_{2.5}$ measurements **(calibrated if low-cost nodes)** on day *t*; $\boldsymbol{\Gamma} = \{\boldsymbol{x_1}, \dots, \boldsymbol{x_{31}}\}$ **denotes 31 nodes' locations and $\boldsymbol{x_i} \in \mathbb{R}^2$ is a vector of the latitude and longitude of node *i*; $\boldsymbol{\mu} \in \mathbb{R}^{31}$ represents the mean function (assumed to be 0 in this study) and $\boldsymbol{\Sigma} \in \mathbb{R}^{31\times 31}$ with $\boldsymbol{\Sigma_{ij}} = \boldsymbol{K}(\boldsymbol{x_i}, \boldsymbol{x_j}; \boldsymbol{\Theta})$ represents the covariance function/kernel function.**

$$\arg\max_{\boldsymbol{\Theta}} L(\boldsymbol{\Theta}) = \arg\max_{\boldsymbol{\Theta}} \sum_{t=1}^{59} \log p(\boldsymbol{r}_t|\boldsymbol{\Theta}) \ = \arg\max_{\boldsymbol{\Theta}} \left(-0.5 \cdot 59 \cdot \log|\boldsymbol{\Sigma}_{\theta}| - 0.5 \sum_{t=1}^{59} \boldsymbol{r}_t{}^{T} \boldsymbol{\Sigma}_{\theta}^{-1} \boldsymbol{r}_t\right) \tag{5}$$

where $\boldsymbol{\Theta} \in \mathbb{R}^{\mathbf{3}}$ is a vector of **the GPR hyperparameters** σ_s^2, l, and σ_n^2."

2.3.4 Update low-cost nodes' (simple linear regression) calibrations based on their conditional means

Once the optimum $\boldsymbol{\Theta}$ for the (initial) GPR was found, we used the learned covariance function to find the mean of each low-cost node i's Gaussian Distribution conditional on the remaining 30 nodes within the network (i.e., $\mu_{A|B}^{it}$) on day t as described mathematically in Eq. (6)–(8) and repeatedly did so until all 59 days' $\mu_{A|B}^{it}$ (i.e., $\boldsymbol{\mu}_{\boldsymbol{A|B}}^{\boldsymbol{i}} \in \mathbb{R}^{\mathbf{59}}$) were found and then re-calibrated that low-cost node i based on the $\boldsymbol{\mu}_{\boldsymbol{A|B}}^{\boldsymbol{i}}$. **The re-calibration was done by first fitting a simple linear regression model to all 59 pairs of daily PM2.5 mass concentrations from the uncalibrated low-cost node $\boldsymbol{i}$ ($\boldsymbol{y_i}$, independent variable) and its conditional mean ($\boldsymbol{\mu}_{\boldsymbol{A|B}}^{\boldsymbol{i}}$, dependent variable) and then using the updated calibration factors (slope $\boldsymbol{\alpha_i}$ and intercept $\boldsymbol{\beta_i}$) obtained from this newly fitted simple linear regression calibration model to calibrate the low-cost node $\boldsymbol{i}$ again (using Eq. 3).** This procedure is summarized graphically in Fig. 3 step four and was performed iteratively for all low-cost nodes one at a time. The reasoning behind this step is given in the Supplement. A high-level interpretation of this step is that the target low-cost node is calibrated by being weighted over the remaining nodes within the network and the $\boldsymbol{\Sigma}_{\boldsymbol{AB}}^{\boldsymbol{it}} \boldsymbol{\Sigma}_{\boldsymbol{BB}}^{\boldsymbol{it}}{}^{-1}$ term computes the weights. In contrast to the inverse distance weighting interpolation which will weight the nodes used for calibration equally if they are equally distant from the target node, the GPR will value sparse information more and lower the importance of redundant information (suppose all the nodes are equally distant from the target node) as shown in Fig. S2.

$$p\left(\begin{bmatrix} r_A^{it} \\ \boldsymbol{r}_{\boldsymbol{B}}^{\boldsymbol{it}} \end{bmatrix}\right) = \ N\left(\begin{bmatrix} r_A^{it} \\ \boldsymbol{r}_{\boldsymbol{B}}^{\boldsymbol{it}} \end{bmatrix}; \begin{bmatrix} \mu_A^{it} \\ \boldsymbol{\mu}_{\boldsymbol{B}}^{\boldsymbol{it}} \end{bmatrix} \begin{bmatrix} \Sigma_{AA}^{it} & \boldsymbol{\Sigma}_{\boldsymbol{AB}}^{\boldsymbol{it}} \\ \boldsymbol{\Sigma}_{\boldsymbol{BA}}^{\boldsymbol{it}} & \boldsymbol{\Sigma}_{\boldsymbol{BB}}^{\boldsymbol{it}} \end{bmatrix}\right) \tag{6}$$

$$r_A^{it}|\boldsymbol{r}_{\boldsymbol{B}}^{\boldsymbol{it}} \sim N\left(\mu_{A|B}^{it}, \Sigma_{A|B}^{it}\right) \tag{7}$$

$$\mu_{A|B}^{it} = \ \mu_A^{it} + \boldsymbol{\Sigma}_{\boldsymbol{AB}}^{\boldsymbol{it}} \boldsymbol{\Sigma}_{\boldsymbol{BB}}^{\boldsymbol{it}}{}^{-1} (\boldsymbol{r}_{\boldsymbol{B}}^{\boldsymbol{it}} - \ \boldsymbol{\mu}_{\boldsymbol{B}}^{\boldsymbol{it}}) \tag{8}$$

where $r_A^{it}$and $\boldsymbol{r}_{\boldsymbol{B}}^{\boldsymbol{it}}$ are the daily PM2.5 measurement(**s**) of the low-cost node i and the remaining 30 nodes on day t; μ_A^{it}, $\boldsymbol{\mu}_{\boldsymbol{B}}^{\boldsymbol{it}}$, and $\mu_{A|B}^{it}$ are the mean (**vector**) of the partitioned Multivariate Gaussian Distribution of the low-cost node i, the remaining 30 nodes, and the low-cost node i conditional on the remaining 30 nodes, respectively, on day t; and Σ_{AA}^{it}, $\boldsymbol{\Sigma}_{\boldsymbol{AB}}^{\boldsymbol{it}}$, $\boldsymbol{\Sigma}_{\boldsymbol{BA}}^{\boldsymbol{it}}$, $\boldsymbol{\Sigma}_{\boldsymbol{BB}}^{\boldsymbol{it}}$, and $\Sigma_{A|B}^{it}$ are the covariance between the low-cost node i and itself, the low-cost node i and the remaining 30 nodes, the remaining 30 nodes and the low-cost node i, the remaining 30 nodes and themselves, and the low-cost node i conditional on the remaining 30 nodes and itself, respectively, on day t.

2.3.5 Optimize alternately and iteratively and converge

Iterative optimizations alternated between the GPR **hyperparameters** and the low-cost node **calibrations using the approaches described in Sect. 2.3.3 and 2.3.4, respectively** (Fig. 3 steps five and six, **respectively**), until the GPR parameters $\boldsymbol{\Theta}$ converged **with the convergence criteria being the differences in all the GPR hyperparameters between the two adjacent runs below 0.01 (i.e., with $\Delta\boldsymbol{\sigma}_{s}^{2} \leq \mathbf{0.01}, \Delta\boldsymbol{l} \leq \mathbf{0.01}, \boldsymbol{and}\ \Delta\boldsymbol{\sigma}_{n}^{2} \leq \mathbf{0.01}$).**

2.3.6 Predict on the holdout reference node and calculate accuracy metrics

The final GPR was used to predict the 59-day $PM_{2.5}$ measurements of the holdout reference node (Fig. 3 step seven) following the Cholesky decomposition algorithm (Rasmussen and Williams, 2006) with the standardized predictions being transformed back to the original $PM_{2.5}$ measurement scale at the end. **The back transformation was done by multiplying the predictions by the standard deviation $\boldsymbol{s_{training}}$ (the standard deviation of the training $PM_{2.5}$ measurements) and then adding back the mean $\boldsymbol{\mu_{training}}$ (the mean of the training $PM_{2.5}$ measurements).** Metrics including root mean square errors (RMSE, Eq. 9) and percent errors defined as RMSE normalized by the average of the true measurements of the holdout reference node in this study (Eq. 10) were calculated for each fold and further averaged over all 22 folds to assess the accuracy and sensitivity of our simultaneous GPR and simple linear regression calibration model.

$$\mathrm{RMSE} = \sqrt{\frac{1}{59}\|\boldsymbol{y}_i - \widehat{\boldsymbol{y}_i}\|_2^2} \qquad (9)$$

where $\boldsymbol{y}_i$ and $\widehat{\boldsymbol{y}_i}$ are the true and model predicted 59 daily $PM_{2.5}$ measurements of the holdout reference node *i*.

$$\text{Percent error} = \frac{\mathrm{RMSE}}{\text{avg. holdout reference PM}_{2.5}\text{ conc.}} \qquad (10)”$$

Modified Figure 3:

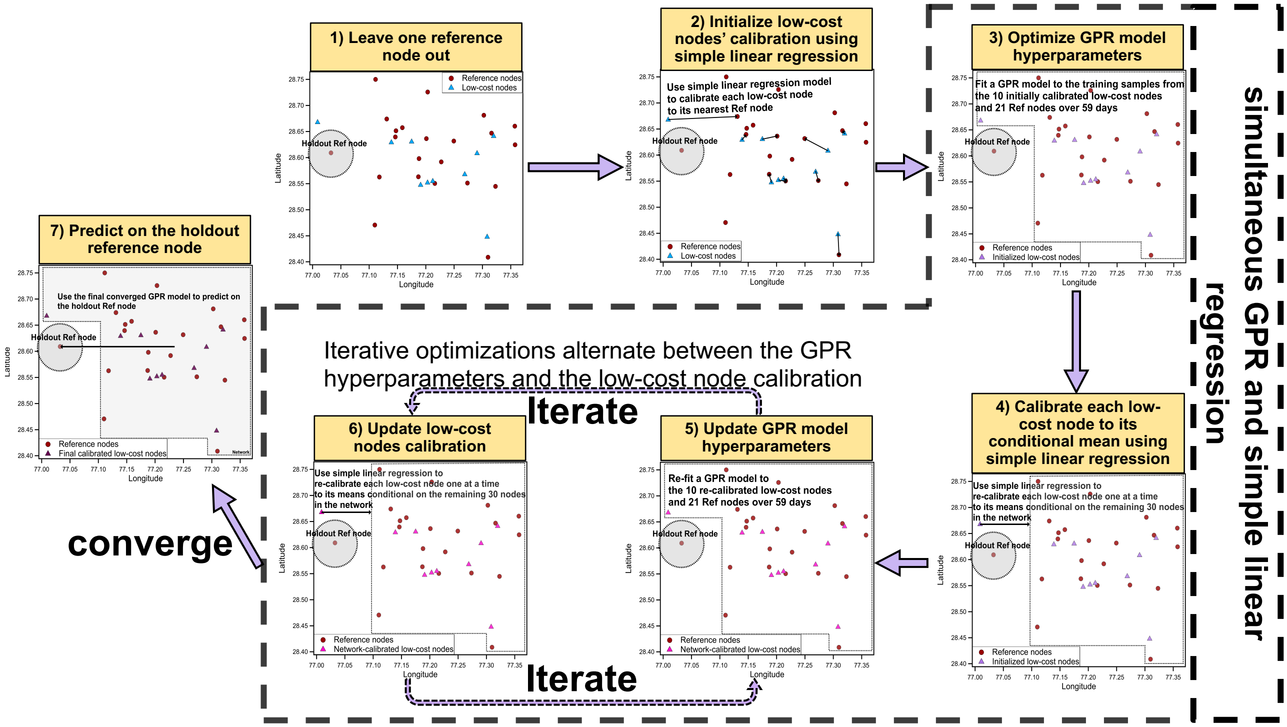
1) Leave one reference node out
Reference nodes
Low-cost nodes
Holdout Ref node
2) Initialize low-cost nodes' calibration using simple linear regression
Use simple linear regression model to calibrate each low-cost node to its nearest Ref node
3) Optimize GPR model hyperparameters
Fit a GPR model to the training samples from the 10 initially calibrated low-cost nodes and 21 Ref nodes over 59 days
Initialized low-cost nodes
4) Calibrate each low-cost node to its conditional mean using simple linear regression
Use simple linear regression to re-calibrate each low-cost node one at a time to its means conditional on the remaining 30 nodes in the network
5) Update GPR model hyperparameters
Re-fit a GPR model to the 10 re-calibrated low-cost nodes and 21 Ref nodes over 59 days
Network-calibrated low-cost nodes
6) Update low-cost nodes calibration
Use simple linear regression to re-calibrate each low-cost node one at a time to its means conditional on the remaining 30 nodes in the network
7) Predict on the holdout reference node
Use the final converged GPR model to predict on the holdout Ref node
Final calibrated low-cost nodes
Iterative optimizations alternate between the GPR hyperparameters and the low-cost node calibration
Iterate
Iterate
converge
simultaneous GPR and simple linear regression
Latitude
Longitude
28.40
28.45
28.50
28.55
28.60
28.65
28.70
28.75
77.00
77.05
77.10
77.15
77.20
77.25
77.30
77.35

Figure 3: The **flow diagram illustrating** the simultaneous GPR and simple linear regression calibration **algorithm. In step one, for each of the 22-fold leave-one-out CVs, one of the 22 reference nodes is held out of modelling for the model predictive performance evaluation in step seven; in step two, fit a simple linear regression model between each low-cost node i and its closest reference node's PM$_{2.5}$, initialize low-cost node i's calibration model to this linear regression model, and calibrate the low-cost node i using this model; in step three, first initialize the GPR hyperparameters to [0.1, 50, 0.01] and then update/optimize the hyperparameters based on the training samples from the 10 initially calibrated low-cost nodes and 21 reference nodes over 59 days; in step four, first compute each low-cost node i's means conditional on the remaining 30 nodes given the optimized GPR hyperparameters, then fit a simple linear regression model between each low-cost node i and its conditional means, update low-cost node i's calibration model to this new linear regression model, and re-calibrate the low-cost node i using this new model; in step five and six, iterative optimizations alternate between the GPR hyperparameters and the low-cost node calibrations using the approaches described in step three and four, respectively, until the GPR hyperparameters converged; in step seven, predict the 59-day PM$_{2.5}$ measurements of the holdout reference node given the finalized GPR hyperparameters and the low-cost node calibrations.**

Second, it appears that both the Gaussian process hyperparameter calibration and the linear regression calibration of the low-cost nodes are carried out over an approximately 60-day period, using all data collected during this period. This would seem to preclude the use of your methods for on-line calibration. You may want to examine how this technique could be used in an on-line fashion, but designating a "current time" within the dataset and only using data collected prior to that time to calibrate the Gaussian Process hyperparameters and linear regression coefficients which are used to correct the data for that time. You could then also examine the effect of time history on your model, analyzing how the performance changes as more or less past data is included in the calibration process. As it currently is, if I am understanding your approach correctly, it can only be applied retroactively to a designated period of time for which all sensor data are available.

Response: We really appreciate the reviewer's insightful suggestions and have examined both the possibility of using our method for online calibration and the effect of time history on our model. We will answer the reviewer's second question first and then circle back to the first question. Regarding **the effect of time history on our model**, we analyzed how the model performance changed when an increment of 2 days' data were included in the model. The model performance was based on the accuracy of model prediction on the 22 reference nodes (within the time periods of the data included) using leave-one-out CV, as described in Sect. 3.2.1. We observed a surprisingly consistent ~30 % error rate and ~3–4 % standard error of the mean (SEM) regardless of how many 2-day increments were used as the training window size. The small effect of training window size on the model performance hints **that using our method for online calibration/prediction is feasible**. We assessed the performance of using simple linear regression calibration factors and GPR hyperparameters that were optimized from one week to calibrate the 10 low-cost nodes and predict each of the 22 reference nodes in the next week. For example, the first/second/third/… week data were used as training data to build GPR models and simple linear regression models. These simple linear regression models were then used to calibrate the low-cost nodes in the second/third/fourth/… week, followed by GPR models to predict each of the 22 reference nodes in that week. The performance was still measured by the accuracy of model prediction on the 22 reference nodes using leave-one-out CV, as described in Sect. 3.2.1. We found similarly stable 26–34 % online calibration error rates and ~3–7 % SEMs throughout the weeks. We have now added two sub-sections (i.e., **Sect. 3.2.3 GPR model performance as a function of training window size** and **Sect. 3.2.4 GPR model dynamic calibration performance**, respectively) to address the time history and online calibration questions, respectively. A figure showing the model performance as a function of training window size for Sect. 3.2.3 was added to the main manuscript as Figure 8. Another figure showing the GPR model dynamic calibration performance for each successive week (from weeks 2 to 8) was added to the supplement as Figure S4. We have also updated the abstract, introduction, and conclusions to include the new results. Finally, all the figure numbers have been changed accordingly.

Added Section 3.2.3:

3.2.3 GPR model performance as a function of training window size

So far, the optimization of both GPR model hyperparameters and the linear regression calibration factors for the low-cost nodes has been carried out over the entire sampling period using all 59 valid daily-averaged data points. It is of critical importance to examine the effect of time history on the algorithm, by analyzing how sensitive the model performance is to training window size. We tracked the model performance change when an increment of 2 days' data were included in the model training. The model performance was measured by the mean accuracy of model prediction on the 22 reference nodes (within the time period of the training window) using leave-one-out CV, as described in Sect. 3.2.1. Figure 8 illustrates that, throughout the 59 days, the error rate and the standard error of the mean (SEM) remained surprisingly consistent at ~30 % and ~3–4 %, respectively, regardless of how many 2-day

increments were used as the training window size. The little influence of training window size on the GPR model performance is possibly a positive side effect of the algorithm's time-invariant mean assumption, strong spatial smoothing effect, and the additional averaging of the error rates of the 22 reference nodes. The markedly low requirement of our algorithm for training data is powerful in that it enables the GPR model hyperparameters and the linear regression calibration factors to always be nearly most updated in the field. This helps realize the algorithm's full potential for automatically surveilling large-scale networks by detecting malfunctioning low-cost nodes within a network (see Sect. 3.3.1) and tracking the drift of low-cost nodes (see Sect. 3.3.2) with as little latency as possible.

Added Figure 8:

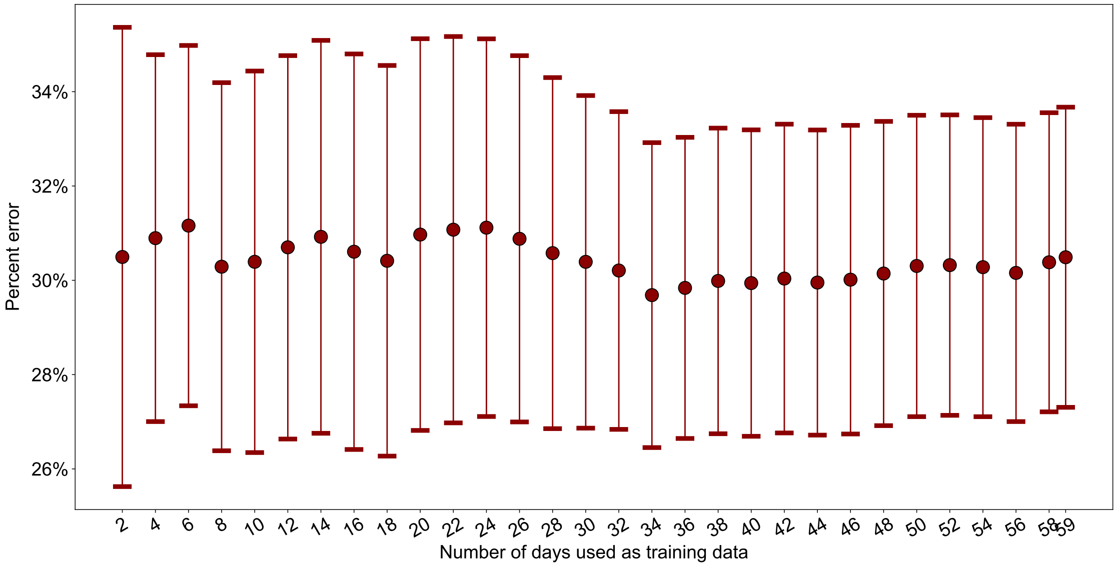

Figure 8: The mean percent error rate of GPR model prediction on the 22 reference nodes using leave-one-out CV (see Sect. 3.2.1) as a function of training window size in an increment of 2 days. The error bars represent the standard error of the mean (SEM) of the GPR prediction errors of the 22 reference nodes.

Added Section 3.2.4:

3.2.4 GPR model dynamic calibration performance

The stationary model performance in response to the increase of training data hints that using our method for dynamic calibration/prediction is feasible. We assessed the algorithm's 1 week-ahead prediction performance, by

using simple linear regression calibration factors and GPR hyperparameters that were optimized from one week to calibrate the 10 low-cost nodes and predict each of the 22 reference nodes, respectively, in the next week. For example, the first/second/third/… week data were used as training data to build GPR models and simple linear regression models. These simple linear regression models were then used to calibrate the low-cost nodes in the second/third/fourth/… week, followed by the GPR models to predict each of the 22 reference nodes in that week. The performance was still measured by the mean accuracy of model prediction on the 22 reference nodes using leave-one-out CV, as described in Sect. 3.2.1. We found similarly stable 26–34 % dynamic calibration error rates and ~3–7 % SEMs throughout the weeks (see Figure S4).

Added Figure S4:

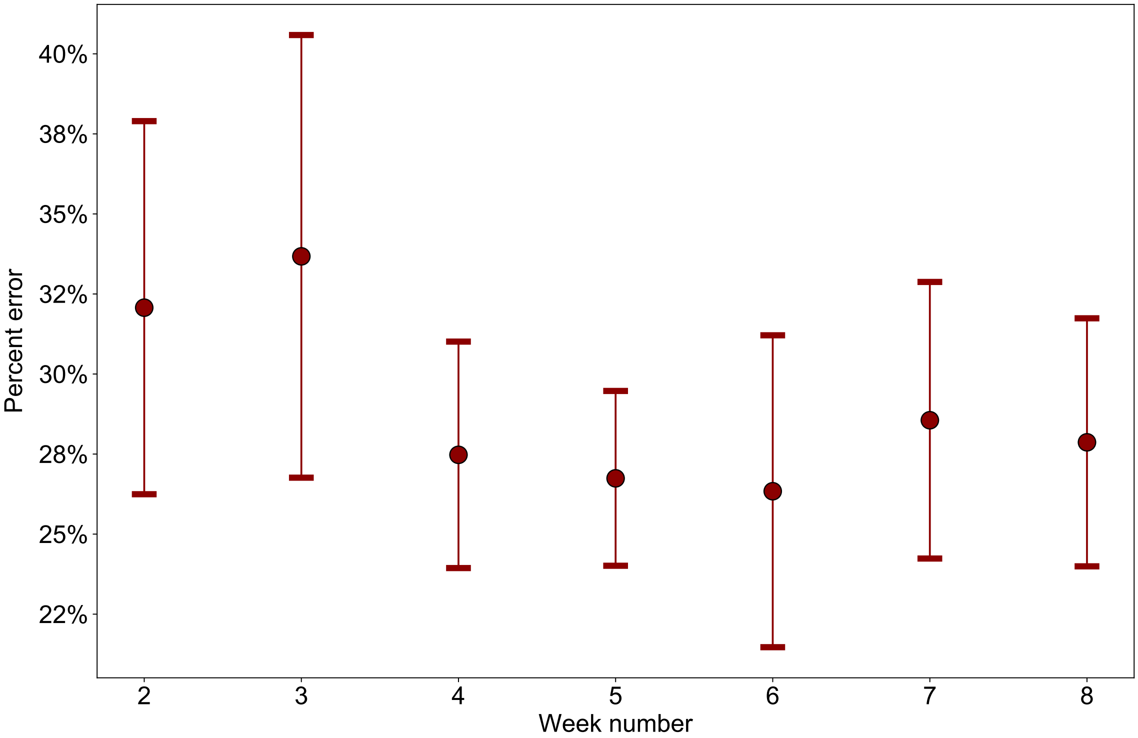

Figure S4: The 1 week-ahead prediction error of the GPR models (which were pre-trained on the current week's data) as a function of the week being predicted. The error bars represent the standard error of the mean (SEM) of the GPR prediction errors of the 22 reference nodes.

Added text for the Abstract on Page 1, line 25:

We further demonstrated that our algorithm performance is insensitive to training window size as the mean prediction error rate and the standard error of the mean (SEM) for the 22 reference stations remained consistent at ~30 % and ~3–4 % when an increment of 2 days' data were included in the model training. The markedly low

requirement of our algorithm for training data enables the models to always be nearly most updated in the field, thus realizing the algorithm's full potential for dynamically surveilling large-scale WLPMSNs by detecting malfunctioning low-cost nodes and tracking the drift with little latency. Our algorithm presented similarly stable 26–34 % mean prediction errors and ~3–7 % SEMs over the sampling period when pre-trained on the current week's data and predicting 1 week ahead, therefore suitable for online calibration.

Added text for the Introduction on Page 3, line 17:

3) examining the sensitivity of our algorithm to the training data size and the feasibility of it for dynamic calibration;

Added text for the Conclusions on Page 13, line 28:

We showed that our algorithm performance is insensitive to training window size as the mean prediction error rate and the standard error of the mean (SEM) for the 22 reference stations remained consistent at ~30 % and ~3–4 % when an increment of 2 days' data were included in the model training. The markedly low requirement of our algorithm for training data enables the models to always be nearly most updated in the field, thus realizing the algorithm's full potential for dynamically surveilling large-scale WLPMSNs by detecting malfunctioning low-cost nodes and tracking the drift with little latency. Our algorithm presented similarly stable 26–34 % mean prediction errors and ~3–7 % SEMs over the sampling period when pre-trained on the current week's data and predicting 1 week ahead, therefore suitable for dynamic calibration.

Third, when analyzing possible failure modes of sensors to determine if the algorithm can detect these modes, only two modes are considered: linear drift over time and replacement of the sensor signal with random noise. Other common failure modes should also be examined. These should include a "random walk" baseline drift (rather than simple linear drift), flatlining of the sensor (either at zero or at a non-zero value), and noisy corruption of a true signal (i.e. adding a random noise to the original signal, rather than completely replacing the true signal with random noise).

Response: We thank the reviewer for his/her expertise in the possible failure modes of sensors and his/her scientific rigor. As we demonstrated in our response to the reviewer's second general comment, the performance of our algorithm is insensitive to the training data size. And we believe that models with a similar prediction accuracy should have a similar failure mode detection power. For example, if the prediction accuracy of the model trained on 59 days' data is virtually the same as the accuracy of the model trained on 2 days' data (as shown previously), and if the model trained on 59 days is able to detect the simulated drift, then so should the model trained on 2 days. Then if we reasonably assume that the drift rate remains roughly unchanged within a 2-day window (as drift is believed to occur on time periods much longer than 2 days), then the drift mode (linear or random), which only dictates how the drift rate jumps (usually smoothly as well) between any adjacent discrete 2-day windows, does not matter that much anymore. All that matters is to track that one fixed drift rate reasonably well within those 2 days, which is virtually the same as what we already did and demonstrated with the entire 59 days' data in Sect. 3.3.2. Therefore, we do not believe that **the mode of drift** is a major issue. Regarding **flatlining**, we thank the reviewer for mentioning and defining this type of failure mode. Flatlining is in fact the most commonly seen failure mode of our PM sensors in Delhi. The raw signals of such malfunctioning PM sensors were observed to flatline at the upper end of the sensor output values (typically thousands of µg m^{-3}). The very distinct signals of these flatlining low-cost PM nodes make it rather easy to separate them from the rest of the nodes and filter them out at the early pre-processing stage before analyses without having to resort to our algorithm. Regarding **noisy corruption of a true signal**, this particular failure mode is commonly seen in low-cost electrochemical sensors (such as ozone and nitrogen dioxide) based on redox reactions, but rarely seen in low-cost PM sensors that employ a light-scattering approach. Therefore, we consider the noisy corruption failure mode not applicable to or out of the scope of our current paper whose main subject is low-cost PM sensors. We have now added the discussion about why we do not need our algorithm to detect flatlining and why the mode of drift will not affect our simulation results to Sect. 3.3.1 and Sect. 3.3.2, respectively.

Added text on Page 11, line 8:

"**It is worth mentioning that flatlining is another commonly seen failure mode of our low-cost PM sensors in Delhi. The raw signals of such malfunctioning PM sensors were observed to flatline at the upper end of the sensor output values (typically thousands of µg m^{-3}). The very distinct signals of these flatlining low-cost PM nodes, however, make it rather easy to separate them from the rest of the nodes and filter them out at the early pre-processing stage before analyses, therefore without having to resort to our algorithm.**"

Modified text on Page 12, lines 6-9:

"~~We can rebuild a model such as every week using a rolling window (to keep the number of observations for model construction roughly unchanged) to assess the drifts in the model space over time. After that, the true calibration factors obtained from the initial collocation with reference instruments prior to deployment can be adjusted accordingly based on the model-estimated drifts. This procedure allows for real-time drift corrections to low-cost node measurements.~~

It should be noted that the mode of drift (linear or random drift) will not significantly affect our simulation results. As we demonstrated in Sect. 3.2.3, the performance of our algorithm is insensitive to the training data size. And we believe that models with a similar prediction accuracy should have a similar drift detection power. For example, if the prediction accuracy of the model trained on 59 days' data is virtually the same as the accuracy of the model trained on 2 days' data, and if the model trained on 59 days is able to detect the simulated drift, then so should the model trained on 2 days. Then if we reasonably assume that the drift rate remains roughly unchanged within a 2-day window, then the drift mode (linear or random), which only dictates how the drift rate jumps (usually smoothly as well) between any adjacent discrete 2-day windows, does not matter anymore. All that matters is to track that one fixed drift rate reasonably well within those 2 days, which is virtually the same as what we already did with the entire 59 days' data."

Finally, while the body of the paper presents a good discussion of the limitations of the proposed approach (mainly its need for spatial homogeneity in the true concentrations to be fully effective), this discussion is missing from the abstract. I believe that this observation is an important result of this paper and should be highlighted in the abstract as well.

Response: We did attempt to convey this message on Page 1, lines 23-25; however, the message might be somewhat subtle. We have now more prominently discussed the limitations of the proposed approach.

Modified text on Page 1, lines 23-25:

"**Of the 22 reference stations, high-quality predictions were observed for those stations whose $PM_{2.5}$ means were close to the Delhi-wide mean (i.e., 138 ± 31 μg m^{-3}) and relatively poor predictions for those nodes whose means differed substantially from the Delhi-wide mean (particularly on the lower end). We also observed washed-out local variability in $PM_{2.5}$ across the 10 low-cost sites** after calibration **using our approach**, **which stands in marked contrast to the true wide variability across the reference sites. These observations revealed that our proposed technique (and more generally the geostatistical technique) requires high spatial homogeneity in the pollutant concentrations to be fully effective.**"

Specific Comments:

Page 1, Lines 25-29: This is a very long and complex sentence; consider splitting in into several sentences and/or revising how the information is presented. For exam- ple: "Simulations conducted using our algorithm suggest that in addition to dynamic calibration, it can also be adapted to automated monitoring of WLPMSNs. In these simulations, the algorithm was able to differentiate malfunctioning or singular low-cost nodes by identifying aberrant model-generated calibration factors (i.e. slopes close to zero and intercepts close to the global mean of true PM2.5). The algorithm was also able to track the drift of low-cost nodes accurately within 4% error for all the simulation scenarios."

Response: Thank you, we have made the suggested revision to this sentence.

Modified text on Page 1, lines 25-29:

"**Simulations conducted using our algorithm suggest that in addition to dynamic calibration, the algorithm can also be adapted for automated monitoring of large-scale WLPMSNs. In these simulations, the algorithm was able to differentiate malfunctioning low-cost nodes (due to either hardware failure or under heavy influence of local sources) within a network by identifying aberrant model-generated calibration factors (i.e., slopes close to zero and intercepts close to the Delhi-wide mean of true $PM_{2.5}$). The algorithm was also able to track the drift of low-cost nodes accurately within 4 % error for all the simulation scenarios.**"

Page 1, Line 27: I am not clear on what is meant by a "singular" node.

Response: "Singular" node means an anomalous/abnormal node that reports signals that are spatially uncorrelated with other normal nodes within the network, due to under heavy influence of local sources. This echoes Section 3.3.1. The word "singular" was meant to differentiate the situation from sensor failure ("malfunctioning"). Given the confusion this word gives, we have removed "singular" throughout the manuscript. Instead, we have clarified that "malfunctioning" corresponds to two situations throughout the manuscript (i.e., sensor hardware failure and sensors under heavy influence of local sources).

Modified text on Page 1, lines 26-28:

"In these simulations, the algorithm was able to differentiate **malfunctioning low-cost nodes (due to either hardware failure or under heavy influence of local sources)** within a network by identifying aberrant model-generated calibration factors (i.e., slopes close to zero and intercepts close to the global mean of true $PM_{2.5}$)."

Modified text on Page 11, lines 2-4:

"These two observations indicate that the GPR model enables automated and streamlined process of instantly spotting any malfunctioning low-cost nodes **(due to either hardware failure or under heavy influence of local sources)** within a large-scale sensor network."

Modified text on Page 13, lines 30-32:

"Simulations proved our algorithm's capability of differentiating malfunctioning low-cost nodes **(due to either hardware failure or under heavy influence of local sources)** within a network and of tracking the drift of low-cost nodes accurately with less than 4 % errors for all the simulation scenarios."

Page 2, Line 14: I assume you mean "since the emergence of low-cost AQ sensors" Rather than "since the emergence of calibration-related issues". It might be better to state that.

Response: Thank you for pointing this out, we have revised the sentence accordingly.

Modified text on Page 2, line 14:

"On the down side, researchers have been plagued by calibration-related issues since **the emergence of low-cost AQ sensors.**"

Page 3, Line 10: These coordinates are likely too precise to denote the city of Delhi generally. It is probably sufficient here to just state "Delhi, India", rather than providing coordinates, unless you are trying to describe a specific location within the city.

Response: Thank you, we have removed the coordinates.

Modified text on Page 3, line 10:

"…collocation calibration by leveraging all available reference monitors across an area (e.g., **Delhi, India**)."

Page 3, Line 18: Rather than "drift nodes" I would say "the drift of nodes".

Response: Thank you, we have made the suggested change to wording.

Modified text on Page 3, line 18:

"…auto-detect the faulty and auto-correct **the drift of nodes** within a network via computational simulation, …"

Page 4: Line 15: Use "the" rather than "our".

Response: Thank you, we have made the suggested change

Modified text on Page 4, line 15:

"…KairosDB as **the** primary fast scalable time series database built on Apache Cassandra, …"

Page 5, Lines 6-7: It is not clear to me why the GPR model would require data from all stations to operate. If it is interpolating between stations then it should be able to fill in for any missing station data as well.

Response: The reviewer is correct. Mathematically, the GPR model would only require data from at least one reference monitoring station to operate. In this paper, the choice of attempting to interpolate all the stations' missing data first was made based on some practical reasons, specifically the speed of the algorithm/program. Theoretically, relying on GPR model to fill in for any missing station data is 59 (the number of daily-averaged data points) times slower. This theoretical upper bound is 59 because the algorithm will have to loop through each of the 59 days if each day's missing reference and low-cost nodes are different. And this process is relatively computationally expensive because it involves many matrix inversions. In reality, the algorithm with interpolating all the stations' missing data first takes ~10 mins to run 22 times (a complete leave-one-out process) while the algorithm without any interpolation takes ~200 mins to run 22 times. If a complete leave-one-out process takes 200 min to run, it will be nearly impossible to implement the simulation experiments shown in Section 3.3. We have now clarified our motivation for requiring data from all the stations to operate the GPR model in this paper.

Modified text on Page 5, lines 6–10:

"**While mathematically the GPR model can operate without requiring data from all the stations to be non-missing on each day by relying on the GPR model to fill in each day's missing station data, we practically required** concurrent measurements of all the stations **in this paper to drastically increase the speed of the algorithm (~10 mins to run a complete 22-fold leave-one-out CV, up to ~20 times faster) by avoiding the expensive computational cost of excessive amount of matrix inversion that can be incurred otherwise.** We linearly interpolated **the** $PM_{2.5}$ values for the hours with missing measurements for each station, after which we averaged the hourly data to daily resolution as the model inputs."

Page 5, Line 20: The meaning of "with that of after missing data imputation" is not clear.

Response: "with that of after missing data imputation" means "with 1 h $PM_{2.5}$'s completeness after missing data imputation". The whole sentence "The comparison of initial 1 h $PM_{2.5}$'s completeness with that of after missing data imputation for both reference and low-cost nodes is detailed in Table 1" means "The comparison between the initial 1 h $PM_{2.5}$'s completeness and the 1 h $PM_{2.5}$'s completeness after missing data imputation for both reference and low-cost nodes is detailed in Table 1". We have now revised the sentence to make its meaning clearer.

Modified text on Page 5, lines 20–21:

"**The comparison of 1 h $PM_{2.5}$'s completeness before and after** missing data imputation for both reference and low-cost nodes is detailed in Table 1 and…"

Page 5, Line 21: I don't know if "imputed" is the correct word to use here.

Response: Imputation just means replacing missing values with estimated values based on available information. Therefore, the word "imputed" seems reasonable to me.

Text remains unmodified.

Page 5, Line 29: Should be "while outliers have scores significantly larger than 1".

Response: Thank you, we have revised the sentence accordingly.

Modified text on Page 5, line 29:

"Normal observations tend to have LOF scores near 1 while outliers **have scores** significantly larger than 1."

Page 6, Line 19 to Page 7, Line 5: This description could be improved. In particular, it is not clear how the alpha and beta parameters of Equation 3 are determined. The description seems to combine a linear regression and a calibration of the hyperparam- eters of the Gaussian Process. These two steps should be described separately.

Response: We agree with the reviewer on that "how the alpha and beta parameters of Equation 3 are determined" should be more clearly described. The α_i and β_i parameters of Equation 3 were determined by fitting a simple linear regression model to all available pairs of daily $PM_{2.5}$ mass concentrations from the uncalibrated low-cost node i (independent variable) and its closest reference node (dependent variable). The α_i and β_i parameters are the slope and intercept of the fitted simple linear regression calibration model, respectively. As shown in Equation 3, the α_i and β_i calibration factors were then used to calibrate each low-cost node i to its closest reference node to bridge disagreements between low-cost and reference node measurements which led to a more consistent spatial interpolation and a faster convergence during model optimization. Therefore, "the linear regression step (called low-cost node initialization, corresponding to step 2 in Fig. 3, described on page 6, lines 19-23) and the training/optimization of the hyperparameters of the GPR model (corresponding to step 3 in Fig. 3, described on page 6, lines 23-29, starting from 'After standardizing')" were previously described separately. To better highlight this fact and in order to avoid confusion, we have now added additional details to the low-cost node initialization step, have split the descriptions of the two steps into two separate paragraphs, have re-organized the places of Equations 3-5, and have added additional texts to explain the terms in Equations 3-5.

Modified text from Page 6, line 19 to Page 7, line 5:

“What separates our method from standard GP applications is the simultaneous incorporation of calibration for the low-cost nodes using a simple linear regression model into the spatial model. Linear regression has previously been shown to be effective at calibrating PM sensors (Zheng et al., 2018). **Linear regression was first used to initialize low-cost nodes' calibrations (step two in Fig. 3). In this step**, each low-cost node $\boldsymbol{i}$ was **linearly** calibrated **to** its closest reference node **using Eq. (3), where the calibration factors $\boldsymbol{\alpha_i}$ (slope) and $\boldsymbol{\beta_i}$ (intercept) were determined by fitting a simple linear regression model to all available pairs of daily PM2.5 mass concentrations from the uncalibrated low-cost node $\boldsymbol{i}$ (independent variable) and its closest reference node (dependent variable). This step aims** to bridge disagreements between low-cost and reference node measurements**, which can lead** to a more consistent spatial interpolation and a faster convergence during the **GPR** model optimization.

$$\boldsymbol{r}_i = \begin{cases} \boldsymbol{y}_i, & \text{if reference node} \\ \alpha_i \cdot \boldsymbol{y}_i + \beta_i, & \text{if low} - \text{cost node} \end{cases} \tag{3}$$

where $\boldsymbol{y_i}$ **is either a vector of all the daily PM2.5 measurements of reference node $\boldsymbol{i}$ or a vector of all the daily raw PM2.5 signals of low-cost node $\boldsymbol{i}$**; $\boldsymbol{r_i}$ **is either a vector of all the daily PM2.5 measurements of reference node $\boldsymbol{i}$ or a vector of all the daily calibrated PM2.5 measurements of** low-cost node i; α_i and β_i are the slope and intercept, respectively, **determined from the fitted simple linear regression** calibration equation **with daily PM2.5 mass concentrations of the uncalibrated** low-cost node i **as independent variable and PM2.5 mass concentrations of low-cost node $\boldsymbol{i}$'s** closest reference node **as dependent variable**.

In the next step (step three in Fig. 3), a GPR model was fit to **each day $\boldsymbol{t}$'s** 31 nodes (i.e., 10 initialized low-cost nodes and 21 reference nodes) as described in Eq. (4). **Prior to the GPR model fitting, all the PM2.5 measurements of the 31 nodes over 59 valid days used for GPR model hyperparameters training were standardized. The standardization was performed by first concatenating all these training PM2.5 measurements (from the 31 nodes over 59 days), then** subtracting **their** mean $\mu_{training}$ and **dividing them by their standard deviation** $s_{training}$(i.e., transforming **all** the **training** PM2.5 measurements to have a zero mean and unit variance). **After the standardization of training samples,** the GPR was trained to maximize the log marginal likelihood over all 59 days **using Eq. 5 and** using an L-BFGS-B optimizer (Byrd et al., 1994). To avoid bad local minima, several random hyperparameter initializations were tried and the initialization **that resulted in** the **largest** log marginal likelihood **after optimization** was chosen **(in this paper, $\boldsymbol{\Theta = [\sigma_s^2, l, \sigma_n^2]}$ was initialized to [0.1, 50, 0.01]).**”

$$\boldsymbol{r}_t|\Gamma \sim N(\boldsymbol{\mu}, \boldsymbol{\Sigma}) \tag{4}$$

where $\boldsymbol{t}$ ranges from 1 (inclusive) to 59 (inclusive); $\boldsymbol{r_t} \in \mathbb{R}^{31}$ is a vector of all 31 nodes' PM2.5 measurements **(calibrated if low-cost nodes)** on day t; $\boldsymbol{\Gamma} = \{\boldsymbol{x_1}, \dots, \boldsymbol{x_{31}}\}$ **denotes 31 nodes' locations and $\boldsymbol{x_i} \in \mathbb{R}^2$ is a vector of the latitude and longitude of node $\boldsymbol{i}$; $\boldsymbol{\mu} \in \mathbb{R}^{31}$ represents the mean function (assumed to be 0 in this study) and $\boldsymbol{\Sigma} \in \mathbb{R}^{31\times31}$ with $\boldsymbol{\Sigma_{ij}} = \boldsymbol{K(x_i, x_j; \Theta)}$ represents the covariance function/kernel function.**

$$\arg\max_{\boldsymbol{\Theta}} L(\boldsymbol{\Theta}) = \arg\max_{\boldsymbol{\Theta}} \sum_{t=1}^{59} \log p(\boldsymbol{r}_t|\boldsymbol{\Theta}) \ = \arg\max_{\boldsymbol{\Theta}} \left(-0.5 \cdot 59 \cdot \log|\boldsymbol{\Sigma}_\theta| - 0.5 \sum_{t=1}^{59} \boldsymbol{r}_t{}^T \boldsymbol{\Sigma}_\theta^{-1} \boldsymbol{r}_t\right) \tag{5}$$

where $\boldsymbol{\Theta} \in \mathbb{R}^3$ is a vector of **the GPR hyperparameters** σ_s^2, l, and σ_n^2.”

Page 6, Lines 23-24: The process of “standardization” is not clear to me. If this is done separately for each node, wouldn’t this eliminate any systematic differences between measurement locations? If this step is only done to the data which are to be used for calibrating the model hyperparameters, then that should be stated. Even so, it is not clear that this is an appropriate step; for example, two node may be systematically higher than other locations, and so should have a mutual correlation, while if the means are subtracted, the data from the nodes would no longer be correlated (in other words, two variables can be made similar in a GP model either by giving them a high mutual correlation or by giving them a smaller prior variance and the same prior mean).

Response: We agree with the reviewer on that the standardization process should be more clearly described. First, the standardization was not done separately for each node. The original text (“After standardizing the PM$_{2.5}$ measurements for each node…”) did not describe the process accurately. All the PM$_{2.5}$ measurements of the 31 nodes over 59 valid days used for GPR model hyperparameters training were standardized at once. The standardization was performed by first concatenating all these training PM$_{2.5}$ measurements (from the 31 nodes over 59 days), then subtracting their mean $\mu_{training}$ and dividing them by their standard deviation $s_{training}$(i.e., transforming all the training PM$_{2.5}$ measurements to have a zero mean and unit variance). Therefore, the standardization done in this way will not eliminate any systematic differences between measurement locations. Second, the standardization was only done to the data used for training/optimizing the hyperparameters of the GPR model (i.e., all the PM$_{2.5}$ measurements of the 31 nodes over 59 valid days). The holdout node’s PM$_{2.5}$ measurements were never used to calculate the $\mu_{training}$ and $s_{training}$. Third, assuming the mean function $\boldsymbol{\mu} \in \mathbb{R}^{31}$ to be $\mathbf{0}$ in this study along with standardizing all the training stations’ PM$_{2.5}$ measurements to have a zero mean and unit variance is absolutely an appropriate step and will not destroy the correlations. The correlations can be learned from the covariance matrix. Assuming a same mean value for all the stations is one of the common modelling formulations on the GPR model and the simplest one. Alternative modelling formulations include a station-specific mean function (lack of prior information for this project), a time-dependent mean function (computationally expensive), and a combination of both. These relatively complex formulations were not considered for this paper.

Modified text on Page 6, lines 23-26:

“**In the next step (step three in Fig. 3)**, a GPR model was fit to **each day *t*’s** 31 nodes (i.e., 10 initialized low-cost nodes and 21 reference nodes) as described in Eq. (4). **Prior to the GPR model fitting, all the PM$_{2.5}$ measurements of the 31 nodes over 59 valid days used for GPR model hyperparameters training were standardized. The standardization was performed by first concatenating all these training PM$_{2.5}$ measurements (from the 31 nodes over 59 days), then** subtracting **their** mean $\mu_{training}$ and **dividing them by their standard deviation** $s_{training}$ (i.e., transforming **all** the **training** PM$_{2.5}$ measurements to have a zero mean and unit variance). **It is worth noting that assuming the mean function**

$\boldsymbol{\mu} \in \mathbb{R}^{31}$ to be 0 along with standardizing all the training PM2.5 samples in this study is one of the common modelling formulations on the GPR model and the simplest one. More complex formulations including a station-specific mean function (lack of prior information for this project), a time-dependent mean function (computationally expensive), and a combination of both were not considered for this paper. After the standardization of training samples, the GPR was trained to maximize the log marginal likelihood over all 59 days **using Eq. 5 and** using an L-BFGS-B optimizer (Byrd et al., 1994)."

Equation 4: What is Gamma?

Response: Gamma, $\Gamma = \{x_1, \ldots, x_{31}\}$, denotes 31 nodes' locations and $x_i \in \mathbb{R}^2$ is a vector of the latitude and longitude of node *i.* This was originally stated on page 6, lines 5-6. We have now also added the description of the Γ term to Equation 4.

Modified Equation 4:

"$$\boldsymbol{r}_t | \Gamma \sim N(\boldsymbol{\mu}, \boldsymbol{\Sigma}) \tag{4}$$

where t ranges from 1 (inclusive) to 59 (inclusive); $\boldsymbol{r_t} \in \mathbb{R}^{31}$ is a vector of all 31 nodes' PM2.5 measurements **(calibrated if low-cost nodes)** on day t; **$\boldsymbol{\Gamma} = \{\boldsymbol{x_1}, \ldots, \boldsymbol{x_{31}}\}$ denotes 31 nodes' locations and $\boldsymbol{x_i} \in \mathbb{R}^2$ is a vector of the latitude and longitude of node i; $\boldsymbol{\mu} \in \mathbb{R}^{31}$ represents the mean function (assumed to be 0 in this study) and $\boldsymbol{\Sigma} \in \mathbb{R}^{31\times31}$ with $\boldsymbol{\Sigma_{ij}} = \boldsymbol{K}(\boldsymbol{x_i}, \boldsymbol{x_j}; \boldsymbol{\Theta})$ represents the covariance function/kernel function.**"

Page 7, line 7: What does the bold-face Theta denote? Are these the hyperparameters of the GP model as described in Equation 2?

Response: The bold-face Theta ($\boldsymbol{\Theta} \in \mathbb{R}^3$) denotes the vector of the GPR hyperparameters σ_s^2, l, and σ_n^2. This was originally stated in Equation 5. Yes, these are the same hyperparameters of the GPR model as described in Equation 2. Thank you for pointing out the discrepancy in the Theta notation between Equations 2 and 5. We have now changed the Theta notation in both Equations 1 and 2 to bold-face Theta ($\boldsymbol{\Theta} \in \mathbb{R}^3$).

Modified Equation 1:

"$$\boldsymbol{y}_t | \Gamma \sim N(\boldsymbol{\mu}, \boldsymbol{\Sigma}) \tag{1}$$

where $\boldsymbol{\mu} \in \mathbb{R}^{31}$ represents the mean function (assumed to be $\boldsymbol{0}$ in this study)**;** $\boldsymbol{\Sigma} \in \mathbb{R}^{31\times31}$ with $\Sigma_{ij} = K(\boldsymbol{x}_i, \boldsymbol{x}_j; \boldsymbol{\Theta})$ represents the covariance function/kernel function and **$\boldsymbol{\Theta}$ is a vector of the GPR hyperparameters.**"

Modified Equation 2:

"$$K(\boldsymbol{x}_i, \boldsymbol{x}_j; \boldsymbol{\Theta}) = \sigma_s^2\, exp\left(-\frac{\|x_i - x_j\|_2^2}{2l^2}\right) + \sigma_n^2 \boldsymbol{I} \quad \text{(Rasmussen and Williams, 2006)} \tag{2}$$

where σ_s^2, l, and σ_n^2 are the model hyperparameters (to be optimized) that control the signal magnitude, characteristic length-scale, and noise magnitude, respectively**; $\boldsymbol{\Theta} \in \mathbb{R}^3$ is a vector of the GPR hyperparameters $\boldsymbol{\sigma_s^2}$, $\boldsymbol{l}$, and $\boldsymbol{\sigma_n^2}$.**"

Page 7, Lines 10-11: It is not clear what it means to re-calibrate a node based on its posterior mean. I am assuming this involves adjusting the alpha and beta parameters, but this is not clear.

Response: We agree with the reviewer on that not enough details were provided to fully clarify what it means to re-calibrate a low-cost node based on its conditional mean. But the reviewer's assumption is correct. "Re-calibrating a low-cost node based on its conditional mean" just means first fitting a simple linear regression model to all 59 pairs of daily $PM_{2.5}$ mass concentrations from the uncalibrated low-cost node *i* ($\boldsymbol{y_i}$, independent variable) and its conditional mean ($\boldsymbol{\mu_{A|B}^i}$, dependent variable) and then using this newly fitted simple linear regression calibration model to calibrate the low-cost node *i* again. As the reviewer said, this is essentially adjusting/updating the calibration factors α_i (slope) and β_i (intercept) in Equation 3. This step is also the "simple linear regression" step of the entire "simultaneous GPR and simple linear regression" algorithm. We have now added additional descriptions to clarify this process.

Modified text on Page 7, lines 8-11:

"Once the optimum $\boldsymbol{\Theta}$ for the (initial) GPR was found, we used the learned covariance function to find the mean of each low-cost node i's Gaussian Distribution conditional on the remaining 30 nodes within the network (i.e., $\mu_{A|B}^{it}$) on day *t* as described mathematically in Eq. (6)–(8) and repeatedly did so until all 59 days' $\mu_{A|B}^{it}$ (i.e., $\boldsymbol{\mu_{A|B}^i} \in \mathbb{R}^{\mathbf{59}}$) were found and then re-calibrated that low-cost node *i* based on the $\boldsymbol{\mu_{A|B}^i}$. **The re-calibration was done by first fitting a simple linear regression model to all 59 pairs of daily $PM_{2.5}$ mass concentrations from the uncalibrated low-cost node *i* ($\boldsymbol{y_i}$, independent variable) and its conditional mean ($\boldsymbol{\mu_{A|B}^i}$, dependent variable) and then using the updated calibration factors (slope $\boldsymbol{\alpha_i}$ and intercept $\boldsymbol{\beta_i}$) obtained from this newly fitted simple linear regression calibration model to calibrate the low-cost node *i* again (using Eq. 3).**"

Page 7, Line 29: What criteria are used for convergence?

Response: The criteria used for convergence are the differences in all the GPR hyperparameters between the two adjacent runs below 0.01 (i.e., with $\Delta\sigma_s^2 \leq 0.01, \Delta l \leq 0.01, and\ \Delta\sigma_n^2 \leq 0.01$).

Modified text on Page 7, line 29:

"…until the GPR parameters $\boldsymbol{\Theta}$ converged **with the convergence criteria being the differences in all the GPR hyperparameters between the two adjacent runs below 0.01 (i.e., with $\boldsymbol{\Delta\sigma_s^2 \leq 0.01, \Delta l \leq 0.01, and\ \Delta\sigma_n^2 \leq 0.01}$).**"

Page 7, Line 31: This relates to a previous comment, I believe, but it should be de- scribed how the predictions are transformed back into the original PM scale.

Response: We agree that how the back transformation of the predictions was done should be more clearly described. Since standardization is just linear transformation, back transformation is relatively simple. The predictions were transformed back by multiplying the standard deviation $s_{training}$ (the standard deviation of the training $PM_{2.5}$ measurements) and then adding back the mean $\mu_{training}$ (the mean of the training $PM_{2.5}$ measurements).

Modified text on Page 7, line 31:

"…with the standardized predictions being transformed back to the original $PM_{2.5}$ measurement scale at the end. **The back transformation was done by multiplying the predictions by the standard deviation $s_{training}$ (the standard deviation of the training $PM_{2.5}$ measurements) and then adding back the mean $\mu_{training}$ (the mean of the training $PM_{2.5}$ measurements).**"

Page 9, Lines 10-12: This sentence can be better written as ". . .the reference node mapping accuracy follows a pattern, with relatively high quality prediction for those nodes whose means are close to the global mean (e.g., global mean ± SD as highlighted with shading in Table 2) and relatively poor prediction for those nodes whose means differ substantially from the global mean (particularly on the lower end)".

Response: We appreciate the suggestion and have revised the sentence accordingly.

Modified text on Page 9, lines 10-12:

". . .the reference node mapping accuracy follows a pattern**,** with relatively **high-quality** prediction for those nodes whose means **were** close to the **Delhi-wide** mean (e.g., **Delhi-wide** mean ± SD as highlighted with shading in Table 2) **and** relatively poor prediction for **those nodes whose means differed substantially from** the **Delhi-wide** mean (particularly **on** the lower end)."

Page 9, Line 21: It is unclear what the "scale of 10" refers to.

Response: The "scale of 10" refers to the number of the low-cost nodes within the network is 10. We have now clarified this.

Modified text on Page 9, line 21:

"While only a marginal improvement **with 10 low-cost nodes in the network**, …"

Page 12, Line 4: It is unclear what "quality drift estimation" is.

Response: "quality drift estimation" means "high-quality drift estimation".

Modified text on Page 12, line 4:

"The **high-quality** drift estimation has therefore presented another convincing case …"

Page 12, Line 11: This should be "Questions which remain unsolved".

Response: Thank you for pointing this out. We have now corrected it.

Modified text on Page 12, line 11:

"Questions **which** remain unsolved are …"

Page 13, Lines 24-27: The end of this sentence may be incomplete.

Response: The sentence on Page 13, lines 21-27 is complete but very long and complex, which has caused confusion. We have now split it into several sentences.

Modified text on Page 13, lines 21-27:

"**We closely investigated** into 1) the large model calibration errors (~50 %) at two Atmos regional background sites (3-month mean $PM_{2.5}$: ~72 μg m^{-3}) where our E-BAMs were collocated; 2) the similarly large model prediction errors at the comparatively clean Pusa and Sector 62 reference sites; **and** 3) the washed-out local variability in the model calibrated low-cost sites**. These observations** revealed that the performance of our technique (and more generally the geostatistical techniques) can calibrate the low-cost nodes dynamically, but effective only if the degree of urban homogeneity in $PM_{2.5}$ is high. **High urban homogeneity scenarios can be that** the local contributions are as small a fraction of the regional ones as possible or the local contributions are prevalent but of similar magnitudes."

Page 13, Line 31: Again, it is not clear what is meant by a singular node.

Response: This was addressed previously. "Singular" node means an anomalous/abnormal node that reports signals that are spatially uncorrelated with other normal nodes within the network, due to under heavy influence of local sources. This echoes Section 3.3.1. The word "singular" was meant to differentiate the situation from sensor failure ("malfunctioning"). Given the confusion this word gives, we have removed "singular" throughout the manuscript. Instead, we have clarified that "malfunctioning" corresponds to two situations throughout the manuscript (i.e., sensor hardware failure and sensors under heavy influence of local sources).

Modified text on Page 13, lines 30-32:

"Simulations proved our algorithm's capability of differentiating malfunctioning low-cost nodes **(due to either hardware failure or under heavy influence of local sources)** within a network and of tracking the drift of low-cost nodes accurately with less than 4 % errors for all the simulation scenarios."

Gaussian Process regression model for dynamically calibrating and surveilling a wireless low-cost particulate matter sensor network in Delhi

Tongshu Zheng[1], Michael H. Bergin[1], Ronak Sutaria[2], Sachchida N. Tripathi[3], Robert Caldow[4], David E. Carlson[1,5]

[1]Department of Civil and Environmental Engineering, Duke University, Durham, NC 27708, USA
[2]Respirer Living Sciences Pvt. Ltd, 7, Maheshwar Nivas, Tilak Road, Santacruz (W), Mumbai 400054, India
[3]Department of Civil Engineering, Indian Institute of Technology Kanpur, Kanpur, Uttar Pradesh 208016, India
[4]TSI Inc., 500 Cardigan Road, Shoreview, MN 55126, USA
[5]Department of Biostatistics and Bioinformatics, Duke University, Durham, NC 27708, USA

Correspondence to: Tongshu Zheng (tongshu.zheng@duke.edu)

Abstract. Wireless low-cost particulate matter sensor networks (WLPMSNs) are transforming air quality monitoring by providing PM information at finer spatial and temporal resolutions; however, large-scale WLPMSN calibration and maintenance remain a challenge because the manual labor involved in initial calibration by collocation and routine recalibration is intensive, the transferability of the calibration models determined from initial collocation to new deployment sites is questionable as calibration factors typically vary with urban heterogeneity of operating conditions and aerosol optical properties, and the stability of low-cost sensors can ~~develop~~ drift or degrade over time. This study presents a simultaneous Gaussian Process regression (GPR) and simple linear regression pipeline to calibrate and monitor dense WLPMSNs on the fly by leveraging all available reference monitors across an area without resorting to pre-deployment collocation calibration. We evaluated our method for Delhi where the $PM_{2.5}$ measurements of all 22 regulatory reference and 10 low-cost nodes were available in 59 valid days from January 1, 2018 to March 31, 2018 ($PM_{2.5}$ averaged 138 ± 31 μg m^{-3} among 22 reference stations) using a leave-one-out cross-validation (CV) over the 22 reference nodes. We showed that our approach can achieve an overall 30 % prediction error (RMSE: 33 μg m^{-3}) at a 24 h scale and is robust as underscored by the small variability in the GPR model parameters and in the model-produced calibration factors for the low-cost nodes among the 22-fold CV. ~~We revealed that the accuracy of our calibrations depends on the degree of homogeneity of PM concentrations, and decreases with increasing local source contributions.~~ Of the 22 reference stations, high-quality predictions were observed for those stations whose $PM_{2.5}$ means were close to the Delhi-wide mean (i.e., 138 ± 31 μg m^{-3}) and relatively poor predictions for those nodes whose means differed substantially from the Delhi-wide mean (particularly on the lower end). We also observed washed-out local variability in $PM_{2.5}$ across the 10 low-cost sites after calibration using our approach, which stands in marked contrast to the true wide variability across the reference sites. These observations revealed that our proposed technique (and more generally the geostatistical technique) requires high spatial homogeneity in the pollutant concentrations to be fully effective. We further demonstrated that our algorithm performance is insensitive to training window size as the mean prediction error rate and the standard error of the mean (SEM) for the 22 reference stations remained consistent at ~30 %

and ~3–4 % when an increment of 2 days' data were included in the model training. The markedly low requirement of our algorithm for training data enables the models to always be nearly most updated in the field, thus realizing the algorithm's full potential for dynamically surveilling large-scale WLPMSNs by detecting malfunctioning low-cost nodes and tracking the drift with little latency. Our algorithm presented similarly stable 26–34 % mean prediction errors and ~3–7 % SEMs over the sampling period when pre-trained on the current week's data and predicting 1 week ahead, therefore suitable for online calibration. ~~As by-products of dynamic calibration, our algorithm can be adapted for automated large-scale WLPMSN monitoring as simulations proved its capability of differentiating malfunctioning or singular low-cost nodes within a network via model-generated calibration factors with the aberrant nodes having slopes close to 0 and intercepts close to the global mean of true $PM_{2.5}$ and of tracking the drift of low-cost nodes accurately within 4 % error for all the simulation scenarios.~~ Simulations conducted using our algorithm suggest that in addition to dynamic calibration, the algorithm can also be adapted for automated monitoring of large-scale WLPMSNs. In these simulations, the algorithm was able to differentiate malfunctioning low-cost nodes (due to either hardware failure or under heavy influence of local sources) within a network by identifying aberrant model-generated calibration factors (i.e., slopes close to zero and intercepts close to the Delhi-wide mean of true $PM_{2.5}$). The algorithm was also able to track the drift of low-cost nodes accurately within 4 % error for all the simulation scenarios. The simulation results showed that ~20 reference stations are optimum for our solution in Delhi and confirmed that low-cost nodes can extend the spatial precision of a network by decreasing the extent of pure interpolation among only reference stations. Our solution has substantial implications in reducing the amount of manual labor for the calibration and surveillance of extensive WLPMSNs, improving the spatial comprehensiveness of PM evaluation, and enhancing the accuracy of WLPMSNs.

1 Introduction

Low-cost air quality (AQ) sensors that report high time resolution data (e.g., ≤ 1 h) in near real time offer excellent potential for supplementing existing regulatory AQ monitoring networks by providing enhanced estimates of the spatial and temporal variabilities of air pollutants (Snyder et al., 2013). Certain low-cost particulate matter (PM) sensors demonstrated satisfactory performance benchmarked against Federal Equivalent Methods (FEMs) or research-grade instruments in some previous field studies (Holstius et al., 2014; Gao et al., 2015; SCAQMD, 2015a–b; Jiao et al., 2016; Kelly et al., 2017; Mukherjee et al., 2017; SCAQMD, 2017a–c; Crilley et al., 2018; Feinberg et al., 2018; Johnson et al., 2018; Zheng et al., 2018). Application-wise, low-cost PM sensors have had success in identifying urban fine particle ($PM_{2.5}$, with a diameter of 2.5 μm and smaller) hotspots in Xi'an, China (Gao et al., 2015), mapping urban air quality with additional dispersion model information in Oslo, Norway (Schneider et al., 2017), monitoring smoke from prescribed fire in Colorado, US (Kelleher et al., 2018), measuring a traveler's exposure to $PM_{2.5}$ in various microenvironments in Southeast Asia (Ozler et al., 2018), and building up a detailed city-wide temporal and spatial indoor $PM_{2.5}$ exposure profile in Beijing, China (Zuo et al., 2018).

On the down side, researchers have been plagued by calibration-related issues since ~~their~~ the emergence of low-cost AQ sensors. One common brute force solution is initial calibration by collocation with reference analyzers before field deployment and follow-up routine recalibration. Yet, the transferability of these pre-determined calibrations at collocation sites to new deployment sites is questionable as calibration factors typically vary with operating conditions such as PM mass concentrations, relative humidity, temperature, and aerosol optical properties (Holstius et al., 2014; Austin et al., 2015; Wang et al., 2015; Lewis and Edwards, 2016; Crilley et al., 2018; Jayaratne et al., 2018; Zheng et al., 2018). Complicating this further, the pre-generated calibration curves may only apply for a short term as the stability of low-cost sensors can develop drift or degrade over time (Lewis and Edwards, 2016; Jiao et al., 2016; Hagler et al., 2018). Routine recalibrations which require frequent transit of the deployed sensors between the field and the reference sites are not only too labor intensive for a large-scale network but also still cannot address the impact of urban heterogeneity of ambient conditions on calibration models (Kizel et al., 2018).

As such, calibrating sensors on-the-fly while they are deployed in the field is highly desirable. Takruri et al. (2009) showed that the Interacting Multiple Model (IMM) algorithm combined with the Support Vector Regression (SVR)-Unscented Kalman Filter (UKF) can automatically and successfully detect and correct low-cost sensor measurement errors in the field; however, the implementation of this algorithm still requires pre-deployment calibrations. Fishbain and Moreno-Centeno (2016) designed a self-calibration strategy for low-cost nodes with no need for collocation by exploiting the raw signal differences between all possible pairs of nodes. The learned calibrated measurements are the vectors whose pairwise differences are closest in normalized projected Cook-Kress (NPCK) distance to the corresponding pairwise raw signal differences given all possible pairs over all time steps. However, this strategy did not include reference measurements in the self-calibration procedure, and therefore the tuned measurements were still essentially raw signals (although instrument noise was dampened). An alternative calibration method involves chain calibration of the low-cost nodes in the field with only the first node calibrated by collocation with reference analyzers and the remaining nodes calibrated sequentially by their respective previous node along the chain (Kizel et al., 2018). While this node-to-node calibration procedure proved its merits in reducing collocation burden and data loss during calibration/relocation/recalibration and accommodating the influence of urban heterogeneity on calibration models, it is only suitable for relatively small networks because calibration errors propagate through chains and can inflate toward the end of a long chain (Kizel et al., 2018).

In this paper, we introduce a simultaneous Gaussian Process regression (GPR) and simple linear regression pipeline to calibrate $PM_{2.5}$ readings of any number of low-cost PM sensors on the fly in the field without resorting to pre-deployment collocation calibration by leveraging all available reference monitors across an area (e.g., Delhi, India ~~N 28.6139, E 77.2089~~). The proposed strategy is theoretically sound since the GPR (also known as Kriging) can capture the spatial covariance inherent in the data and has been widely used for spatial data interpolation (e.g., Holdaway, 1996; Di et al., 2016; Schneider et al., 2017) and the simple linear regression calibration can adjust for disagreements between low-cost sensor and reference instrument measurements and lead to more consistent spatial interpolation. This paper focuses on 1) quantifying experimentally the daily performance of our dynamic calibration model in Delhi during winter season based on model prediction accuracy on the holdout reference nodes during leave-one-out cross-validations (CV) and low-cost node calibration accuracy; 2) revealing the potential pitfalls of employing a dynamic calibration algorithm; 3) examining the sensitivity of our algorithm to the training data size and the feasibility of it for dynamic calibration; ~~3~~4) demonstrating the ability of our algorithm to auto-detect the faulty and auto-correct the drift of nodes within a network via computational simulation, therefore the practicality of adapting our algorithm for automated large-scale sensor network monitoring; and ~~4~~5) studying computationally the optimal number of reference stations across Delhi to support our technique and the usefulness of low-cost sensors for extending the spatial precision of a sensor network. To the best of our knowledge, this is the first study to apply such a non-static calibration technique to a wireless low-cost PM sensor network in a heavily polluted region such as India and the first to present methods of auto-monitoring dense AQ sensor networks.

2 Materials and methods

2.1 Low-cost node configuration

The low-cost packages used in the present study (dubbed "Atmos") shown in Fig. 1a were developed by Respirer Living Sciences (http://atmos.urbansciences.in/, last access: 30 November 2018) and cost ~ USD 300 per unit. The Atmos monitor measures 20.3 cm L × 12.1 cm W × 7.6 cm H, weighs 500 g, and is housed in an IP65 (Ingress Protection rating 65) enclosure with a liquid crystal display (LCD) on the front showing real-time PM mass concentrations and various debugging messages. It includes a Plantower PMS7003 sensor (~ USD 25; dimension: 4.8 cm L × 3.7 cm W × 1.2 cm H) to measure PM$_1$, PM$_{2.5}$, and PM$_{10}$ mass concentrations, an Adafruit DHT22 sensor to measure temperature and relative humidity, and an ultra-compact Quectel L80 GPS model to retrieve accurate locations in real time. The operating principle and configuration of PMS7003 are similar to its PMS1003, PMS3003, and PMS5003 counterparts and have been extensively discussed in previous studies (Kelly et al., 2017; Zheng et al., 2018; and Sayahi et al., 2018, respectively). The inlet and outlet of PMS7003 were aligned with two slots on the box to ensure unrestricted airflow into the sensor. The PM and meteorology data are read over the serial TTL interface every three seconds, aggregated every 1 min in memory on the device, before being transmitted by a Quectel M66 GPRS module through the mobile 2G cellular network to an online database. The Atmos can also store the data on a local microSD card in case of transmission failure. Users have the option to configure the frequencies of data transfer and logging to 5, 10, 15, 30, and 60 minutes via a press key on the device and are able to view the settings on the LCD. All components of the Atmos monitors (key parts are labelled in Fig. 1b) are integrated to a custom-designed printed circuit board (PCB) which is controlled by a STMicroelectronics microcontroller (model STM32F051). Each Atmos was continuously powered up by a 5V 2A USB wall charger but also comes with a fail-safe 3.7V–2600 mAh rechargeable Li-ion battery in case of power outage that can last up to 10 hours at a 1 min transmission frequency and 20 hours at a 5 min frequency.

The Atmos network's server architecture was also developed by Respirer Living Sciences and built on the following open-source components: KairosDB as ~~our~~ the primary fast scalable time series database built on Apache Cassandra, custom-made Java libraries for ingesting data and for providing XML/JSON/CSV-based access to aggregated time series data, HTML5/JavaScript for creating the front-end dashboard, and LeafletJS for visualizing Atmos networks on maps.

2.2 Data description

2.2.1 Reference $PM_{2.5}$ data

Hourly ground-level $PM_{2.5}$ concentrations from 21 monitoring stations operated by the Central Pollution Control Board (CPCB), the Delhi Pollution Control Committee (DPCC), the India Meteorological Department (IMD), and the Uttar Pradesh and Haryana States Pollution Control Boards (SPCBs) (https://app.cpcbccr.com/ccr/#/caaqm-dashboard/caaqm-landing, last access: 18 September 2018) and from one monitoring station operated by the U.S. Embassy in New Delhi (https://www.airnow.gov/index.cfm?action=airnow.global_summary#India$New_Delhi, last access: 18 September 2018) were available in our study domain of Delhi and its satellite cities including Gurgaon, Faridabad, Noida, and Ghaziabad from January 1, 2018 to March 31, 2018 (winter season) and were used as the reference measurements in our Delhi PM sensor network. The topographical, climatic, and air quality conditions of Delhi are well documented by Tiwari et al. (2012 and 2015) and Gorai et al. (2018). Briefly, Delhi experiences unusually high $PM_{2.5}$ concentrations over winter season due to a combination of increased biomass burning for heating, shallower boundary layer mixing height, diminished wet scavenging by precipitation, lower wind speed, and trapping of air pollutants by the Himalayan topology. Figure 2 visualizes the spatial distribution of these 22 reference monitors (red icons) and Table 1 lists their latitudes and longitudes. No station of the 22 reference monitors is known for regional background monitoring. The complex local built environment in Delhi arising from the densely and intensively mixed land use (Tiwari, 2002) and the significant contributions to air pollution from all vehicular, industrial (small scale industries and major power plants), commercial (diesel generators and tandoors), and residential (diesel generators and biomass burning) sectors (CPCB, 2009; Gorai et al., 2018) render the $PM_{2.5}$ concentrations relatively unconnected to the land-use patterns. We removed 104 1 h observations (labeled invalid and missing) from the U.S. Embassy dataset based on its reported QA/QC (quality assurance/quality control) remarks; however, the same procedure was not applied to the remaining 21 Indian government monitoring stations due to lack of relevant information. While mathematically the GPR model can operate without requiring data from all the stations to be non-missing on each day by relying on the GPR model to fill in each day's missing station data, we practically required concurrent measurements of all the stations in this paper to drastically increase the speed of the algorithm (~10 mins to run a complete 22-fold leave-one-out CV, up to ~20 times faster) by avoiding the expensive computational cost of excessive amount of matrix inversion that can be incurred otherwise. ~~GPR requires concurrent measurements of all the stations~~ . ~~but certain stations had a high fraction of missing values. Therefore, to maximize the number of complete concurrent observations for modelling in order to~~

~~significantly increase the model accuracy, we~~ We linearly interpolated the $PM_{2.5}$ values for the hours with missing measurements for each station, after which we averaged the hourly data to daily resolution as the model inputs.

2.2.2 Low-cost node $PM_{2.5}$ data

Hourly uncalibrated $PM_{2.5}$ measurements from 10 Atmos low-cost nodes across Delhi between January 1, 2018 and March 31, 2018 were downloaded using our custom-designed Application Program Interface (API). Figure 2 shows the sampling locations of these 10 low-cost nodes as blue icons and Table 1 specifies their latitudes and longitudes. In our current study, the factors governing the siting of these nodes consist of the ground contact personnel availability, the resource availability such as strong mobile network signal and 24/7 main power supply, the location physical accessibility, and some other common criteria for sensor deployment (e.g., locations away from major pollution sources, situated in a place where free flow of air is available, and protected from vandalism and extreme weather). Similar to the preprocessing of the reference $PM_{2.5}$ data, we linearly interpolated the missing hourly $PM_{2.5}$ for each low-cost node and then aggregated the hourly data at a daily interval. The comparison of ~~initial~~ 1 h $PM_{2.5}$'s completeness ~~with that of~~ before and after missing data imputation for both reference and low-cost nodes is detailed in Table 1 and the periods over which data were imputed for each site are illustrated in Fig. S1. To remove the prospective outliers such as erroneous surges/nadirs existing in the datasets of the 21 Indian government reference nodes and the 10 low-cost nodes or unreasonable interpolated measurements introduced during handling the missing data, we employed the Local Outlier Factor (LOF) algorithm with 20 neighbors considered (a number that works well in general) to remove a conservative ~10% of the 32-dimensional (22 reference + 10 low-cost nodes) 24 h $PM_{2.5}$ datasets. LOF is an unsupervised anomaly detection method that assigns each multi-dimensional data point an LOF score, defined as the ratio of the average local density of its k nearest neighboring data points (k = 20 in our study) to its own local density, to measure the relative degree of isolation of the given data point with respect to its neighbors (Breunig, et al., 2000). Normal observations tend to have LOF scores near 1 while outliers have scores significantly larger than 1. The LOF therefore identifies the outliers as those multi-dimensional observations with the top x% (x = 10 in our study) LOF scores. A total of 59 days' $PM_{2.5}$ measurements common to all 32 nodes in the network were left (see Fig. S1) and used for our model evaluation.

2.3 Simultaneous GPR and simple linear regression calibration model

~~Figure 3 shows the overall schema for the simultaneous GPR and simple linear regression dynamic calibration model.~~ The simultaneous GPR and simple linear regression calibration algorithm is introduced here as Algorithm 1. The critical steps of the algorithm are linked to sub-sections under which the respective details can be found. Complementing Algorithm 1, a flow diagram illustrating the algorithm is given in Figure 3.

Algorithm 1: Algorithm of simultaneous GPR and simple linear regression

```
for each reference node (denote: Ref_k) in the network do
    leave Ref_k out as test sample (see Sect. 2.3.1 for details)
    for each low-cost node (denote: Low-cost_i) in the network do
        find Low-cost_i's closest reference node (denote: Ref_i) (Sect. 2.3.2)
        fit a simple linear regression model between Ref_i and Low-cost_i's PM2.5: $\boldsymbol{Ref_i} = \alpha_i \cdot \boldsymbol{Low-cost_i} + \beta_i$ (Sect. 2.3.2)
        initialize the simple linear regression calibration factors to $\alpha_i$ (slope) and $\beta_i$ (intercept) for Low-cost_i (Sect. 2.3.2)
        initialize the calibration of Low-cost_i using $\alpha_i$ and $\beta_i$ (Sect. 2.3.2)
    end for
    initialize GPR hyperparameters $\boldsymbol{\Theta} = [\sigma_s^2, l, \sigma_n^2]$ to [0.1, 50, 0.01] (Sect. 2.3.3)
    standardize the 10 calibrated low-cost and 21 reference nodes at once (Sect. 2.3.3)
    while convergence criteria not met do
        update/optimize GPR hyperparameters $\boldsymbol{\Theta}$ using the 31 standardized training nodes (Sect. 2.3.3 and .5)
        for each low-cost node (denote: Low-cost_i) in the network do
            for each day (denote: t) of the 59 days do
                calculate Low-cost_i's mean conditional on the remaining 30 nodes on day t (denote $\mu_{A|B}^{it}$) (Sect. 2.3.4 and .5)
            end for
            fit a linear regression between $\boldsymbol{\mu}_{A|B}^{i} \in \mathbb{R}^{59}$ and Low-cost_i: $\boldsymbol{\mu}_{A|B}^{i} = \alpha_i \cdot \boldsymbol{Low-cost_i} + \beta_i$ (Sect. 2.3.4 and .5)
            update calibration factors $\alpha_i$ and $\beta_i$ for Low-cost_i (Sect. 2.3.4 and .5)
            update the calibration of Low-cost_i using $\alpha_i$ and $\beta_i$ (Sect. 2.3.4 and .5)
        end for
        check convergence criteria (Sect. 2.3.5)
    end while
    use the final GPR model to predict on Ref_k (Sect. 2.3.6)
    transform the prediction back to original PM2.5 scale (Sect. 2.3.6)
    calculate RMSE and percent error (Sect. 2.3.6)
end for
```

2.3.1 Leave one reference node out

~~Under the context of not knowing beforehand~~Because the true calibration factors for the low-cost nodes are not known beforehand, a leave-one-out CV approach (i.e., holding one of the 22 reference nodes out of modelling each run for model predictive performance evaluation) was adopted as a surrogate to estimate our proposed model accuracy of calibrating the low-cost nodes. For each of the 22-fold CV, 31 node locations (denoted $\Gamma = \{\boldsymbol{x}_1, \dots, \boldsymbol{x}_{31}\}$) were available, where $\boldsymbol{x}_i$ is the latitude and longitude of node i. Let y_{it} represent the daily PM$_{2.5}$ measurement of node i on day t and $\boldsymbol{y}_t \in \mathbb{R}^{31}$ denote the concatenation of the daily PM2.5 measurements recorded by the 31 nodes on day t. Given a finite number of node locations, a Gaussian Process (GP) becomes a Multivariate Gaussian Distribution over the nodes in the form of:

$$\boldsymbol{y}_t|\Gamma \sim N(\boldsymbol{\mu}, \boldsymbol{\Sigma}) \tag{1}$$

where $\boldsymbol{\mu} \in \mathbb{R}^{31}$ represents the mean function (assumed to be $\mathbf{0}$ in this study); ~~and~~ $\boldsymbol{\Sigma} \in \mathbb{R}^{31\times31}$ with $\Sigma_{ij} = K\left(\boldsymbol{x}_i, \boldsymbol{x}_j; \boldsymbol{\Theta}$~~$\theta$~~$\right)$ represents the covariance function/kernel function and $\boldsymbol{\Theta}$ is a vector of the GPR hyperparameters.

For simplicity's sake, the kernel function was set to a squared exponential (SE) covariance term to capture the spatially-correlated signals coupled with another component to constrain the independent noise:

$$K\left(\boldsymbol{x}_i, \boldsymbol{x}_j; \boldsymbol{\Theta}\cancel{\theta}\right) = \sigma_s^2\, exp\left(-\frac{\left\|x_i - x_j\right\|_2^2}{2l^2}\right) + \sigma_n^2 \boldsymbol{I} \text{ (Rasmussen and Williams, 2006)} \tag{2}$$

where σ_s^2, l, and σ_n^2 are the model hyperparameters (to be optimized) that control the signal magnitude, characteristic length-scale, and noise magnitude, respectively; $\boldsymbol{\Theta} \in \mathbb{R}^3$ is a vector of the GPR hyperparameters σ_s^2, l, and σ_n^2~~.~~

2.3.2 Initialize low-cost nodes' (simple linear regression) calibrations

What separates our method from standard GP applications is the simultaneous incorporation of calibration for the low-cost nodes using a simple linear regression model into the spatial model. Linear regression has previously been shown to be effective at calibrating PM sensors (Zheng et al., 2018). Linear regression was first used to initialize low-cost nodes' calibrations (step two in Fig. 3). In this step~~Initially (step two in Fig. 3)~~, each low-cost node i was linearly calibrated ~~based on~~to its closest reference node using ~~(~~Eq. 3~~)~~, where the calibration factors α_i (slope) and β_i (intercept) were determined by fitting a simple linear regression model to all available pairs of daily PM2.5 mass concentrations from the uncalibrated low-cost node i (independent variable) and its closest reference node (dependent variable). This step aims to bridge disagreements between low-cost and reference node measurements, which can ~~led~~ lead to a more consistent spatial interpolation and a faster convergence during the GPR model optimization.

$$\boldsymbol{r}_i = \begin{cases} \boldsymbol{y}_i, & \text{if reference node} \\ \alpha_i \cdot \boldsymbol{y}_i + \beta_i, & \text{if low} - \text{cost node} \end{cases} \tag{3}$$

where $\boldsymbol{y_i}$ is either a vector of all the daily PM2.5 measurements of reference node i or a vector of all the daily raw PM2.5 signals of low-cost node i; $\boldsymbol{r_i}$ is either a vector of all the daily PM2.5 measurements of reference node i or a vector of all the daily calibrated PM2.5 measurements of low-cost node i; α_i and β_i are the slope and intercept, respectively, determined from the fitted simple linear regression calibration equation with daily PM2.5 mass concentrations of the uncalibrated low-cost node i as independent variable and PM2.5 mass concentrations of low-cost node i's closest reference node as dependent variable.

2.3.3 Optimize GPR model (hyperparameters)

~~After standardizing the $PM_{2.5}$ measurements for each node by subtracting the mean and scaling to unit variance (i.e., transforming the $PM_{2.5}$ measurements to have a zero mean and unit variance)~~ In the next step (step three in Fig. 3), a GPR model was fit to each day t's~~all~~ 31 nodes (i.e., 10 initialized low-cost nodes and 21 reference nodes) as described in Eq. (4). Prior to the GPR model fitting, all the $PM_{2.5}$ measurements of the 31 nodes over 59 valid days used for GPR model hyperparameters training were standardized. The standardization was performed by first concatenating all these training $PM_{2.5}$ measurements (from the 31 nodes over 59 days), then subtracting their mean $\mu_{training}$ and dividing them by their standard deviation $s_{training}$ (i.e., transforming all the training $PM_{2.5}$ measurements to have a zero mean and unit variance). ~~and step three in Fig. 3.~~ It is worth noting that assuming the mean function $\boldsymbol{\mu} \in \mathbb{R}^{31}$ to be 0 along with standardizing all the training $PM_{2.5}$ samples in this study is one of the common modelling formulations on the GPR model and the simplest one. More complex formulations including a station-specific mean function (lack of prior information for this project), a time-dependent mean function (computationally expensive), and a combination of both were not considered for this paper. After the standardization of training samples, ~~Then~~ the GPR was trained to maximize the log marginal likelihood over all 59 days ~~(~~using Eq. 5~~)~~ and using an L-BFGS-B optimizer (Byrd et al., 1994). To avoid bad local minima, several random hyperparameter initializations were tried and the initialization that resulted in~~with~~ the ~~best~~ largest log marginal likelihood after optimization was chosen (in this paper, $\boldsymbol{\Theta} = [\sigma_s^2, l, \sigma_n^2]$ was initialized to [0.1, 50, 0.01]).

$$\boldsymbol{r}_i = \begin{cases} \boldsymbol{y}_i, & \text{if reference node} \\ \alpha_i \cdot \boldsymbol{y}_i + \beta_i, & \text{if low} - \text{cost node} \end{cases}$$

~~(3)~~

$$\boldsymbol{r}_t | \Gamma \sim N(\boldsymbol{\mu}, \boldsymbol{\Sigma}) \tag{4}$$

where t ranges from 1 (inclusive) to 59 (inclusive); $\boldsymbol{r}_t \in \mathbb{R}^{31}$ is a vector of all 31 nodes' $PM_{2.5}$ measurements (calibrated if low-cost nodes) on day t; $\Gamma = \{\boldsymbol{x}_1, \dots, \boldsymbol{x}_{31}\}$ denotes 31 nodes' locations and $\boldsymbol{x}_i \in \mathbb{R}^2$ is a vector of the latitude and longitude of node i; $\boldsymbol{\mu} \in \mathbb{R}^{31}$ represents the mean function (assumed to be $\mathbf{0}$ in this study) and $\boldsymbol{\Sigma} \in \mathbb{R}^{31\times31}$ with $\Sigma_{ij} = K(\boldsymbol{x}_i, \boldsymbol{x}_j; \boldsymbol{\Theta})$ represents the covariance function/kernel function.

~~where α_i and β_i are the slope and intercept, respectively, of the calibration equation for low-cost node i based on its closest reference node; $\boldsymbol{r}_i$ is all the daily $PM_{2.5}$ measurements of either the initially-calibrated low-cost node i or reference node i; and $\boldsymbol{r}_t$ is the concatenation of all 31 nodes' $PM_{2.5}$ measurements on day t.~~

$$\arg\max_{\boldsymbol{\Theta}} L(\boldsymbol{\Theta}) = \arg\max_{\boldsymbol{\Theta}} \sum_{t=1}^{59} \log p(\boldsymbol{r}_t | \boldsymbol{\Theta}) = \arg\max_{\boldsymbol{\Theta}} (-0.5 \cdot 59 \cdot \log|\boldsymbol{\Sigma}_\theta| - 0.5 \sum_{t=1}^{59} \boldsymbol{r}_t{}^T \boldsymbol{\Sigma}_\theta^{-1} \boldsymbol{r}_t) \tag{5}$$

where $\boldsymbol{\Theta} \in \mathbb{R}^3$ is a vector of the GPR hyperparameters σ_s^2, l, and σ_n^2.

2.3.4 Update low-cost nodes' (simple linear regression) calibrations based on their conditional means

Once the optimum $\boldsymbol{\Theta}$ for the (initial) GPR was found, we used the learned covariance function to find the mean of each low-cost node i's Gaussian Distribution conditional on the remaining 30 nodes within the network (i.e., $\mu_{A|B}^{it}$) on day t as described mathematically in Eq. (6)–(8) and repeatedly did so until all 59 days' $\mu_{A|B}^{it}$ (i.e., $\boldsymbol{\mu}_{\boldsymbol{A|B}}^{\boldsymbol{i}} \in \mathbb{R}^{59}$) were found and then re-calibrated that low-cost node i based on the $\boldsymbol{\mu}_{\boldsymbol{A|B}}^{\boldsymbol{i}}$. The re-calibration was done by first fitting a simple linear regression model to all 59 pairs of daily PM2.5 mass concentrations from the uncalibrated low-cost node i ($\boldsymbol{y_i}$, independent variable) and its conditional mean ($\boldsymbol{\mu}_{\boldsymbol{A|B}}^{\boldsymbol{i}}$, dependent variable) and then using the updated calibration factors (slope α_i and intercept β_i) obtained from this newly fitted simple linear regression calibration model to calibrate the low-cost node i again (using Eq. 3). This procedure is summarized graphically in Fig. 3 step four and was performed iteratively for all low-cost nodes one at a time. The reasoning behind this step is given in the Supplement. A high-level interpretation of this step is that the target low-cost node is calibrated by being weighted over the remaining nodes within the network and the $\boldsymbol{\Sigma}_{\boldsymbol{AB}}^{\boldsymbol{it}}{\boldsymbol{\Sigma}_{\boldsymbol{BB}}^{\boldsymbol{it}}}^{-1}$ term computes the weights. In contrast to the inverse distance weighting interpolation which will weight the nodes used for calibration equally if they are equally distant from the target node, the GPR will value sparse information more and lower the importance of redundant information (suppose all the nodes are equally distant from the target node) as shown in Fig. S2.

$$p\left(\begin{bmatrix} r_A^{it} \\ \boldsymbol{r}_{\boldsymbol{B}}^{\boldsymbol{it}} \end{bmatrix}\right) = N\left(\begin{bmatrix} r_A^{it} \\ \boldsymbol{r}_{\boldsymbol{B}}^{\boldsymbol{it}} \end{bmatrix}; \begin{bmatrix} \mu_A^{it} \\ \boldsymbol{\mu}_{\boldsymbol{B}}^{\boldsymbol{it}} \end{bmatrix} \begin{bmatrix} \Sigma_{AA}^{it} & \boldsymbol{\Sigma}_{\boldsymbol{AB}}^{\boldsymbol{it}} \\ \boldsymbol{\Sigma}_{\boldsymbol{BA}}^{\boldsymbol{it}} & \boldsymbol{\Sigma}_{\boldsymbol{BB}}^{\boldsymbol{it}} \end{bmatrix}\right) \tag{6}$$

$$r_A^{it} | \boldsymbol{r}_{\boldsymbol{B}}^{\boldsymbol{it}} \sim N\left(\mu_{A|B}^{it}, \Sigma_{A|B}^{it}\right) \tag{7}$$

$$\mu_{A|B}^{it} = \mu_A^{it} + \boldsymbol{\Sigma}_{\boldsymbol{AB}}^{\boldsymbol{it}}{\boldsymbol{\Sigma}_{\boldsymbol{BB}}^{\boldsymbol{it}}}^{-1}(\boldsymbol{r}_{\boldsymbol{B}}^{\boldsymbol{it}} - \boldsymbol{\mu}_{\boldsymbol{B}}^{\boldsymbol{it}}) \tag{8}$$

where r_A^{it} and $\boldsymbol{r}_{\boldsymbol{B}}^{\boldsymbol{it}}$ are the daily PM2.5 measurement(**s**) of the low-cost node i and the remaining 30 nodes on day t; μ_A^{it}, $\boldsymbol{\mu}_{\boldsymbol{B}}^{\boldsymbol{it}}$, and $\mu_{A|B}^{it}$ are the mean (**vector**) of the partitioned Multivariate Gaussian Distribution of the low-cost node i, the remaining 30 nodes, and the low-cost node i conditional on the remaining 30 nodes, respectively, on day t; and Σ_{AA}^{it}, $\boldsymbol{\Sigma}_{\boldsymbol{AB}}^{\boldsymbol{it}}$, $\boldsymbol{\Sigma}_{\boldsymbol{BA}}^{\boldsymbol{it}}$, $\boldsymbol{\Sigma}_{\boldsymbol{BB}}^{\boldsymbol{it}}$, and $\Sigma_{A|B}^{it}$ are the covariance between the low-cost node i and itself, the low-cost node i and the remaining 30 nodes, the remaining 30 nodes and the low-cost node i, the remaining 30 nodes and themselves, and the low-cost node i conditional on the remaining 30 nodes and itself, respectively, on day t.

2.3.5 Optimize alternately and iteratively and converge

Iterative optimizations alternated between the GPR ~~covariance function~~hyperparameters and the low-cost node calibrations using the approaches described in Sect. 2.3.3 and 2.3.4, respectively~~measurements~~ (Fig. 3 steps five and six, respectively), until the GPR parameters $\boldsymbol{\Theta}$ converged with the convergence criteria being the differences in all the GPR hyperparameters between the two adjacent runs below 0.01 (i.e., with $\Delta\sigma_s^2 \le 0.01, \Delta l \le 0.01, and\ \Delta\sigma_n^2 \le 0.01$).

2.3.6 Predict on the holdout reference node and calculate accuracy metrics

The final GPR was used to predict the 59-day PM2.5 measurements of the holdout reference node (Fig. 3 step seven) following the Cholesky decomposition algorithm (Rasmussen and Williams, 2006) with the standardized predictions being transformed back to the original PM2.5 measurement scale at the end. The back transformation was done by multiplying the predictions by the standard deviation $s_{training}$ (the standard deviation of the training $PM_{2.5}$ measurements) and then adding back the mean $\mu_{training}$ (the mean of the training $PM_{2.5}$ measurements). Metrics including root mean square errors (RMSE, Eq. 9) and percent errors defined as RMSE normalized by the average of the true measurements of the holdout reference node in this study (Eq. 10) were calculated for each fold and further averaged over all 22 folds to assess the accuracy and sensitivity of our simultaneous GPR and simple linear regression calibration model.

$$\mathrm{RMSE} = \sqrt{\frac{1}{59}\|\boldsymbol{y}_i - \widehat{\boldsymbol{y}}_i\|_2^2} \qquad (9)$$

where $\boldsymbol{y}_i$ and $\widehat{\boldsymbol{y}}_i$ are the true and model predicted 59 daily $PM_{2.5}$ measurements of the holdout reference node i.

$$\text{Percent error} = \frac{\mathrm{RMSE}}{\text{avg. holdout reference } \mathrm{PM}_{2.5} \text{ conc.}} \qquad (10)$$

3 Results and discussion

3.1 Spatial variation of $PM_{2.5}$ across Delhi

Figure 4a presents the box plot of the daily averaged $PM_{2.5}$ at each available reference site across Delhi from January 1, 2018 to March 31, 2018. The Vasundhara and DTU sites were the most polluted stations with the $PM_{2.5}$ averaging 194 ± 104 µg m^{-3} and 193 ± 90 µg m^{-3}, respectively. The Pusa and Sector 62 sites had the lowest mean $PM_{2.5}$, averaging 86 ± 40 µg m^{-3} and 88 ± 36 µg m^{-3}, respectively. Spatially, the ~~global~~ Delhi-wide average of the 3-month mean $PM_{2.5}$ of the 22 reference stations was found to be 138 ± 31 µg m^{-3}. This pronounced spatial variation in mean $PM_{2.5}$ in Delhi (as reflected by the high SD of 31 µg m^{-3}) coupled with the stronger temporal variation for each station even at a 24 h scale (range: 35–104 µg m^{-3}, see Fig. 4a) caused nonuniform calibration performance of the GPR model across Delhi, as detailed in Sect. 3.2.

3.2 Assessment of GPR model performance

The optimum values of the GPR model parameters including the signal variance (σ_s^2), the characteristic length-scale (l), and the noise variance (σ_n^2) are shown in Fig. S3. The σ_s^2, l, and σ_n^2 from the 22-fold leave-one-out CV averaged 0.53 ± 0.02, 97.89 ± 5.47 km, and 0.47 ± 0.01, respectively. The small variability in all the parameters among all the folds indicates that the model is fairly robust to the different combinations of reference nodes. The learned length-scale can be interpreted as the modeled spatial pattern of $PM_{2.5}$ being relatively consistent within approximately 98 km, suggesting that the optimized model majorly captures a global trend rather than fine-grained local variations in Delhi.

3.2.1 Accuracy of reference node prediction

We start by showing the accuracy of model prediction on the 22 reference nodes using leave-one-out CV (when the low-cost node measurements were included in our spatial prediction). Without any prior knowledge of the true calibration factors for the low-cost nodes, the holdout reference node prediction accuracy is a statistically sound proxy for estimating how well our technique can calibrate the low-cost nodes. The performance scores (including RMSE and percent error) for each reference station sorted by the 3-month mean PM$_{2.5}$ in descending order are listed in Table 2. An overall 30 % prediction error (equivalent to an RMSE of 33 μg m^{-3}) at a 24 h scale was achieved on the reference nodes following our calibration procedure. Although the technique's performance is decent especially considering the minimal amount of field work involved, its calibration error is nearly 3 times higher than the one of the low-cost nodes that were well calibrated by collocation with an environmental β-attenuation monitors (E-BAM) in our previous study (error: 11 %; RMSE: 13 μg m^{-3}) under similar PM$_{2.5}$ concentrations at the same temporal resolution (Zheng et al., 2018). The suboptimal on-the-fly mapping accuracy is a result of the optimized model's ability to simulate only the global trend well. From a different perspective, the GPR method would have modeled the spatial pattern of PM$_{2.5}$ in Delhi well had the natural spatial covariance among the nodes not been disturbed by the complex and prevalent local sources there. As a substantiation of the flawed local PM$_{2.5}$ variation modelling, the reference node mapping accuracy follows a pattern, with relatively high-quality prediction for those nodes whose means were close to the ~~global~~ Delhi-wide mean (e.g., ~~global~~ Delhi-wide mean ± SD as highlighted with shading in Table 2) ~~while~~ and relatively poor prediction for those nodes whose~~the~~ means ~~wide of~~differed substantially from the ~~global~~ Delhi-wide mean (~~and~~ particularly ~~in~~ on the lower end).

It is of particular interest to validate the value of establishing a relatively dense wireless sensor network in Delhi by examining if the addition of the low-cost nodes can truly lend a performance boost to the spatial interpolation among sensor locations. We juxtapose the interpolation performance using the full sensor network (including both the reference and low-cost nodes) with that using only the reference nodes in Fig. 5. In this context, the unnormalized RMSE is less representative than the percent error of the model interpolation performance because of the unequal numbers of overlapping 24 h observations for all the nodes (59 data points) and for only the reference nodes (87 data points). The comparison revealed that the inclusion of the 10 low-cost devices on top of the regulatory grade monitors can reduce mean and median interpolation error by roughly 2 %. While only a marginal improvement with 10 low-cost nodes in the network~~at the scale of 10~~, the outcome hints that densely-deployed low-cost nodes can have great promise of significantly decreasing the amount of pure interpolation among sensor locations, therefore benefitting the spatial precision of a network. We will explore more about the significance of the low-cost nodes for the network performance in Sect. 3.3.3.

3.2.2 Accuracy of low-cost node calibration

Next we describe the technique's accuracy of low-cost node calibration. The model-produced calibration factors are shown in Fig. 6. The intercepts and slopes for each unique low-cost device varied little among all the 22 CV folds, reiterating the stability of the GPR model. The values of these calibration factors resemble those obtained in the previous field work, with slopes comparable to South Coast Air Quality Management District's evaluations on the Plantower PMS models (SCAQMD, 2017a–c) and intercepts comparable to our Kanpur, India post-monsoon study (Zheng et al., 2018).

Two low-cost nodes (i.e., MRU and IITD) were collocated with two E-BAMs throughout the entire study. This allows us to take their model-derived calibration factors and calibrate the corresponding raw values of the low-cost nodes before computing the calibration accuracy based on the ground truth (i.e., E-BAM measurements). Figures 7a and 7b show the scatterplots of the collocated E-BAM measurements against the model-calibrated low-cost nodes at the MRU and the IITD sites, respectively. The two sites had similarly large calibration errors (~50 %) because their concentrations were both near the lower end of $PM_{2.5}$ spectrum in Delhi. These high error rates echo the conditions found at the comparatively clean Pusa and Sector 62 reference sites. The scatterplots also reveal the reason why the technique especially has trouble calibrating low-concentration sites—the technique overpredicted the $PM_{2.5}$ concentrations at the low-concentration sites to match the levels as if subject to the natural spatial variation. The washed-out local variability after model calibration more obviously manifests in Fig. 4b, which stands in marked contrast to the true wide variability across the reference sites (Fig. 4a). In other words, the geostatistical techniques can calibrate the low-cost nodes dynamically, with the important caveat that it is effective only if the degree of urban homogeneity in $PM_{2.5}$ is high (e.g., the local contributions are as small a fraction of the regional ones as possible or the local contributions are prevalent but of similar magnitudes). Otherwise, quality predictions will only apply for those nodes whose means are close to the ~~global~~ Delhi-wide mean. In this study, our MRU and IITD sites are similar to the IITM site from the studies by Tiwari et al. (2012 and 2015), which are all on campus and free from major pollution sources and therefore qualified to be regional background sites. The $PM_{2.5}$ regional background concentration during winter in Delhi was then estimated to be approximately 72 µg m^{-3}. The ~~global~~ Delhi-wide mean of the 22 reference sites was 138 µg m^{-3}, thus the mean local contribution across Delhi was roughly 66 µg m^{-3}. Clearly this ~1:1 regional–to–local ratio did not fully support the technique. Alternatively, prior information about urban $PM_{2.5}$ spatial patterns such as high-spatial-resolution annual average concentration basemap from air pollution dispersion models can dramatically improve the on-the-fly calibration performance by correcting for the concentration range-specific biases (Schneider et al., 2017).

3.2.3 GPR model performance as a function of training window size

So far, the optimization of both GPR model hyperparameters and the linear regression calibration factors for the low-cost nodes has been carried out over the entire sampling period using all 59 valid daily-averaged data points. It is of critical importance to examine the effect of time history on the algorithm, by analyzing how sensitive the model performance is to training window size. We tracked the model performance change when an increment of 2 days' data were included in the model training. The model performance was measured by the mean accuracy of model prediction on the 22 reference nodes (within the time period of the training window) using leave-one-out CV, as described in Sect. 3.2.1. Figure 8 illustrates that, throughout the 59 days, the error rate and the standard error of the mean (SEM) remained surprisingly consistent at ~30 % and ~3–4 %, respectively, regardless of how many 2-day increments were used as the training window size. The little influence of training window size on the GPR model performance is possibly a positive side effect of the algorithm's time-invariant mean assumption, strong spatial smoothing effect, and the additional averaging of the error rates of the 22 reference nodes. The markedly low requirement of our algorithm for training data is powerful in that it enables the GPR model hyperparameters and the linear regression calibration factors to always be nearly most updated in the field. This helps realize the algorithm's full potential for automatically surveilling large-scale networks by detecting malfunctioning low-cost nodes within a network (see Sect. 3.3.1) and tracking the drift of low-cost nodes (see Sect. 3.3.2) with as little latency as possible.

3.2.4 GPR model dynamic calibration performance

The stationary model performance in response to the increase of training data hints that using our method for dynamic calibration/prediction is feasible. We assessed the algorithm's 1 week-ahead prediction performance, by using simple linear regression calibration factors and GPR hyperparameters that were optimized from one week to calibrate the 10 low-cost nodes and predict each of the 22 reference nodes, respectively, in the next week. For example, the first/second/third/… week data were used as training data to build GPR models and simple linear regression models. These simple linear regression models were then used to calibrate the low-cost nodes in the second/third/fourth/… week, followed by the GPR models to predict each of the 22 reference nodes in that week. The performance was still measured by the mean accuracy of model prediction on the 22 reference nodes using leave-one-out CV, as described in Sect. 3.2.1. We found similarly stable 26–34 % dynamic calibration error rates and ~3–7 % SEMs throughout the weeks (see Figure S4).

3.3 Simulation results

While the exact values of the calibration factors derived from the GPR model fell short of faithfully recovering the original picture of $PM_{2.5}$ spatiotemporal gradients in Delhi, these values of one low-cost node relative to another in the network (Sect. 3.3.1) or relative to itself over time (Sect. 3.3.2) turned out to be useful in facilitating automated large-scale sensor network monitoring.

3.3.1 Simulation of low-cost node failure or under heavy influence of local sources

One way to simulate the conditions of low-cost node failure or under heavy influence of local sources is to replace their true signals with values from random number generators so that the inherent spatial correlations are corrupted. In this study, we simulated how the model-produced calibration factors change when all (10), nine, seven, three, and one of the low-cost nodes within the network malfunction or are subject to strong local disturbance. We have three major observations from evaluating the simulation results (Fig. ~~8~~ 9 and Fig. ~~S4~~S5). First, the normal calibration factors are quite distinct from those of the low-cost nodes with random signals. Compared to the normal values (see Fig. ~~8~~ 9 bottom right panel), the ones of the low-cost nodes with random signals have slopes close to 0 and intercepts close to the ~~global~~ Delhi-wide mean of true $PM_{2.5}$ in Delhi (most clearly shown in Fig. ~~8~~ 9 top left panel). Second, the calibration factors of the normal low-cost nodes are not affected by the aberrant nodes within the network (see Fig. ~~8~~ 9 top right, middle left, middle right, and bottom left panels).

These two observations indicate that the GPR model enables automated and streamlined process of instantly spotting any malfunctioning ~~or singular~~ low-cost nodes (due to either hardware failure or under heavy influence of local sources) within a large-scale sensor network. Third, the performance of the GPR model seems to be rather uninfluenced by changing the true signals to random numbers (see Fig. ~~S4~~S5, 33 % error rate when all low-cost nodes are random vs. baseline 30 % error rate). One possible explanation is that the prevalent and intricate air pollution sources in Delhi have already dramatically weakened the natural spatial correlations. This means that a significant degree of randomness has already been imposed on the low-cost nodes in Delhi prior to our complete randomness experiment. It is worth mentioning that flatlining is another commonly seen failure mode of our low-cost PM sensors in Delhi. The raw signals of such malfunctioning PM sensors were observed to flatline at the upper end of the sensor output values (typically thousands of μg m^{-3}). The very distinct signals of these flatlining low-cost PM nodes, however, make it rather easy to separate them from the rest of the nodes and filter them out at the early pre-processing stage before analyses, therefore without having to resort to our algorithm. Nevertheless, our not so accurate on-the-fly calibration model has created a useful algorithm for supervising large-scale sensor networks in real time as a by-product.

3.3.2 Simulation of low-cost node drift

We further investigated the feasibility of applying the GPR model to track the drift of low-cost nodes accurately over time. We simulated drift conditions by first setting random percentages of intercept and slope drift, respectively, for each individual low-cost node and for each simulation run. Next, we adjusted the signals of each low-cost node over the entire study period given these randomly selected percentages using Eq. (11). Then, we rebuilt a GPR model based on these drift-adjusted signals and evaluated if the new model-generated calibration factors matched our expected predetermined percentage drift relative to the true (baseline) calibration factors.

$$\boldsymbol{y_{i\_drift}} = \frac{\boldsymbol{y_i}}{(1-\text{percentage slope drift}_\text{i})} + \frac{\text{percentage intercept drift}_\text{i} \cdot \text{true intercept}_\text{i}}{(1-\text{percentage slope drift}_\text{i})\cdot \text{true slope}_\text{i}} \tag{11}$$

where $\boldsymbol{y_i}$, $\text{true intercept}_\text{i}$, $\text{true slope}_\text{i}$, $\text{percentage intercept drift}_\text{i}$, $\text{percentage slope drift}_\text{i}$, and $\boldsymbol{y_{i\_drift}}$ are a vector of the true signals, the standard model-derived intercept, the standard model-derived slope, the randomly generated percentage of intercept drift, the randomly generated percentage of slope drift, and a vector of the drift-adjusted signals, respectively, over the full study period for low-cost node *i*.

The performance of the model for predicting the drift was examined under a variety of scenarios including assuming that all (10), eight, six, four, and two of the low-cost nodes developed various degrees of drift such as significant (11 %–99 %), marginal (1 %–10 %), and a balanced mixture of significant and marginal. The testing results for 10, six, and two low-cost nodes are displayed in Table 3 and those for eight and four nodes are in Table S1. Overall, the model demonstrates excellent drift predictive power with less than 4 % errors for all the simulation scenarios. The model proves to be most accurate (within 1 % error) when low-cost nodes only drifted marginally regardless of the number of nodes drift. In contrast, significant and particularly a mixture of significant and marginal drifts might lead to marginally larger errors. We also notice that the intercept drifts are slightly harder to accurately capture than the slope drifts. Similar to the simulation of low-cost node failure/under strong local impact as described in Sect 3.3.1, the performance of the model for predicting the measurements of the 22 holdout reference nodes across the 22-fold leave-one-out CV was untouched by the drift conditions (see Fig. ~~S5~~S6). This unaltered performance can be attributable to the fact that the drift simulations only involve simple linear transformations as shown in Eq. (11). The high-quality drift estimation has therefore presented another convincing case of how useful our original algorithm can be applied to dynamically monitoring dense sensor networks, as a by-product of calibrating low-cost nodes. ~~We can rebuild a model such as every week using a rolling window (to keep the number of observations for model construction roughly unchanged) to assess the drifts in the model space over time. After that, the true calibration factors obtained from the initial collocation with reference instruments prior to deployment can be adjusted accordingly based on the model-estimated drifts. This procedure allows for real-time drift corrections to low-cost node measurements.~~

It should be noted that the mode of drift (linear or random drift) will not significantly affect our simulation results. As we demonstrated in Sect. 3.2.3, the performance of our algorithm is insensitive to the training data size. And we believe that models with a similar prediction accuracy should have a similar drift detection power. For example, if the prediction accuracy of the model trained on 59 days' data is virtually the same as the accuracy of the model trained on 2 days' data, and if the model trained on 59 days is able to detect the simulated drift, then so should the model trained on 2 days. Then if we reasonably assume that the drift rate remains roughly unchanged within a 2-day window, then the drift mode (linear or random), which only dictates how the drift rate jumps (usually smoothly as well) between any adjacent discrete 2-day windows, does not matter anymore. All that matters is to track that one fixed drift rate reasonably well within those 2 days, which is virtually the same as what we already did with the entire 59 days' data.

3.3.3 Optimal number of reference nodes

Questions which remain unsolved are 1) what the optimum or minimum number of reference instruments is to sustain this technique and 2) if the inclusion of low-cost nodes can effectively assist in lowering the technique's calibration/mapping inaccuracy. It is interesting to note that optimizing the model's calibration accuracy can not only directly fulfill the fundamental calibration task, but also help better the sensor network monitoring capability as an added bonus. To address these two outstanding issues, we randomly sampled subsets of all the 22 reference nodes within the network in increments of one node (i.e. from 1 to 21 nodes) and implemented our algorithm with and without incorporating the low-cost nodes, before finally computing the mean percent errors in predicting all the holdout reference nodes. To get the performance scores as close to truth as possible but without incurring excessive computational cost in the meantime, the sampling was repeated 100 times for each subset size. The calibration error in this section was defined as the mean percent errors in predicting all the holdout reference nodes further averaged over 100 simulation runs for each subset size.

Figure ~~9~~ 10 describes the 24 h calibration percent error rate of the model as a function of the number of reference stations used for modelling with and without involving the low-cost nodes. The error rates generally decrease as the number of reference instruments increases (full network: from ~40 % with 1 node to ~29 % with 21 nodes; network excluding low-cost nodes: from ~43 % to ~30 %) but are somewhat locally variable and most pronounced when five, seven, and eight reference nodes are simulated. These bumps might simply be the result of five, seven, and eight reference nodes being relatively non-ideal (with regard to their neighboring numbers) for the technique, although the possibility of non-convergence due to the limited 100 simulation runs for each scenario cannot be ruled out. The 19 or 20 nodes emerge as the optimum numbers of reference nodes with the lowest errors of close to 28 %, while 17 to 21 nodes all yield comparably low inaccuracies (all below 30 %). The pattern discovered in our research shares certain similarities with Schneider et al. (2017) who studied the relationship between the accuracy of using colocation-calibrated low-cost nodes to map urban AQ and the number of simulated low-cost nodes for their urban-scale air pollution dispersion model and kriging-fueled data fusion technique in Oslo, Norway. Both studies indicate that at least roughly 20 nodes are essential to start producing acceptable degree of accuracy. Unlike Schneider et al. (2017) who further expanded the scope to 150 nodes by generating new synthetic stations from their established model and showed a “the more, the merrier” trend up to 50 stations, we restricted ourselves to only realistic data to investigate the relationship since we suspect that stations created from our model with approximately 30 % errors might introduce large noise which could misrepresent the true pattern. We agree with Schneider et al. (2017) that such relationships are location-specific and cannot be blindly transferred to other study sites. At last, including low-cost nodes in the model building can most of the time reduce the model’s errors notably when more than nine reference nodes are sampled (i.e., when the number of simulated reference nodes is favorable for carrying out the technique). And for the comparatively ideal 17–20 nodes, we even observed approximately non-overlapping 95 % confidence intervals, suggesting significantly lower errors are yielded when low-cost nodes are incorporated. The accuracy gains are still relatively minor because of the suboptimal size of the low-cost node network (i.e., 10). We postulate that once the low-cost node network scales up to 100s, the model constructed using the full network information can be more accurate than the one with only the information of reference nodes by considerable margins.

4 Conclusions

This study introduced a simultaneous GPR and simple linear regression pipeline to calibrate wireless low-cost PM sensor networks (up to any scale) on the fly in the field by capitalizing on all available reference monitors across an area without the requirement of pre-deployment collocation calibration. We evaluated our method for Delhi where 22 reference and 10 low-cost nodes were available from January 1, 2018 to March 31, 2018 (~~global~~ Delhi-wide average of the 3-month mean $PM_{2.5}$

among 22 reference stations: 138 ± 31 µg m^{-3}) using a leave-one-out CV over the 22 reference nodes. We demonstrated that our approach can achieve excellent robustness and decent accuracy, as underscored by the low variability in the GPR model parameters and model-produced calibration factors for low-cost nodes and by an overall 30 % prediction error (equivalent to an RMSE of 33 µg m^{-3}) at a 24 h scale, respectively, among the 22-fold CV. ~~Closer investigations~~We closely investigated into 1) the large model calibration errors (~50 %) at two Atmos regional background sites (3-month mean $PM_{2.5}$: ~72 µg m^{-3}) where our E-BAMs were collocated; 2) the similarly large model prediction errors at the comparatively clean Pusa and Sector 62 reference sites; and 3) ~~and~~ the washed-out local variability in the model calibrated low-cost sites. These observations revealed that the performance of our technique (and more generally the geostatistical techniques) can calibrate the low-cost nodes dynamically, but effective only if the degree of urban homogeneity in $PM_{2.5}$ is high. High urban homogeneity scenarios can be that~~(e.g.,~~ the local contributions are as small a fraction of the regional ones as possible or the local contributions are prevalent but of similar magnitudes~~)~~. Otherwise, quality predictions will only apply for those nodes whose means are close to the ~~global~~ Delhi-wide mean. We showed that our algorithm performance is insensitive to training window size as the mean prediction error rate and the standard error of the mean (SEM) for the 22 reference stations remained consistent at ~30 % and ~3–4 % when an increment of 2 days' data were included in the model training. The markedly low requirement of our algorithm for training data enables the models to always be nearly most updated in the field, thus realizing the algorithm's full potential for dynamically surveilling large-scale WLPMSNs by detecting malfunctioning low-cost nodes and tracking the drift with little latency. Our algorithm presented similarly stable 26–34 % mean prediction errors and ~3–7 % SEMs over the sampling period when pre-trained on the current week's data and predicting 1 week ahead, therefore suitable for dynamic calibration. Despite our algorithm's non-ideal calibration accuracy for Delhi, it holds the promise of being adapted for automated and streamlined large-scale wireless sensor network monitoring and of significantly reducing the amount of manual labor involved in the surveillance and maintenance. Simulations proved our algorithm's capability of differentiating malfunctioning ~~or singular~~ low-cost nodes (due to either hardware failure or under heavy influence of local sources) within a network and of tracking the drift of low-cost nodes accurately with less than 4 % errors for all the simulation scenarios. Finally, our simulation results confirmed that the low-cost nodes are beneficial for the spatial precision of a sensor network by decreasing the extent of pure interpolation among only reference stations, highlighting the substantial significance of dense deployments of low-cost AQ devices for a new generation of AQ monitoring network.

Two directions are possible for our future work. The first one is to expand both the longitudinal and the cross-sectional scopes of field studies and examine how well our solution works for more extensive networks in a larger geographical area over longer periods of deployment (when sensors are expected to actually drift, degrade, or malfunction). This enables us to validate the practical use of our method for calibration and surveillance more confidently. The second is to explore the infusion of information about urban $PM_{2.5}$ spatial patterns such as high-spatial-resolution annual average concentration basemap from air pollution dispersion models (Schneider et al., 2017) into our current algorithm to further improve the on-the-fly calibration performance by correcting for the concentration range-specific biases.

Data availability

The data are available upon request to Tongshu Zheng (tongshu.zheng@duke.edu).

Competing interests

Author Ronak Sutaria is the founder of Respirer Living Sciences Pvt. Ltd, a startup based in Mumbai, India which is the developer of the Atmos low-cost AQ monitor. Ronak Sutaria ~~only~~ was involved in developing and refining the hardware of Atmos and its server and dashboard and in deploying the sensors, but not in data analysis. Author Robert Caldow is the director of engineering at TSI and only responsible for the funding and technical support, but not for data analysis.

Acknowledgments

Sachchida N. Tripathi and Ronak Sutaria are supported under the Research Initiative for Real-time River Water and Air Quality Monitoring program funded by the Department of Science and Technology, Government of India and Intel Corporation, and administered by the Indo-US Science and Technology Forum. The authors would like to thank CPCB, DPCC, IMD, SPCBs, and AirNow DOS (Department of State) for providing the Delhi 1 h reference $PM_{2.5}$ measurements used in the current study.

References

Austin, E., Novosselov, I., Seto, E. and Yost, M. G.: Laboratory evaluation of the Shinyei PPD42NS low-cost particulate matter sensor, PLoS One, 10(9), 1–17, doi:10.1371/journal.pone.0137789, 2015.

Breunig, M. M., Kriegel, H. P., Ng, R. T. and Sander, J.: LOF: Identifying Density-Based Local Outliers., available at: http://www.dbs.ifi.lmu.de/Publikationen/Papers/LOF.pdf, last access: 10 Dec 2018, 2000.

Byrd, R. H., Lu, P., Nocedal, J. and Zhu, C.: A limited memory algorithm for bound constrained optimization, available at: http://users.iems.northwestern.edu/~nocedal/PDFfiles/limited.pdf, last access: 10 Dec 2018, 1994.

CPCB: Air quality monitoring, emission inventory, and source apportionment studies for Delhi, available at: http://cpcb.nic.in/cpcbold/Delhi.pdf, last access: 10 Dec 2018, 2009.

Crilley, L. R., Shaw, M., Pound, R., Kramer, L. J., Price, R., Young, S., Lewis, A. C. and Pope, F. D.: Evaluation of a low-cost optical particle counter (Alphasense OPC-N2) for ambient air monitoring, Atmos. Meas. Tech., 11(2), 709–720, doi:10.5194/amt-11-709-2018, 2018.

Di, Q., Kloog, I., Koutrakis, P., Lyapustin, A., Wang, Y. and Schwartz, J.: Assessing PM2.5Exposures with High Spatiotemporal Resolution across the Continental United States, Environ. Sci. Technol., 50(9), 4712–4721, doi:10.1021/acs.est.5b06121, 2016.

Feinberg, S., Williams, R., Hagler, G. S. W., Rickard, J., Brown, R., Garver, D., Harshfield, G., Stauffer, P., Mattson, E., Judge, R. and Garvey, S.: Long-term evaluation of air sensor technology under ambient conditions in Denver, Colorado, Atmos. Meas. Tech., 11(8), 4605–4615, doi:10.5194/amt-11-4605-2018, 2018.

Fishbain, B. and Moreno-Centeno, E.: Self Calibrated Wireless Distributed Environmental Sensory Networks, Sci. Rep., 6, 1–10, doi:10.1038/srep24382, 2016.

Gao, M., Cao, J. and Seto, E.: A distributed network of low-cost continuous reading sensors to measure spatiotemporal variations of PM2.5 in Xi’an, China, Environ. Pollut., 199, 56–65, doi:10.1016/j.envpol.2015.01.013, 2015.

Gorai, A. K., Tchounwou, P. B., Biswal, S. and Tuluri, F.: Spatio-Temporal Variation of Particulate Matter ($PM_{2.5}$) Concentrations and Its Health Impacts in a Mega City, Delhi in India, Environ. Health Insights, 12, 117863021879286, doi:10.1177/1178630218792861, 2018.

Hagler, G. S. W., Williams, R., Papapostolou, V. and Polidori, A.: Air Quality Sensors and Data Adjustment Algorithms: When Is It No Longer a Measurement?, Environ. Sci. Technol., 52(10), 5530–5531, doi:10.1021/acs.est.8b01826, 2018.

Holdaway, M. R.: Spatial modeling and interpolation of monthly temperature using kriging, Clim. Res., 6(3), 215–225, doi:10.3354/cr006215, 1996.

Holstius, D. M., Pillarisetti, A., Smith, K. R. and Seto, E.: Field calibrations of a low-cost aerosol sensor at a regulatory monitoring site in California, Atmos. Meas. Tech., 7(4), 1121–1131, doi:10.5194/amt-7-1121-2014, 2014.

Jayaratne, R., Liu, X., Thai, P., Dunbabin, M. and Morawska, L.: The influence of humidity on the performance of a low-cost air particle mass sensor and the effect of atmospheric fog, Atmos. Meas. Tech., 11(8), 4883–4890, doi:10.5194/amt-11-4883-2018, 2018.

Jiao, W., Hagler, G., Williams, R., Sharpe, R., Brown, R., Garver, D., Judge, R., Caudill, M., Rickard, J., Davis, M., Weinstock, L., Zimmer-Dauphinee, S. and Buckley, K.: Community Air Sensor Network (CAIRSENSE) project: Evaluation of low-cost sensor performance in a suburban environment in the southeastern United States, Atmos. Meas. Tech., 9(11), 5281–5292, doi:10.5194/amt-9-5281-2016, 2016.

Johnson, K. K., Bergin, M. H., Russell, A. G. and Hagler, G. S. W.: Field test of several low-cost particulate matter sensors in high and low concentration urban environments, Aerosol Air Qual. Res., 18(3), 565–578, doi:10.4209/aaqr.2017.10.0418, 2018.

Kelleher, S., Quinn, C., Miller-Lionberg, D. and Volckens, J.: A low-cost particulate matter ($PM_{2.5}$) monitor for wildland fire smoke, Atmos. Meas. Tech., 11(2), 1087–1097, doi:10.5194/amt-11-1087-2018, 2018.

Kelly, K. E., Whitaker, J., Petty, A., Widmer, C., Dybwad, A., Sleeth, D., Martin, R. and Butterfield, A.: Ambient and laboratory evaluation of a low-cost particulate matter sensor, Environ. Pollut., 221, 491–500, doi:10.1016/j.envpol.2016.12.039, 2017.

Kizel, F., Etzion, Y., Shafran-Nathan, R., Levy, I., Fishbain, B., Bartonova, A. and Broday, D. M.: Node-to-node field calibration of wireless distributed air pollution sensor network, Environ. Pollut., 233, 900–909, doi:10.1016/j.envpol.2017.09.042, 2018.

Lewis, A. and Edwards, P.: Validate personal air-pollution sensors, Nature, 535(7610), 29–31, doi:10.1038/535029a, 2016.

Mukherjee, A., Stanton, L. G., Graham, A. R. and Roberts, P. T.: Assessing the utility of low-cost particulate matter sensors over a 12-week period in the Cuyama valley of California, Sensors (Switzerland), 17(8), doi:10.3390/s17081805, 2017.

Ozler, S., Johnson, K. K., Bergin, M. H. and Schauer, J. J.: Personal Exposure to $PM_{2.5}$ in the Various Microenvironments as a Traveler in the Southeast Asian Countries, , doi:10.3844/ajessp.2018.170.184, 2018.

Rasmussen, C. E. and Williams, C. K. I.: 2. Regression, in: Gaussian Processes for Machine Learning, the MIT Press, 8–31, 2006.

Sayahi, T., Butterfield, A. and Kelly, K. E.: Long-term field evaluation of the Plantower PMS low-cost particulate matter sensors, Env. Pollut, in revision, doi:10.1016/j.envpol.2018.11.065, 2018.

Schneider, P., Castell, N., Vogt, M., Dauge, F. R., Lahoz, W. A. and Bartonova, A.: Mapping urban air quality in near real-time using observations from low-cost sensors and model information, Environ. Int., 106(May), 234–247, doi:10.1016/j.envint.2017.05.005, 2017.

South Coast Air Quality Management District (SCAQMD): Field Evaluation AirBeam PM Sensor, available at: http://www.aqmd.gov/docs/default-source/aq-spec/field-evaluations/airbeam---field-evaluation.pdf?sfvrsn=4, last access: 10 Jan 2018, 2015a.

South Coast Air Quality Management District (SCAQMD): Field Evaluation AlphaSense OPC-N2 Sensor, available at: http://www.aqmd.gov/docs/default-source/aq-spec/field-evaluations/alphasense-opc-n2---field-evaluation.pdf?sfvrsn=0, last access: 10 Jan 2018, 2015b.

South Coast Air Quality Management District (SCAQMD): Field Evaluation Laser Egg PM Sensor, available at: http://www.aqmd.gov/docs/default-source/aq-spec/field-evaluations/laser-egg---field-evaluation.pdf, last access: 10 Jan 2018, 2017a.

South Coast Air Quality Management District (SCAQMD): Field Evaluation Purple Air PM Sensor, available at: http://www.aqmd.gov/docs/default-source/aq-spec/field-evaluations/purpleair---field-evaluation.pdf, last access: 10 Jan 2018, 2017b.

South Coast Air Quality Management District (SCAQMD): Field Evaluation Purple Air (PA-II) PM Sensor, available at: http://www.aqmd.gov/docs/default-source/aq-spec/field-evaluations/purple-air-pa-ii---field-evaluation.pdf?sfvrsn=2, last access: 10 Jan 2018, 2017c.

Takruri, M., Challa, S. and Yunis, R.: Data fusion techniques for auto calibration in wireless sensor networks, Inf. Fusion, 132–139, available at: http://ieeexplore.ieee.org/xpls/abs_all.jsp?arnumber=5203880, last access: 10 Dec 2018, 2009.

Tiwari, G..: Urban Transport Priorities, Cities, 19(2), 95–103, available at: http://www.mumbaidp24seven.in/reference/geetam.pdf, last access: 10 Dec 2018, 2002.

Tiwari, S., Chate, D. M., Pragya, P., Ali, K. and Bisht, D. S. F.: Variations in mass of the PM_{10}, $PM_{2.5}$ and PM_1 during the monsoon and the winter at New Delhi, Aerosol Air Qual. Res., 12(1), 20–29, doi:10.4209/aaqr.2011.06.0075, 2012.

Tiwari, S., Hopke, P. K., Pipal, A. S., Srivastava, A. K., Bisht, D. S., Tiwari, S., Singh, A. K., Soni, V. K. and Attri, S. D.:

Intra-urban variability of particulate matter (PM$_{2.5}$ and PM$_{10}$) and its relationship with optical properties of aerosols over Delhi, India, Atmos. Res., 166, 223–232, doi:10.1016/j.atmosres.2015.07.007, 2015.

Wang, Y., Li, J., Jing, H., Zhang, Q., Jiang, J. and Biswas, P.: Laboratory Evaluation and Calibration of Three Low-Cost Particle Sensors for Particulate Matter Measurement, Aerosol Sci. Technol., 49(11), 1063–1077, doi:10.1080/02786826.2015.1100710, 2015.

Zheng, T., Bergin, M. H., Johnson, K. K., Tripathi, S. N., Shirodkar, S., Landis, M. S., Sutaria, R. and Carlson, D. E.: Field evaluation of low-cost particulate matter sensors in high-and low-concentration environments, Atmos. Meas. Tech., 11(8), 4823–4846, doi:10.5194/amt-11-4823-2018, 2018.

Zuo, J. X., Ji, W., Ben, Y. J., Hassan, M. A., Fan, W. H., Bates, L. and Dong, Z. M.: Using big data from air quality monitors to evaluate indoor PM2.5 exposure in buildings: Case study in Beijing, Environ. Pollut., 240, 839–847, doi:10.1016/j.envpol.2018.05.030, 2018.

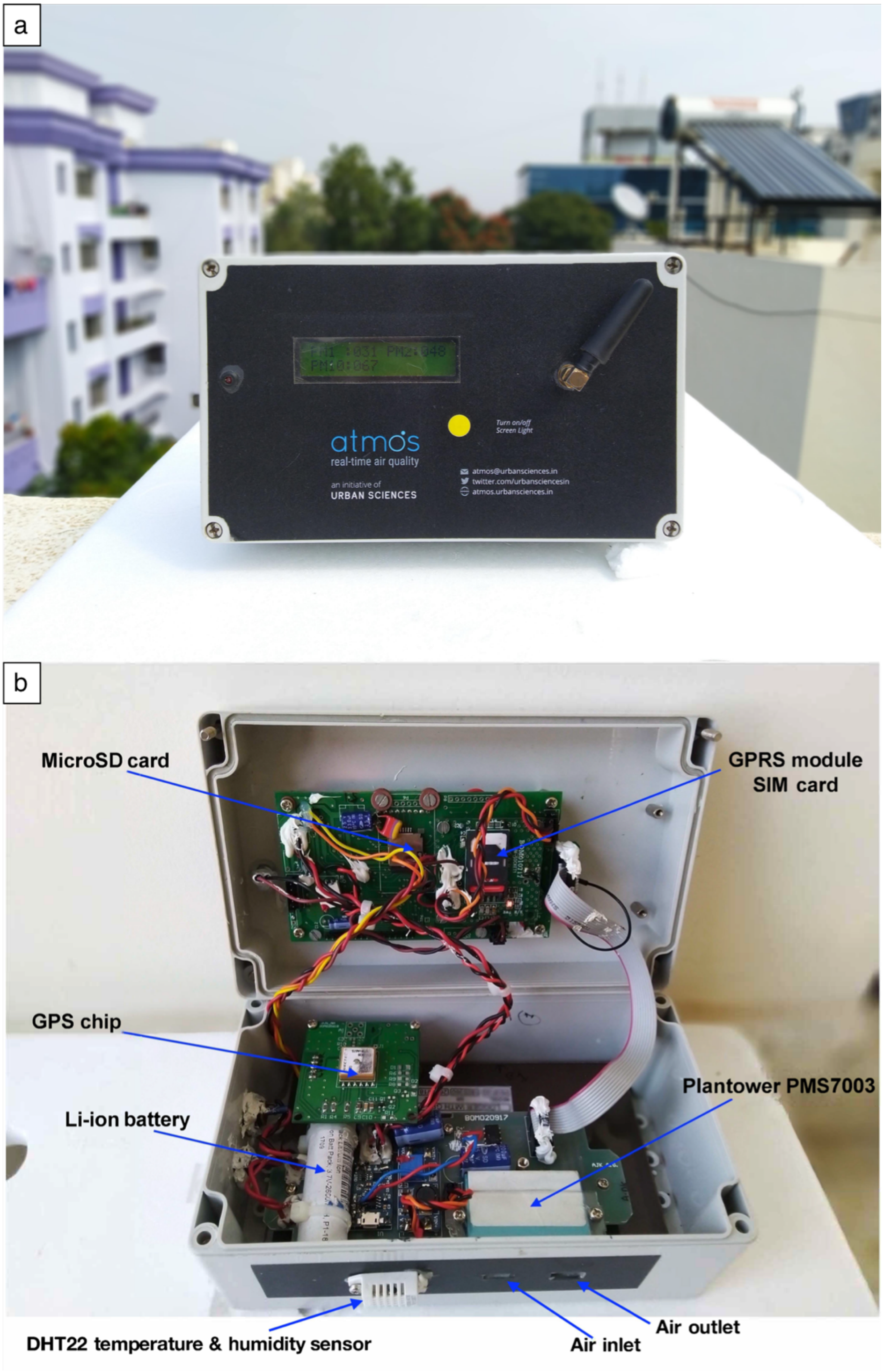

Figure 1: (a) Front view of the low-cost node. (b) Key components of the low-cost node.

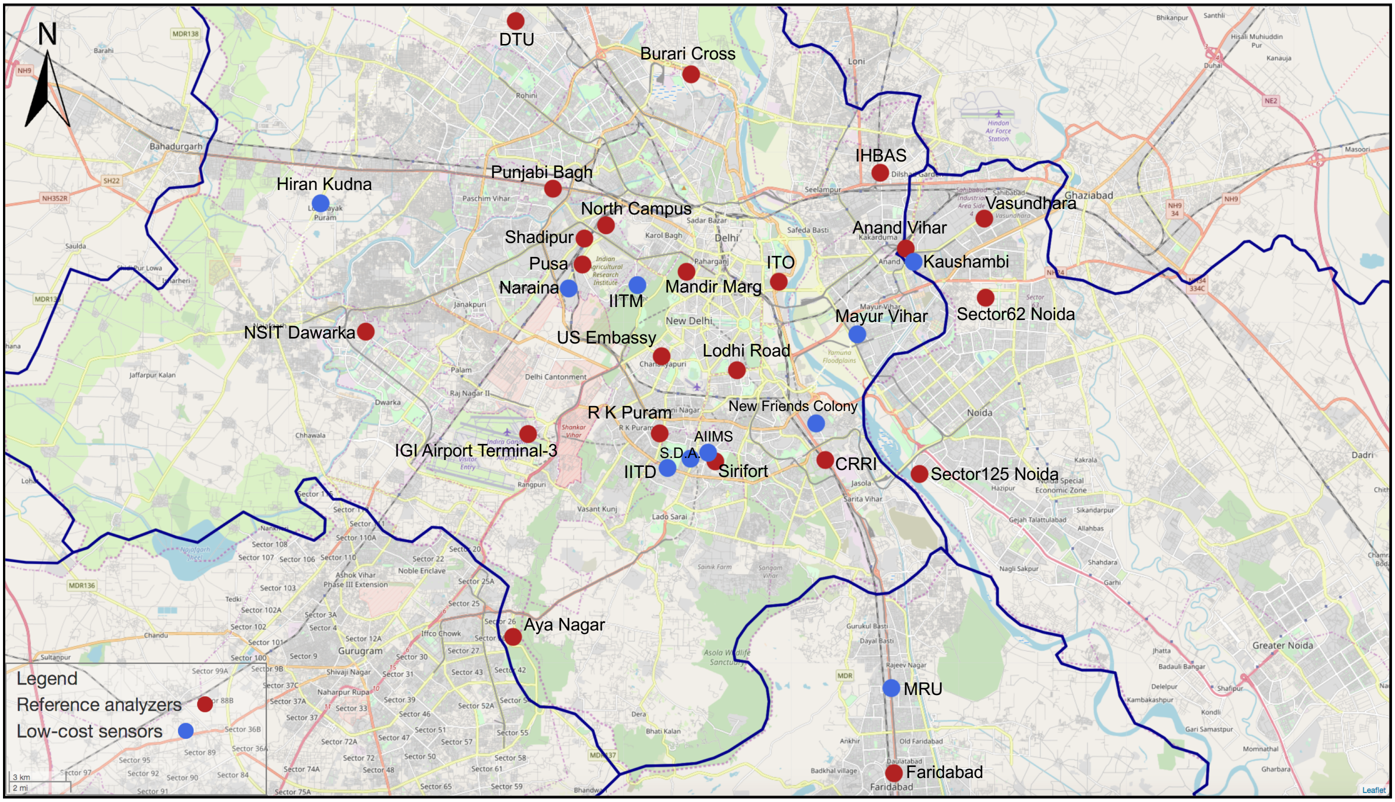

Figure 2: Locations of the 22 reference nodes (red icons) and 10 low-cost nodes (blue icons) that form the Delhi PM sensor network.

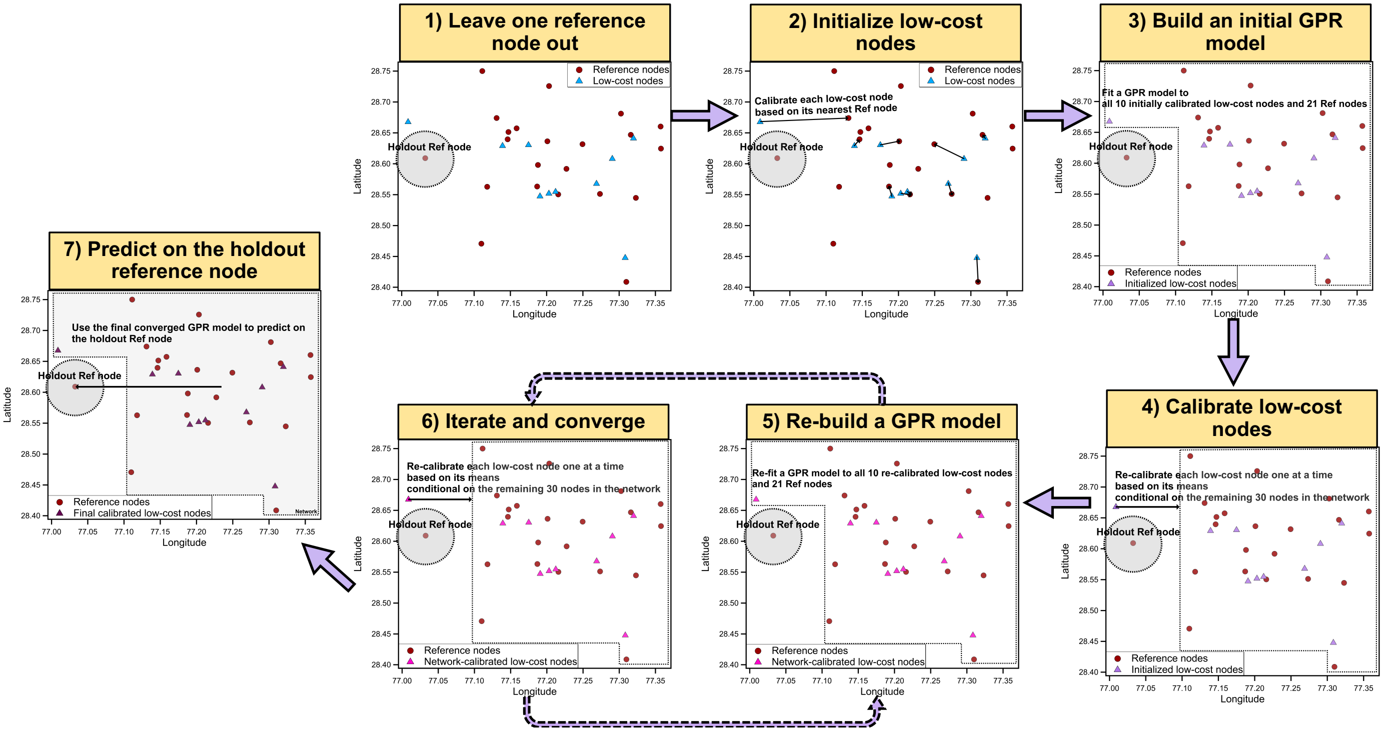
1) Leave one reference node out
Holdout Ref node
Reference nodes
Low-cost nodes
2) Initialize low-cost nodes
Calibrate each low-cost node based on its nearest Ref node
3) Build an initial GPR model
Fit a GPR model to all 10 initially calibrated low-cost nodes and 21 Ref nodes
Initialized low-cost nodes
4) Calibrate low-cost nodes
Re-calibrate each low-cost node one at a time based on its means conditional on the remaining 30 nodes in the network
5) Re-build a GPR model
Re-fit a GPR model to all 10 re-calibrated low-cost nodes and 21 Ref nodes
Network-calibrated low-cost nodes
6) Iterate and converge
7) Predict on the holdout reference node
Use the final converged GPR model to predict on the holdout Ref node
Final calibrated low-cost nodes
Latitude
Longitude

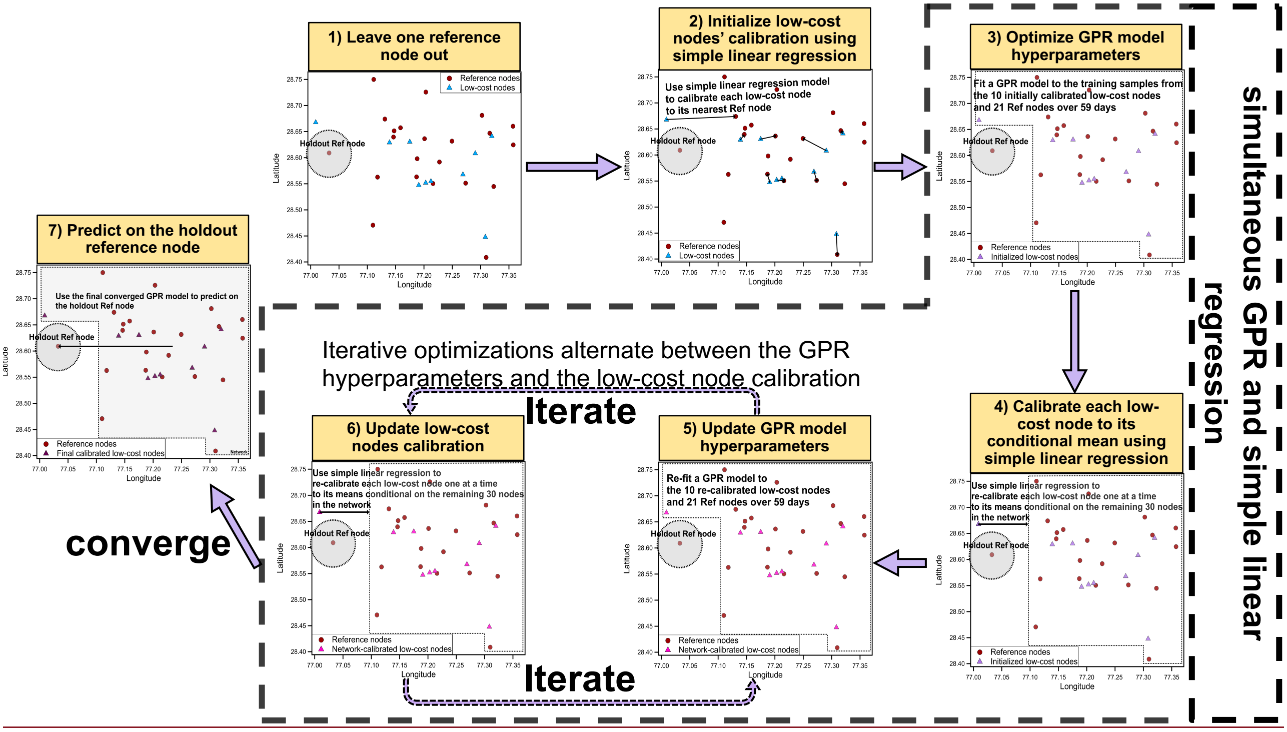
1) Leave one reference node out
Holdout Ref node
Reference nodes
Low-cost nodes
2) Initialize low-cost nodes' calibration using simple linear regression
Use simple linear regression model to calibrate each low-cost node to its nearest Ref node
3) Optimize GPR model hyperparameters
Fit a GPR model to the training samples from the 10 initially calibrated low-cost nodes and 21 Ref nodes over 59 days
Initialized low-cost nodes
4) Calibrate each low-cost node to its conditional mean using simple linear regression
Use simple linear regression to re-calibrate each low-cost node one at a time to its means conditional on the remaining 30 nodes in the network
5) Update GPR model hyperparameters
Re-fit a GPR model to the 10 re-calibrated low-cost nodes and 21 Ref nodes over 59 days
Network-calibrated low-cost nodes
6) Update low-cost nodes calibration
Iterative optimizations alternate between the GPR hyperparameters and the low-cost node calibration
Iterate
Iterate
converge
7) Predict on the holdout reference node
Use the final converged GPR model to predict on the holdout Ref node
Final calibrated low-cost nodes
simultaneous GPR and simple linear regression
Latitude
Longitude

Figure 3: The ~~overall schema for~~flow diagram illustrating the simultaneous GPR and simple linear regression calibration ~~model~~algorithm. In step one, for each of the 22-fold leave-one-out CVs, one of the 22 reference nodes is held out of modelling for the model predictive performance evaluation in step seven; in step two, fit a simple linear regression model between each low-cost

node i and its closest reference node's $PM_{2.5}$, initialize low-cost node i's calibration model to this linear regression model, and calibrate the low-cost node i using this model; in step three, first initialize the GPR hyperparameters to [0.1, 50, 0.01] and then update/optimize the hyperparameters based on the training samples from the 10 initially calibrated low-cost nodes and 21 reference nodes over 59 days; in step four, first compute each low-cost node i's means conditional on the remaining 30 nodes given the optimized GPR hyperparameters, then fit a simple linear regression model between each low-cost node i and its conditional means, update low-cost node i's calibration model to this new linear regression model, and re-calibrate the low-cost node i using this new model; in step five and six, iterative optimizations alternate between the GPR hyperparameters and the low-cost node calibrations using the approaches described in step three and four, respectively, until the GPR hyperparameters converged; in step seven, predict the 59-day $PM_{2.5}$ measurements of the holdout reference node given the finalized GPR hyperparameters and the low-cost node calibrations.

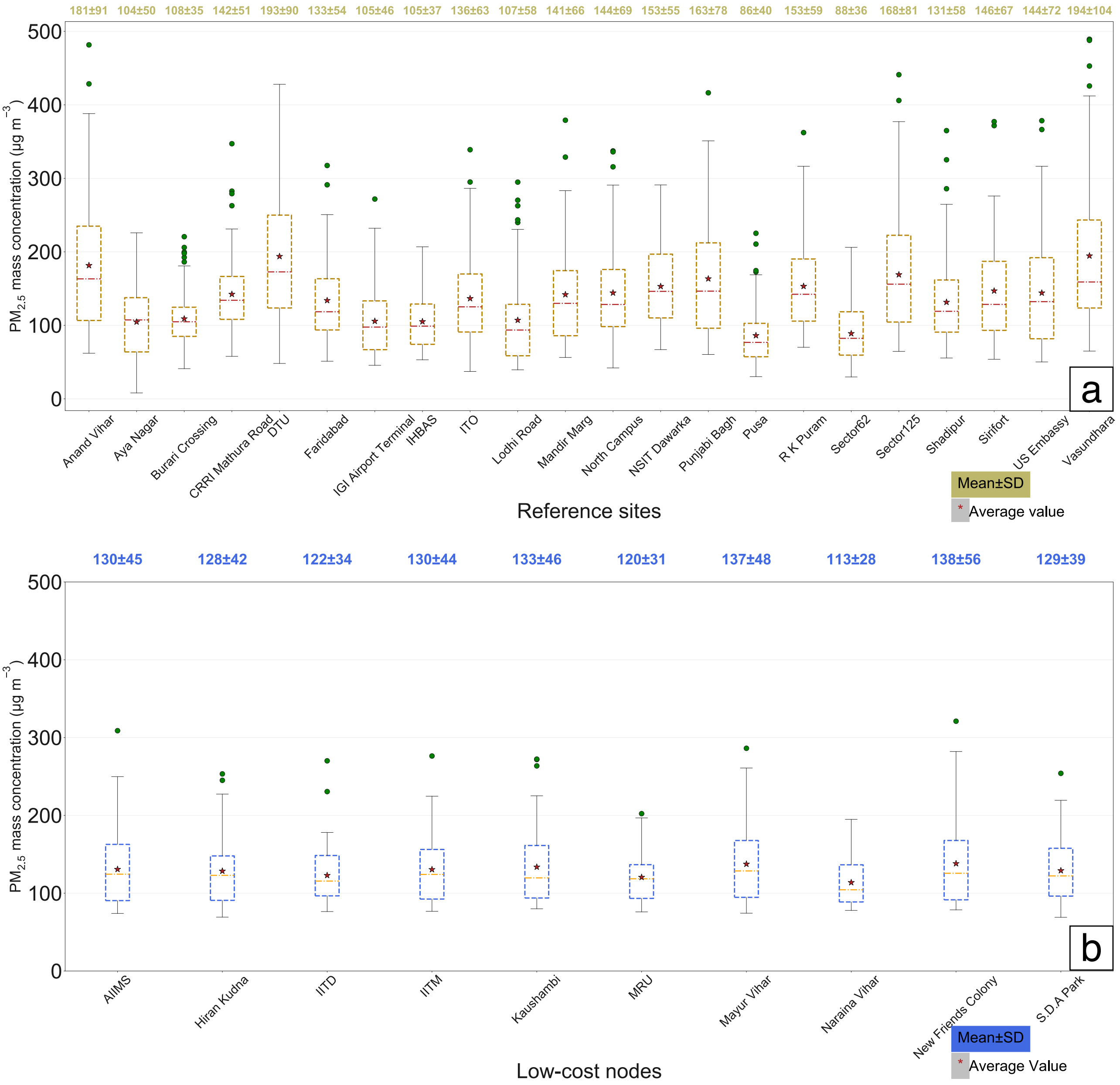

Figure 4: a) Box plots of the 24 h aggregated true ambient $PM_{2.5}$ mass concentrations measured by the 22 government reference monitors across Delhi from January 1 to March 31, 2018. b) Box plots of the low-cost node 24 h aggregated $PM_{2.5}$ mass concentrations calibrated by the optimized GPR model. In both a) and b), mean and SD of the $PM_{2.5}$ mass concentrations for each individual site are superimposed on the box plots.

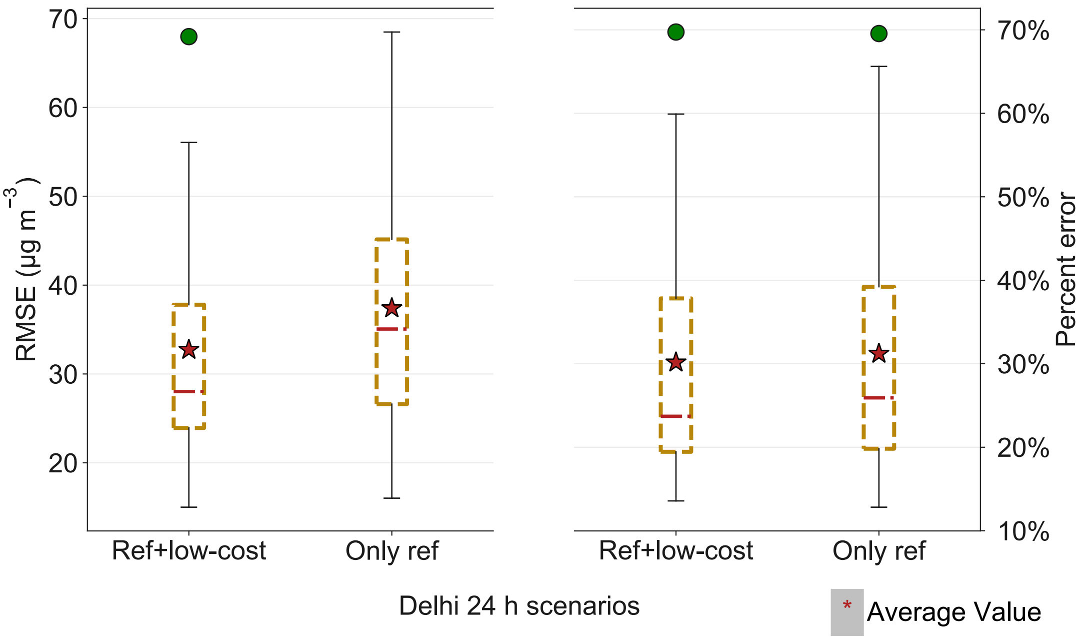

Figure 5: Box plots of the GPR model 24 h performance scores (including RMSE and percent error) for predicting the measurements of the 22 holdout reference nodes across the 22-fold leave-one-out CV under two scenarios — using the full sensor network by including both reference and low-cost nodes and using only the reference nodes for the model construction. Note both scenarios were given the initial parameter values and bounds that maximize the model performance.

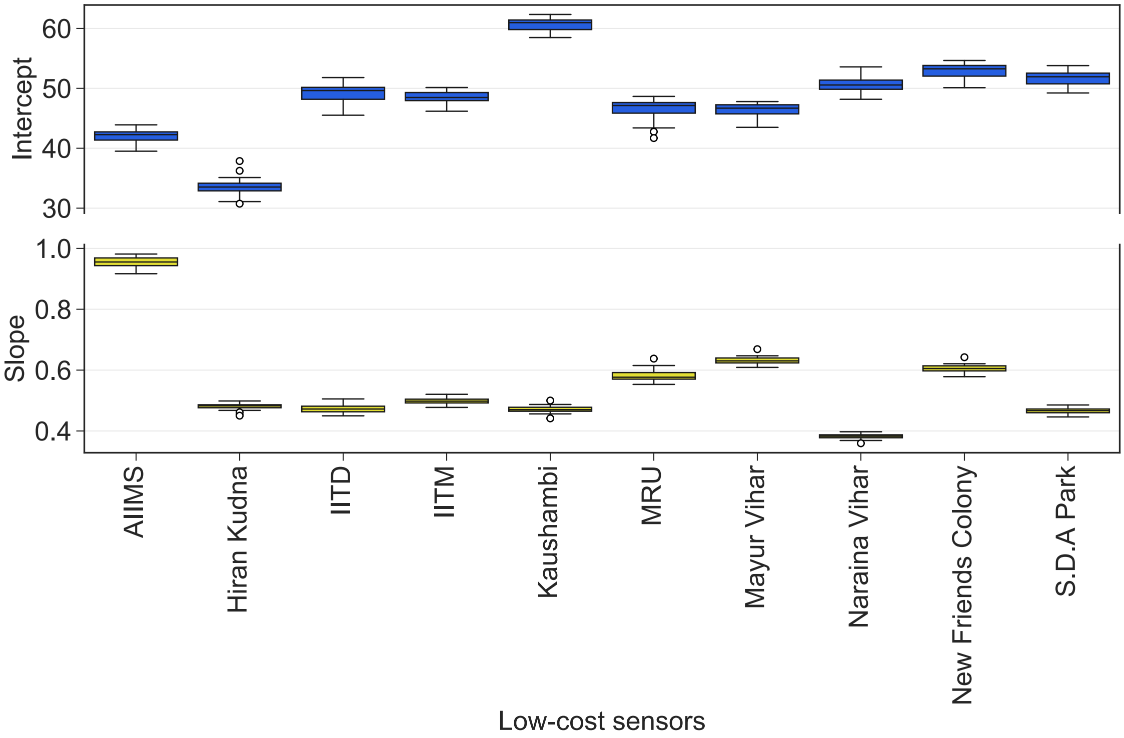

Figure 6: Box plots of the learned calibration factors (i.e., intercept and slope) for each individual low-cost node from the 22 optimized GPR models across the 22-fold leave-one-out CV.

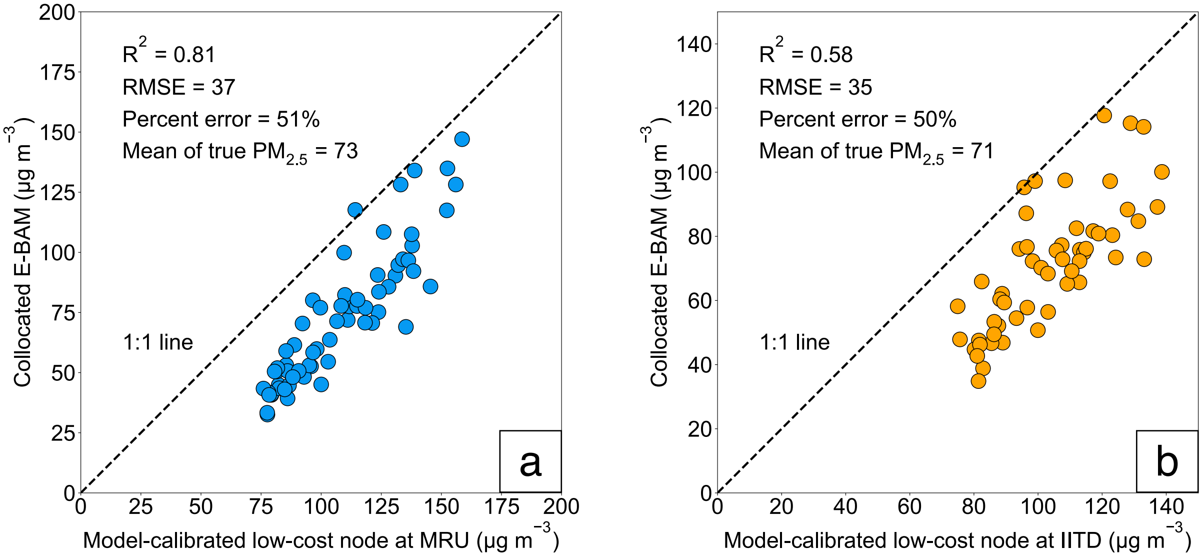

Figure 7: Correlation plots comparing the GPR model-calibrated low-cost node $PM_{2.5}$ mass concentrations to the collocated E-BAM measurements at a) MRU and b) IITD sites. In both a) and b), correlation of determination (*R^2*), RMSE, percent error, and mean of the true ambient $PM_{2.5}$ mass concentrations throughout the study (from January 1 to March 31, 2018) are superimposed on the correlation plots.

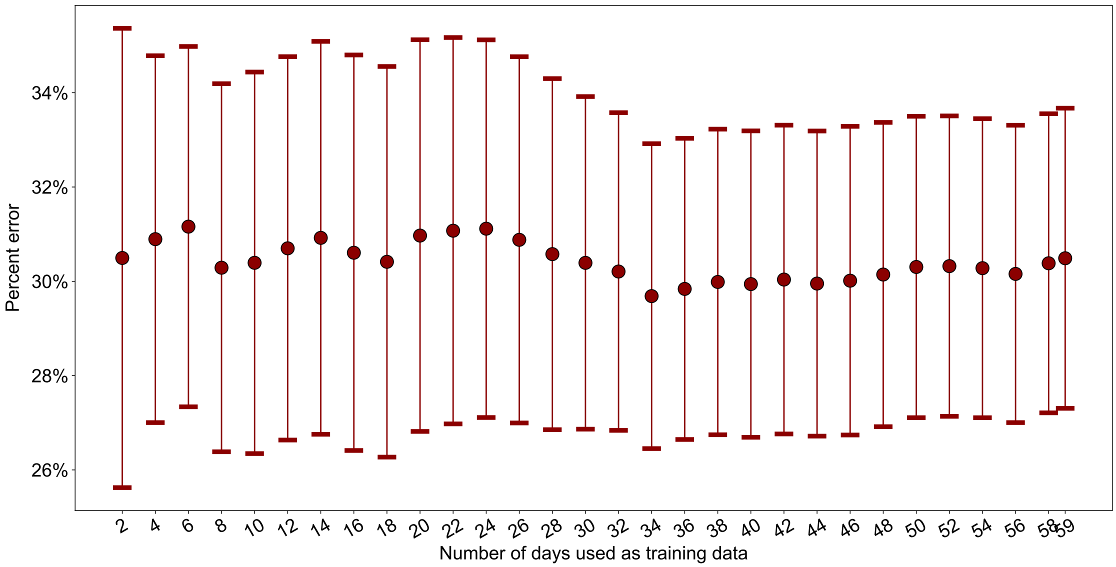

Figure 8: The mean percent error rate of GPR model prediction on the 22 reference nodes using leave-one-out CV (see Sect. 3.2.1) as a function of training window size in an increment of 2 days. The error bars represent the standard error of the mean (SEM) of the GPR prediction errors of the 22 reference nodes.

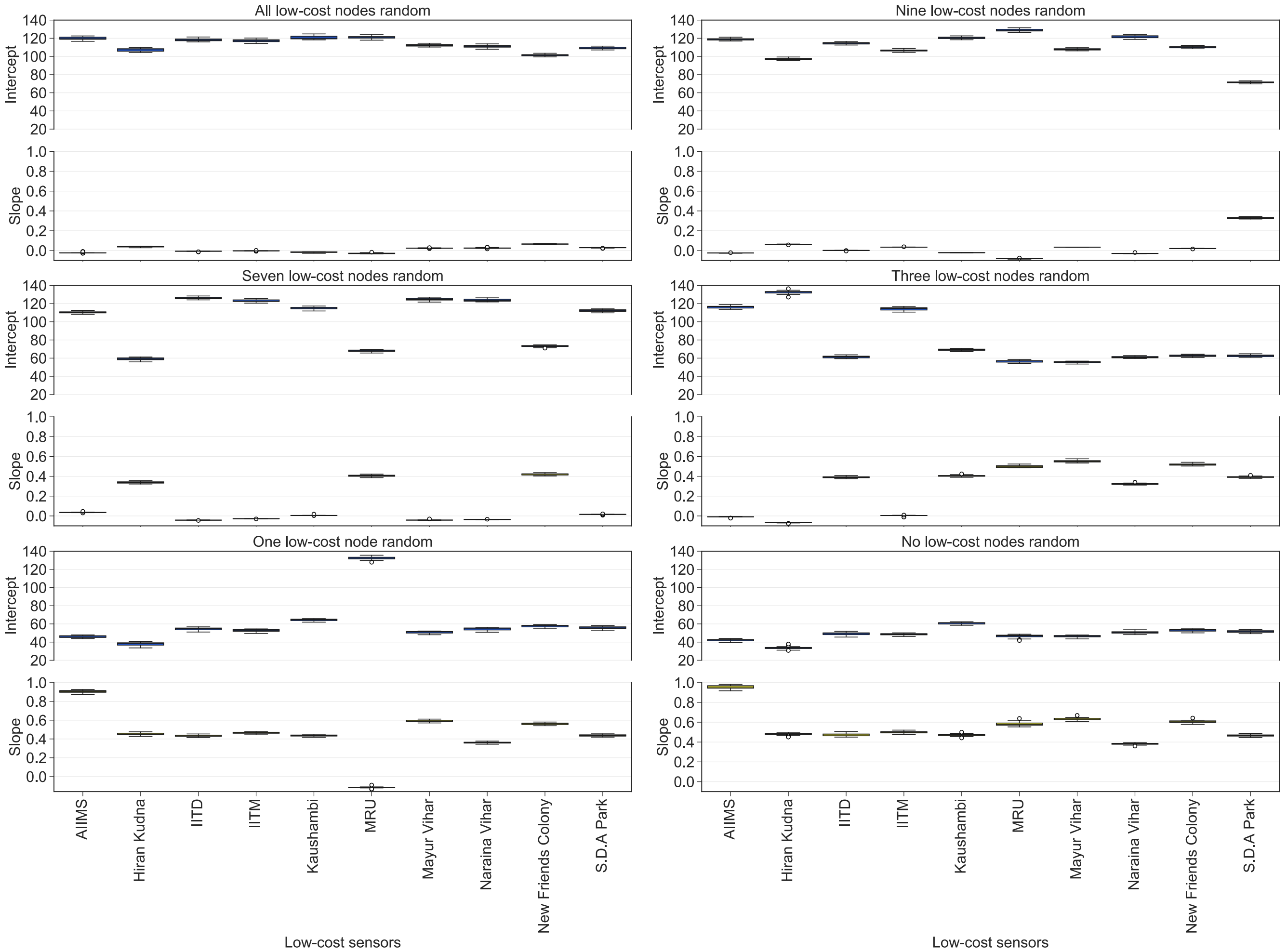

Figure ~~8~~9: Learned calibration factors for each individual low-cost node from the optimized GPR models by replacing measurements of all (top left), nine (top right), seven (middle left), three (middle right), one (bottom left), and zero (bottom right) of the low-cost nodes with random integers bounded by the min and max of the true signals reported by the corresponding low-cost nodes. Note that the nine, seven, three, and one low-cost nodes (whose true signals are replaced with random integers) were randomly chosen.

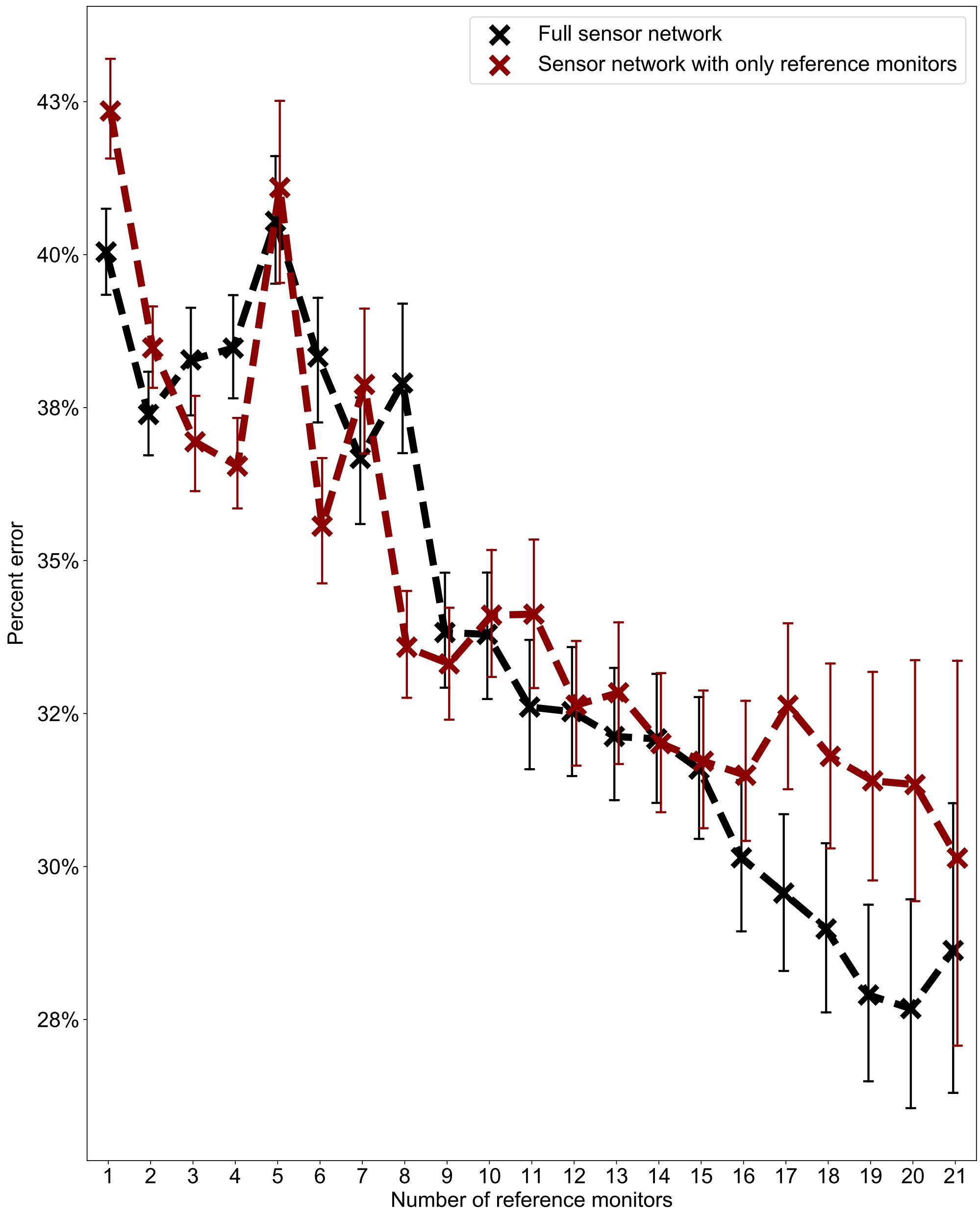

Figure ~~9~~10: Average 24 h percent errors of the GPR model for predicting the holdout reference nodes in the network as a function of the number of reference stations used for the model construction under two scenarios — using the full sensor network information by including both reference and low-cost nodes and using only the reference nodes for the model construction. Note each data point (mean value) is derived from 100 simulation runs. The error bars indicating 95 % CI of the means are based on 1000 bootstrap iterations. All scenarios were given the initial parameter values and bounds that maximize the model performance.

Table 1: Delhi PM sensor network sites along with the 1 h data completeness (from January 1, 2018 00:00 to March 31, 2018 23:59, Indian Standard Time, IST) before and after missing-data imputation for each individual site.

Category	Site names	Latitude	Longitude	Initial 1 h data completeness	1 h data completeness after missing-data imputation
Reference	Anand Vihar	N 28.6468350	E 77.3160320	88 %	100 %
	Aya Nagar	N 28.4706914	E 77.1099364	97 %	100 %
	Burari Cross	N 28.7258390	E 77.2033350	98 %	100 %
	CRRI Mathura Road	N 28.5512005	E 77.2735737	98 %	100 %
	Delhi Technological University (DTU)	N 28.7500499	E 77.1112615	96 %	100 %
	Faridabad	N 28.4088421	E 77.3099081	98 %	100 %
	IGI Airport Terminal-3	N 28.5627763	E 77.1180053	95 %	100 %
	IHBAS, Dilshad Garden	N 28.6811736	E 77.3025234	98 %	100 %
	ITO Metro Station (ITO)	N 28.6316945	E 77.2494387	98 %	100 %
	Lodhi Road	N 28.5918245	E 77.2273074	93 %	100 %
	Mandir Marg	N 28.6364290	E 77.2010670	96 %	100 %
	North Campus	N 28.6573814	E 77.1585447	94 %	100 %
	NSIT Dawarka	N 28.6090900	E 77.0325413	95 %	100 %
	Punjabi Bagh	N 28.6740450	E 77.1310230	94 %	100 %
	Pusa	N 28.6396450	E 77.1462620	99 %	100 %
	R K Puram	N 28.5632620	E 77.1869370	95 %	100 %
	Sector62 Noida	N 28.6245479	E 77.3577104	93 %	99 %
	Sector125 Noida	N 28.5447608	E 77.3231257	90 %	97 %
	Shadipur	N 28.6514781	E 77.1473105	97 %	100 %
	Sirifort	N 28.5504249	E 77.2159377	78 %	100 %
	US Embassy	N 28.5980970	E 77.1880330	95 %	100 %
	Vasundhara, Ghaziabad	N 28.6603346	E 77.3572563	100 %	100 %
Low-cost	All India Institute of Medical Science (AIIMS)	N 28.5545006	E 77.2124023	89 %	100 %
	Hiran Kudna	N 28.6674995	E 77.0089035	80 %	97 %
	Indian Institute of Technology Delhi (IITD)	N 28.5473003	E 77.1909027	88 %	99 %
	Indian Institute of Tropical Meteorology (IITM)	N 28.6303400	E 77.1750400	98 %	100 %
	Kaushambi	N 28.6410008	E 77.3199005	84 %	100 %
	Manav Rachna University (MRU)	N 28.4477005	E 77.3084030	87 %	100 %
	Mayur Vihar	N 28.6079998	E 77.2906036	85 %	93 %
	Naraina Vihar	N 28.6289005	E 77.1391983	70 %	79 %
	New Friends Colony	N 28.5676994	E 77.2687988	99 %	100 %
	S.D.A. Park	N 28.5517006	E 77.2031021	66 %	97 %

Table 2: Summary of the GPR model 24 h performance scores (including RMSE and percent error) for predicting the measurements of the 22 holdout reference nodes across the 22-fold leave-one-out CV when the full sensor network is used. The mean of the true ambient $PM_{2.5}$ mass concentrations throughout the study (from January 1 to March 31, 2018) for each individual reference node is provided. The reference nodes with the means of true $PM_{2.5}$ inside the range of [~~global~~ Delhi-wide mean ± SD, i.e., 138 ± 31] are indicated with shading.

Reference nodes	RMSE	Percent error	Mean of true $PM_{2.5}$
	(μg m^{-3})		(μg m^{-3})
Vasundhara, Ghaziabad	68	44 %	195
DTU	56	36 %	194
Anand Vihar	47	32 %	181
Sector125 Noida	31	23 %	169
Punjabi Bagh	26	20 %	163
NSIT Dawarka	25	19 %	153
R K Puram	26	20 %	153
Sirifort	22	18 %	147
US Embassy	21	18 %	144
North Campus	27	24 %	144
CRRI Mathura Road	27	21 %	142
Mandir Marg	16	14 %	142
ITO	15	14 %	136
Faridabad	21	18 %	133
Shadipur	23	22 %	132
Burari Cross	36	39 %	109
Lodhi Road	34	41 %	107
IGI Airport Terminal–3	29	32 %	106
Aya Nagar	34	38 %	105
IHBAS, Dilshad Garden	38	41 %	105
Sector62 Noida	47	60 %	89
Pusa	48	70 %	86
~~Global~~ Delhi-wide mean	33	30 %	138
SD	13	14 %	31

Table 3: Comparison of predetermined percentages of drift to those estimated from the GPR model for intercept and slope, respectively, for each individual low-cost node, assuming all (10), six, and two of the low-cost nodes developed various degrees of drift such as significant (11 %–99 %), marginal (1 %–10 %), and a balanced mixture of significant and marginal. Note the sensors that drifted, the percentages of drift, and which sensors drifted significantly or marginally are randomly chosen. The results reported under each scenario are based on averages of 10 simulation runs.

Drift category	Low-cost nodes	All low-cost nodes drift				Six low-cost nodes drift				Two low-cost nodes drift			
		Intercept drift (%)		Slope drift (%)		Intercept drift (%)		Slope drift (%)		Intercept drift (%)		Slope drift (%)	
		True	Estimated	True	Estimated	True	Estimated	True	Estimated	True	Estimated	True	Estimated
Significant	AIIMS	58 %	57 %	54 %	54 %	74 %	71 %	46 %	47 %	0 %	-1 %	0 %	-1 %
	Hiran Kudna	43 %	30 %	50 %	52 %	66 %	61 %	53 %	53 %	62 %	64 %	45 %	44 %
	IITD	51 %	52 %	52 %	51 %	0 %	-1 %	0 %	-2 %	0 %	1 %	0 %	-3 %
	IITM	54 %	53 %	56 %	55 %	61 %	58 %	48 %	48 %	0 %	-1 %	0 %	-2 %
	Kaushambi	61 %	62 %	73 %	72 %	70 %	70 %	49 %	48 %	0 %	0 %	0 %	-2 %
	MRU	55 %	56 %	56 %	56 %	58 %	61 %	41 %	39 %	0 %	-1 %	0 %	-2 %
	Mayur Vihar	60 %	65 %	48 %	47 %	0 %	1 %	0 %	-3 %	0 %	1 %	0 %	-3 %
	Naraina Vihar	56 %	54 %	76 %	76 %	0 %	-4 %	0 %	1 %	0 %	-1 %	0 %	-1 %
	New Friends Colony	66 %	68 %	68 %	67 %	55 %	55 %	48 %	47 %	59 %	61 %	37 %	36 %
	S.D.A. Park	53 %	47 %	48 %	50 %	0 %	-4 %	0 %	2 %	0 %	-1 %	0 %	0 %
	Mean absolute difference	**3 %**		**1 %**		**2 %**		**1 %**		**1 %**		**2 %**	
50 % significant and 50 % marginal	AIIMS	4 %	2 %	5 %	6 %	0 %	-4 %	0 %	2 %	0 %	1 %	0 %	-2 %
	Hiran Kudna	51 %	42 %	51 %	52 %	50 %	42 %	50 %	52 %	0 %	1 %	0 %	-2 %
	IITD	6 %	4 %	6 %	6 %	5 %	2 %	6 %	8 %	0 %	0 %	0 %	-2 %
	IITM	56 %	52 %	40 %	40 %	64 %	58 %	47 %	48 %	0 %	1 %	0 %	-3 %
	Kaushambi	60 %	60 %	42 %	41 %	5 %	2 %	5 %	7 %	0 %	0 %	0 %	-2 %
	MRU	6 %	5 %	4 %	3 %	0 %	-6 %	0 %	3 %	6 %	3 %	5 %	5 %
	Mayur Vihar	57 %	59 %	55 %	55 %	5 %	2 %	5 %	6 %	0 %	1 %	0 %	-2 %
	Naraina Vihar	4 %	0 %	5 %	7 %	0 %	-4 %	0 %	2 %	57 %	65 %	64 %	63 %
	New Friends Colony	6 %	5 %	6 %	5 %	0 %	-3 %	0 %	2 %	0 %	-1 %	0 %	-1 %
	S.D.A. Park	53 %	48 %	61 %	61 %	59 %	58 %	64 %	64 %	0 %	0 %	0 %	-1 %
	Mean absolute difference	**3 %**		**1 %**		**4 %**		**2 %**		**2 %**		**2 %**	
Marginal	AIIMS	5 %	5 %	5 %	4 %	8 %	8 %	5 %	5 %	0 %	0 %	0 %	-1 %
	Hiran Kudna	3 %	4 %	6 %	5 %	0 %	0 %	0 %	0 %	0 %	0 %	0 %	0 %
	IITD	5 %	6 %	7 %	5 %	7 %	8 %	5 %	4 %	6 %	7 %	5 %	4 %
	IITM	5 %	5 %	5 %	5 %	0 %	0 %	0 %	-1 %	0 %	0 %	0 %	-1 %
	Kaushambi	5 %	5 %	5 %	4 %	5 %	6 %	7 %	6 %	0 %	0 %	0 %	-1 %
	MRU	5 %	7 %	4 %	2 %	6 %	8 %	5 %	3 %	5 %	7 %	6 %	4 %
	Mayur Vihar	7 %	7 %	5 %	4 %	0 %	1 %	0 %	-1 %	0 %	1 %	0 %	-1 %
	Naraina Vihar	6 %	6 %	7 %	6 %	7 %	7 %	6 %	5 %	0 %	0 %	0 %	-1 %
	New Friends Colony	7 %	8 %	7 %	5 %	0 %	1 %	0 %	-2 %	0 %	1 %	0 %	-1 %
	S.D.A. Park	5 %	5 %	7 %	6 %	6 %	6 %	6 %	6 %	0 %	0 %	0 %	-1 %
	Mean absolute difference	**1 %**		**1 %**		**1 %**		**1 %**		**1 %**		**1 %**	

Reasoning behind step four of the schema for the simultaneous GPR and simple linear regression calibration model

Once the optimum $\boldsymbol{\Theta}$ for the (initial) GPR was found, we used the learned covariance function to find the mean of each low-cost node *i*'s Gaussian Distribution conditional on the remaining 30 nodes within the network (i.e., $\mu_{A|B}^{it}$) on day *t* as described mathematically in Eq. (S1)–(S4) and repeatedly did so until all 59 days' $\mu_{A|B}^{it}$ (i.e., $\boldsymbol{\mu_{A|B}^{i}}$) were found and then re-calibrated that low-cost node *i* based on the $\boldsymbol{\mu_{A|B}^{i}}$. This procedure was performed iteratively for all low-cost nodes one at a time.

$$p\left(\begin{bmatrix} r_A^{it} \\ \boldsymbol{r_B^{it}} \end{bmatrix}\right) = N\left(\begin{bmatrix} r_A^{it} \\ \boldsymbol{r_B^{it}} \end{bmatrix}; \begin{bmatrix} \mu_A^{it} \\ \boldsymbol{\mu_B^{it}} \end{bmatrix} \begin{bmatrix} \Sigma_{AA}^{it} & \boldsymbol{\Sigma_{AB}^{it}} \\ \boldsymbol{\Sigma_{BA}^{it}} & \boldsymbol{\Sigma_{BB}^{it}} \end{bmatrix}\right) \tag{S1}$$

$$r_A^{it} \middle| \boldsymbol{r_B^{it}} \sim N\left(\mu_{A|B}^{it}, \Sigma_{A|B}^{it}\right) \tag{S2}$$

$$\mu_{A|B}^{it} = \mu_A^{it} + \boldsymbol{\Sigma_{AB}^{it}}\boldsymbol{\Sigma_{BB}^{it}}^{-1}\left(\boldsymbol{r_B^{it}} - \boldsymbol{\mu_B^{it}}\right) \tag{S3}$$

$$\Sigma_{A|B}^{it} = \Sigma_{AA}^{it} - \boldsymbol{\Sigma_{AB}^{it}}\boldsymbol{\Sigma_{BB}^{it}}^{-1}\boldsymbol{\Sigma_{BA}^{it}} = a\ constant\ for\ low - cost\ node\ i\ regardless\ of\ day\ t = \Sigma_{A|B}^{i} \tag{S4}$$

where $r_A^{it}$and $\boldsymbol{r_B^{it}}$ are the daily $PM_{2.5}$ measurement(**s**) of the low-cost node *i* and the remaining 30 nodes on day *t*; μ_A^{it}, $\boldsymbol{\mu_B^{it}}$, and $\mu_{A|B}^{it}$ are the mean (**vector**) of the partitioned Multivariate Gaussian Distribution of the low-cost node *i,* the remaining 30 nodes, and the low-cost node *i* conditional on the remaining 30 nodes, respectively, on day *t*; and Σ_{AA}^{it}, $\boldsymbol{\Sigma_{AB}^{it}}$, $\boldsymbol{\Sigma_{BA}^{it}}$, $\boldsymbol{\Sigma_{BB}^{it}}$, and $\Sigma_{A|B}^{it}$ are the covariance between the low-cost node *i* and itself, the low-cost node *i* and the remaining 30 nodes, the remaining 30 nodes and the low-cost node *i*, the remaining 30 nodes and themselves, and the low-cost node *i* conditional on the remaining 30 nodes and itself, respectively, on day *t*.

The reasoning behind recalibrating each low-cost node *i* based on the $\boldsymbol{\mu_{A|B}^{i}}$ is given as follows:

The conditional log-likelihood under the Univariate Gaussian distribution on day *t* is:

$$\log p\left(r_A^{it} \middle| \boldsymbol{r_B^{it}}\right) = constant - 0.5{\Sigma_{A|B}^{it}}^{-2}\left(r_A^{it} - \mu_{A|B}^{it}\right)^2 \tag{S5}$$

Then the complete log-likelihood over all 59 days is therefore given by:

$$\textstyle\sum_{t=1}^{59} \log p\left(r_A^{it} \middle| \boldsymbol{r_B^{it}}\right) = constant - positive\ constant \cdot \sum_{t=1}^{59}\left(r_A^{it} - \mu_{A|B}^{it}\right)^2 \tag{S6}$$

The objective is to maximize the complete log-likelihood over all 59 days (i.e., S6), that is equivalent to minimizing the term of $\sum_{t=1}^{59}\left(r_A^{it} - \mu_{A|B}^{it}\right)^2$:

$$\max_{\boldsymbol{r_A^i}} \textstyle\sum_{t=1}^{59} \log p\left(r_A^{it} \middle| \boldsymbol{r_B^{it}}\right) = \min_{\boldsymbol{r_A^i}} \left\| \boldsymbol{r_A^i} - \boldsymbol{\mu_{A|B}^{i}} \right\|_2^2 \tag{S7}$$

$$\text{and } \boldsymbol{r_A^i} = \boldsymbol{Y_i}\boldsymbol{\beta_i} \tag{S8}$$

where $\boldsymbol{Y_i} = \begin{bmatrix} 1 & y_{it} \\ \vdots & \vdots \\ 1 & y_{i59} \end{bmatrix}$ and $\boldsymbol{\beta_i}$ is a vector of the intercept and slope (to be learned) of the simple linear regression calibration equation for low cost node *i*.

And to minimize $\left\| \boldsymbol{Y}_{\boldsymbol{i}}\boldsymbol{\beta_i} - \boldsymbol{\mu}^{\boldsymbol{i}}_{\boldsymbol{A|B}} \right\|_2^2$ is then equivalent to optimizing a simple linear regression model to re-calibrate the raw low-cost node signals based on the mean of each node's Gaussian Distribution conditional on the remaining 30 nodes within the network (i.e., $\boldsymbol{\mu}^{\boldsymbol{i}}_{\boldsymbol{A|B}}$).

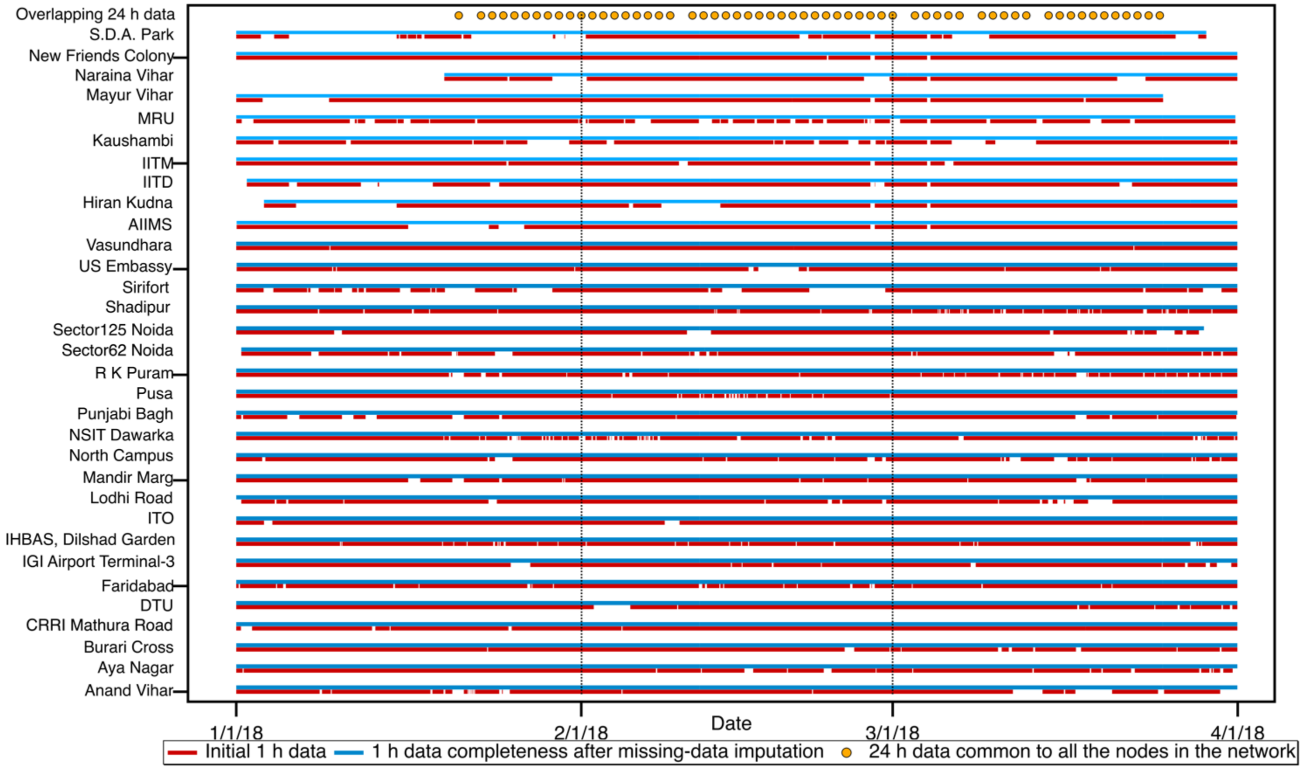

Figure S1: Periods over which 1 h data were available for each individual site before and after missing-data imputation and a total of 59 24 h aggregated observations common to all the nodes in the network used for the on-the-fly calibration feasibility test. Note that there is no obvious pattern in the missing data.

5

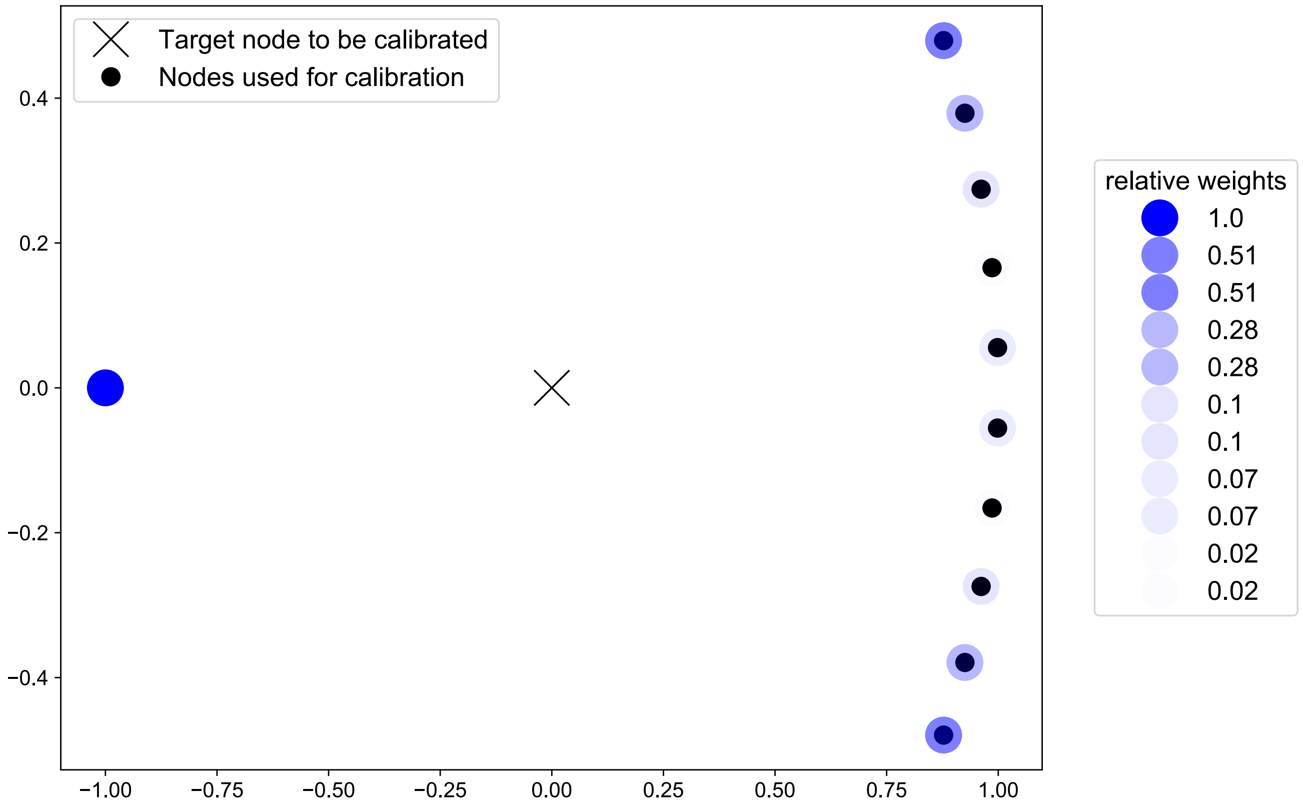

Figure S2: Simplified illustration of the relative importance (i.e., importance normalized by the max value) of each node within the network when using GPR to calibrate the target low-cost node and when all the nodes used for calibration are equally distant from the target node.

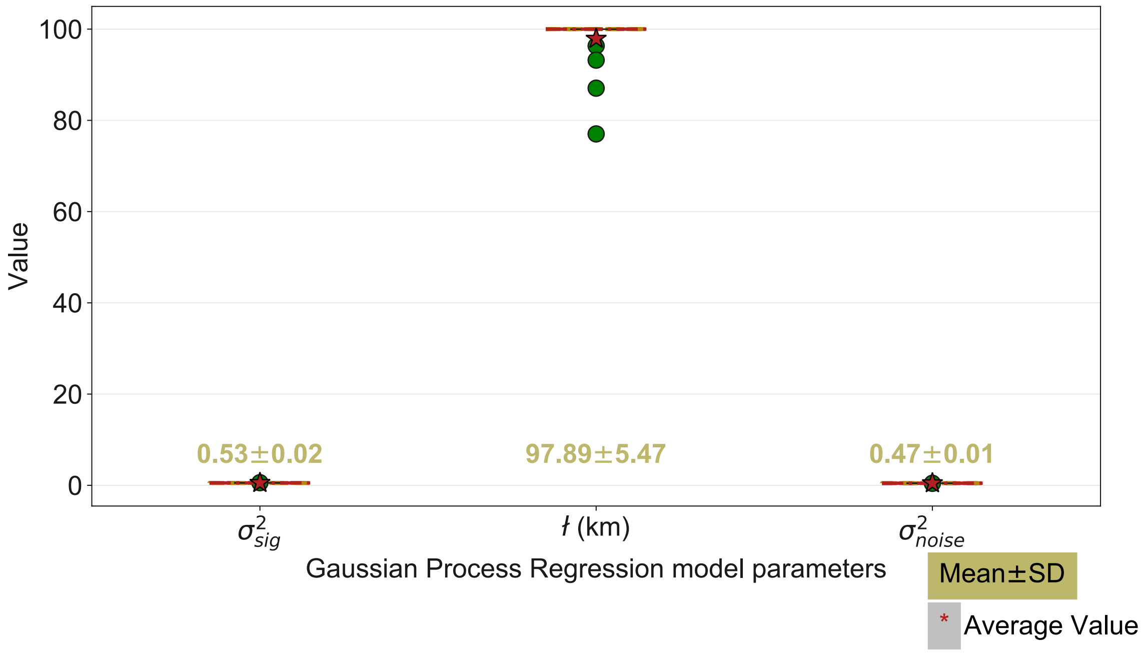

Figure S3: Box plots of the learned optimum Gaussian Process Regression model parameters including the signal variance (σ^2_{sig}), the characteristic length scale (l), and the noise variance (σ^2_{noise}) from the 22-fold leave-one-out cross-validation. The mean and SD of each parameter are superimposed on the box plots.

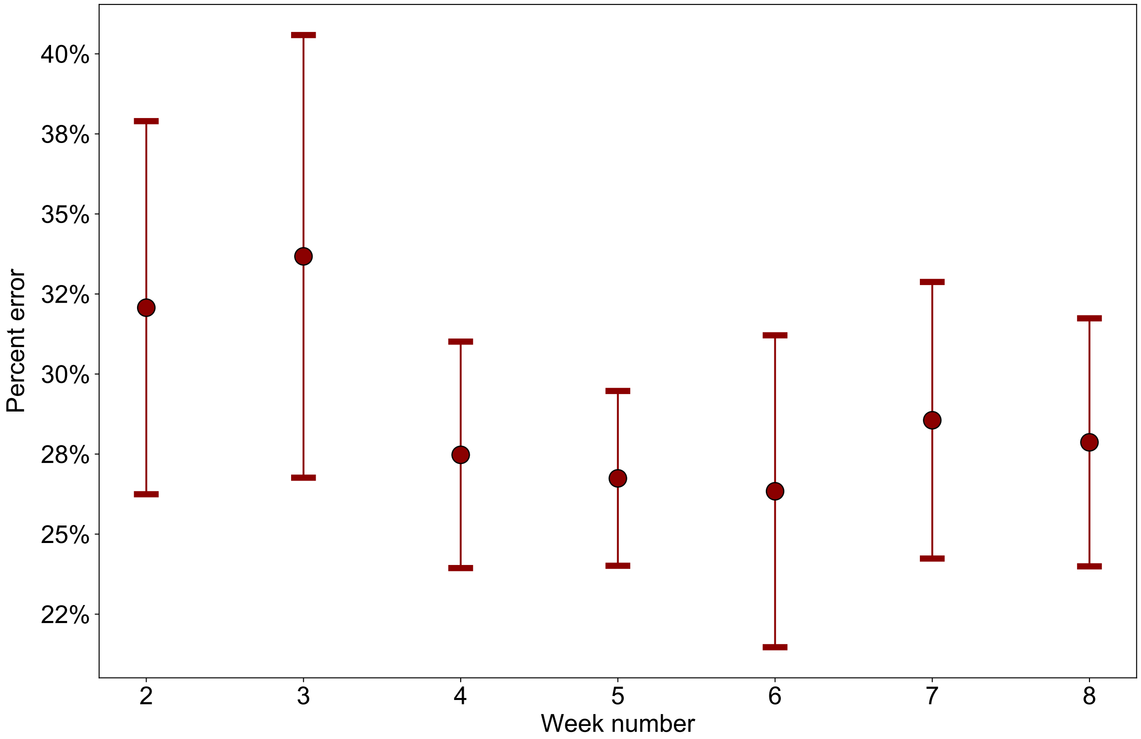

Figure S4: The 1 week-ahead prediction error of the GPR models (which were pre-trained on the current week's data) as a function of the week being predicted. The error bars represent the standard error of the mean (SEM) of the GPR prediction errors of the 22 reference nodes.

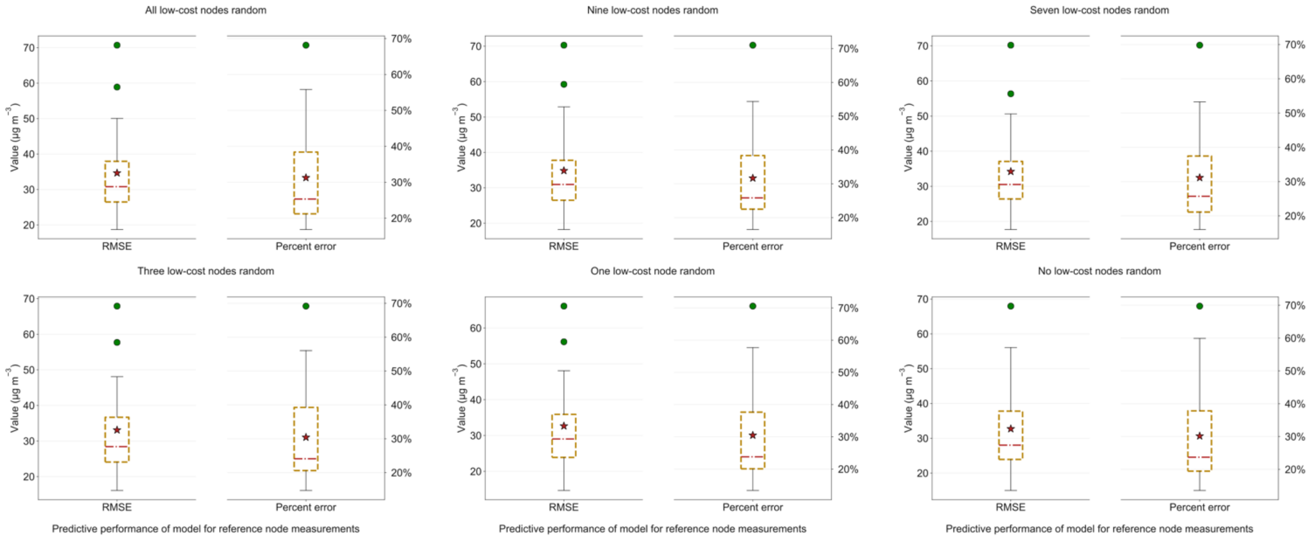

Figure ~~S4~~S5: Gaussian Process Regression model 24 h performance scores (including RMSE and percent error) for predicting the measurements of the 22 holdout reference nodes across the 22-fold leave-one-out cross-validation using the full sensor network, when measurements of all (top left), nine (top center), seven (top right), three (bottom left), one (bottom center), and zero (bottom right) of the low-cost nodes are replaced with random integers bounded by the min and max of the true signals reported by the corresponding low-cost nodes.

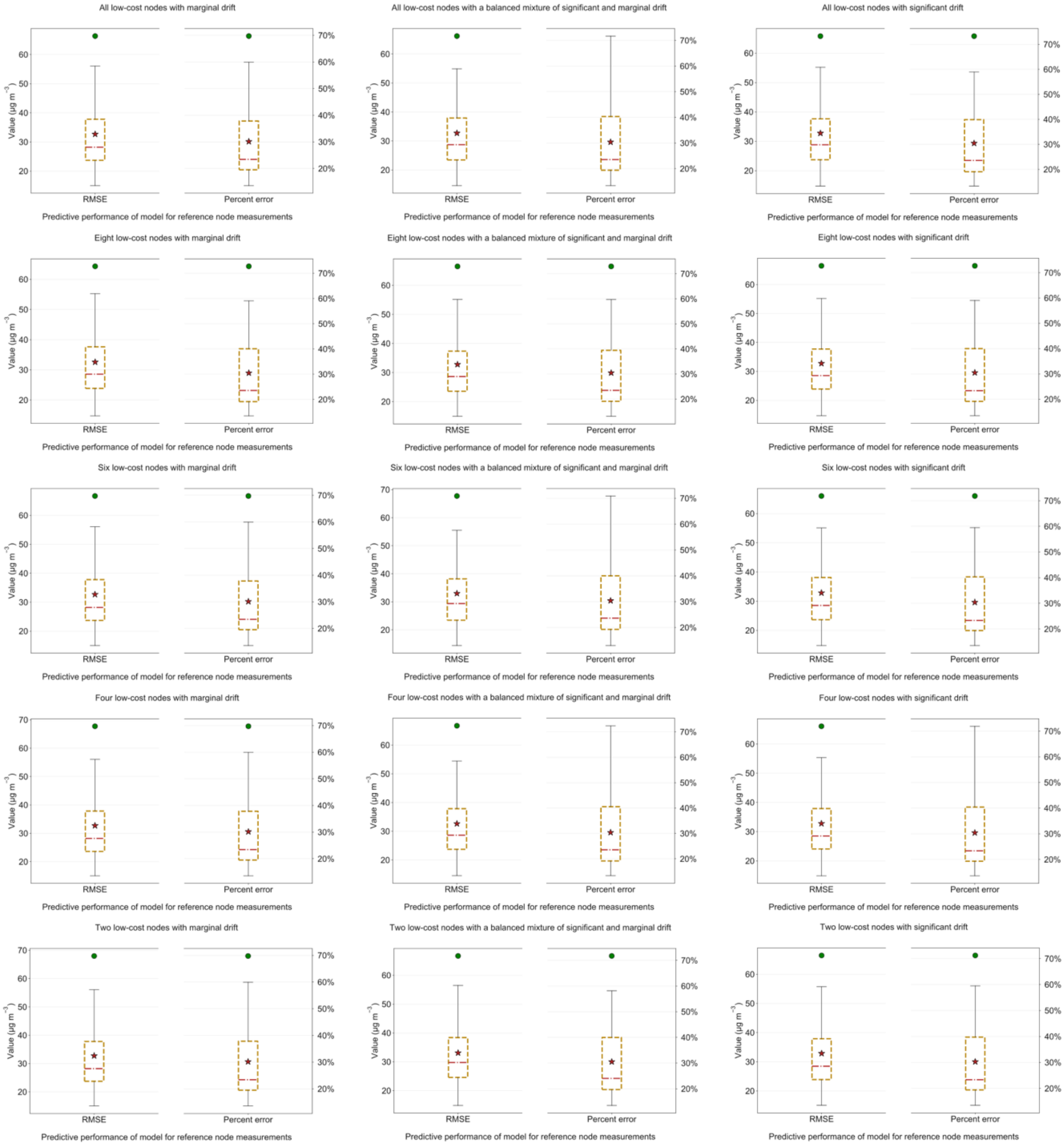

Figure ~~S5~~S6: Gaussian Process Regression model 24 h performance scores (including RMSE and percent error) for predicting the measurements of the 22 holdout reference nodes across the 22-fold leave-one-out cross-validation using the full sensor network, when measurements of two (bottom/1st row), four (2nd row), six (3rd row), eight (4th row), and all ten (top/5th row) of the low-cost nodes developed significant (11 %–99 %, left column), marginal (1 %–10 %, right column), and a balanced mixture of significant and marginal drifts. Note the sensors that drifted, the percentages of drift, and which sensors drifted significantly or marginally are randomly chosen. The results reported under each scenario are based on averages of 10 simulation runs.

Table S1: Comparison of pre-determined percentages of drift to those estimated from the Gaussian Process Regression model for intercept and slope, respectively, for each individual low-cost node, assuming eight and four of the low-cost nodes developed various degrees of drift such as significant (11 %–99 %), marginal (1 %–10 %), and a balanced mixture of significant and marginal. Note the sensors that drifted, the percentages of drift, and which sensors drifted significantly or marginally are randomly chosen. The results reported under each scenario are based on averages of 10 simulation runs.

Drift category	Low-cost nodes	Eight low-cost nodes drift				Four low-cost nodes drift			
		Intercept drift (%)		Slope drift (%)		Intercept drift (%)		Slope drift (%)	
		True	Estimated	True	Estimated	True	Estimated	True	Estimated
Significant	AIIMS	55 %	54 %	55 %	55 %	0 %	-2 %	0 %	0 %
	Hiran Kudna	57 %	43 %	54 %	56 %	47 %	42 %	54 %	54 %
	IITD	68 %	70 %	61 %	61 %	0 %	-1 %	0 %	-1 %
	IITM	0 %	-2 %	0 %	-1 %	0 %	-2 %	0 %	-1 %
	Kaushambi	0 %	-1 %	0 %	-1 %	0 %	-1 %	0 %	-1 %
	MRU	45 %	46 %	52 %	51 %	0 %	-4 %	0 %	1 %
	Mayur Vihar	56 %	59 %	48 %	47 %	42 %	44 %	57 %	56 %
	Naraina Vihar	63 %	61 %	57 %	57 %	51 %	51 %	48 %	48 %
	New Friends Colony	53 %	53 %	57 %	57 %	70 %	71 %	39 %	38 %
	S.D.A. Park	55 %	50 %	55 %	56 %	0 %	-4 %	0 %	2 %
	Mean absolute difference	**3 %**		**1 %**		**2 %**		**1 %**	
50 % significant and 50 % marginal	AIIMS	0 %	-1 %	0 %	-1 %	0 %	-1 %	0 %	-1 %
	Hiran Kudna	47 %	40 %	58 %	58 %	0 %	-9 %	0 %	3 %
	IITD	57 %	62 %	58 %	57 %	0 %	0 %	0 %	-2 %
	IITM	6 %	5 %	6 %	3 %	4 %	3 %	7 %	6 %
	Kaushambi	4 %	4 %	5 %	1 %	0 %	0 %	0 %	-2 %
	MRU	47 %	54 %	55 %	53 %	0 %	-1 %	0 %	-1 %
	Mayur Vihar	56 %	62 %	46 %	43 %	44 %	48 %	70 %	68 %
	Naraina Vihar	5 %	3 %	4 %	3 %	58 %	56 %	46 %	47 %
	New Friends Colony	6 %	7 %	6 %	2 %	5 %	6 %	6 %	3 %
	S.D.A. Park	0 %	-3 %	0 %	1 %	0 %	-3 %	0 %	2 %
	Mean absolute difference	**3 %**		**2 %**		**2 %**		**2 %**	
Marginal	AIIMS	5 %	6 %	4 %	3 %	0 %	0 %	0 %	-1 %
	Hiran Kudna	6 %	6 %	7 %	6 %	0 %	0 %	0 %	0 %
	IITD	6 %	7 %	6 %	4 %	0 %	1 %	0 %	-1 %
	IITM	5 %	5 %	5 %	4 %	0 %	0 %	0 %	-1 %
	Kaushambi	5 %	5 %	5 %	4 %	5 %	6 %	7 %	6 %
	MRU	7 %	9 %	4 %	2 %	7 %	8 %	5 %	4 %
	Mayur Vihar	0 %	1 %	0 %	-1 %	6 %	7 %	4 %	3 %
	Naraina Vihar	6 %	7 %	6 %	5 %	0 %	0 %	0 %	-1 %
	New Friends Colony	0 %	1 %	0 %	-2 %	0 %	1 %	0 %	-1 %
	S.D.A. Park	5 %	6 %	4 %	3 %	7 %	7 %	5 %	4 %
	Mean absolute difference	**1 %**		**1 %**		**1 %**		**1 %**	